OLD DOMINION UNIVERSITY RESEARCH FOUNDATION

DEPARTMENT OF PHYSICS AND GEOPHYSICAL SCIENCES
SCHOOL OF SCIENCES AND HEALTH PROFESSIONS
OLD DOMINION UNIVERSITY
NORFOLK, VIRGINIA

Technical Report PGSTR-PH77-48

(NASA-CR-149789) A HIGH-TEMPERATURE WIDEBAND PRESSURE TRANSDUCER Final Report (Old Dominion Univ. Research Foundation) 106 p HC A06/MF A01 CSCL 14B
N77-20405
Unclas
G3/35 22802

A HIGH-TEMPERATURE WIDEBAND PRESSURE TRANSDUCER

By

Allan J. Zuckerwar

Final Report

Prepared for the
National Aeronautics and Space Administration
Langley Research Center
Hampton, Virginia

Under
Grant NSG 1039
Harlan K. Holmes, Technical Monitor
Acoustics and Vibration Instrumentation Section

March 1977

ABSTRACT

A condenser microphone AM carrier system, which has been developed to measure pressure fluctuations at elevated temperatures, consists of the following components a condenser microphone designed for operation at elevated temperatures, existing carrier electronics developed under two previous research grants but adapted to meet present requirements, a 6 m (20 ft) cable operating as a half-wavelength transmission line between the microphone and carrier electronics, and a voltage-controlled oscillator used in a feedback loop for automatic tuning control Both theoretical and practical aspects of the development program are considered

Specifications achieved with a prototype system are the following maximum operating temperature (continuous duty) >427°C, harmonic distortion at 170 dB SPL = 1 4 percent, noise floor (22.4 Hz to 22 4 kHz) = 105 dB, frequency response (±2 dB) = 20 Hz to 10 kHz, thermal shock, <2 dB change in sensitivity during cooling at rate of 162°C/min; vibration sensitivity <0 5 $N/m^2/g$ The three predominant effects of temperature changes are changes in the membrane-backplate gap, membrane tension, and air viscosity The microphone is designed so that changes in gap and membrane tension tend to have compensating effects upon the microphone sensitivity

CONTENTS

PRECEDING PAGE BLANK NOT FILMED

LIST OF TABLES

LIST OF FIGURES

A HIGH-TEMPERATURE WIDEBAND PRESSURE TRANSDUCER

By

Allan J. Zuckerwar[1]

I. INTRODUCTION

A. Statement of the Problem

The "powered-lift" concept in STOL aircraft design entails the impingement of a jet exhaust upon structural surfaces of the aircraft either by (1) upper surface blowing or (2) externally blown flaps. The interaction of the exhaust stream with the wing and flaps enhances lift, but the associated turbulence simultaneously produces pressure fluctuations with undesirable side effects. acoustic fatigue of the structure and deteriorating ride quality. A study of these effects is contingent upon the availability of a transducer which is capable of measuring the pressure fluctuations right within the jet exhaust. Presently available commercial transducers are of limited applicability to these studies because of their inability to withstand the high ambient temperatures The purpose of the present research is to develop a dynamic pressure transducer specifically for measurements within the high-temperature environment of a jet exhaust.

A typical experimental arrangement to study pressure fluctuations on externally blown flaps is shown in figure 1 The transducers are flush mounted in selected locations on the wing and flaps for the purpose of obtaining the spatial distribution of fluctuating pressure levels.

The specifications on such a transducer are quite severe in view of several requirements peculiar to this particular application first, the transducer must operate continuously at temperatures up to 427°C (800°F), and even higher for future experiments, secondly, it must be insensitive to the vibrations of the panel on which it is mounted, thirdly, it must operate through rapid changes in temperature ("thermal shock"), finally, it must have

[1] Research Associate Professor of Physics, Department of Physics and Geophysical Sciences, Old Dominion University, Norfolk, Virginia 23508

a smooth, plane exterior surface for flush mounting in the test panels, so as not to influence ambient aerodynamic conditions. A list of the most essential specifications is given in table 1.

Table 1. Essential transducer specifications.

1.	Dynamic range (re 2×10^{-5} N/m^2)	110 to 180 dB
2.	Noise floor	100 dB
3.	Frequency response (± 1 dB)	5 Hz to 20 kHz
4.	Maximum operating temperature (continuous duty)	427°C (800°F)
5.	Smooth exterior finish for flush mounting in panels	
6.	Insensitivity to thermal shock [167°C (300°F)/min over range 10° to 427°C]	
7.	Maximum sensitivity to panel vibrations	<0.6895 N/m^2/g (0.0001 psi/g)

From Specification No. 1-59-3821, April 24, 1973, NASA-Langley Research Center.

B. Past Work

Past efforts to measure the pressure fluctuations have centered about the semiconductor pressure transducer manufactured by Kulite Semiconductor Products, Inc. The Kulite transducer, utilizing the piezoresistive effect, has a maximum temperature rating of 260°C (500°F). This limitation is inherent in the nature of the transducer and rules out its use at the higher-temperature locations on the wing and flaps, even though, for the most part, it otherwise meets specifications It has been used successfully in tests where transducer locations were restricted to low-temperature regions of the flaps, or where the exhaust nozzle was modified to produce lower exhaust temperatures (ref 1)

An eddy-current transducer, developed at Kaman Sciences Corporation, is capable of operating at the remarkably high temperature of 1093°C (2000°F), but

at this writing is not available commercially and is not designed to meet the present specifications regarding noise floor and frequency response (ref 2).

C Method of Solution

The response of each of the transducers described above depends upon a material property--the piezoresistive coefficient and the electrical conductivity (of the membrane) in the cases of the Kulite and Kaman units respectively. These properties are sensitive not only to the temperature itself, but also to any contamination or deterioration of the material which might result from continuous duty at high temperature. For this reason it is advantageous to consider a transducer whose operation is based primarily upon geometrical changes and only to a lesser extent upon the properties of its constituent materials. Such a transducer is the condenser microphone.

The electronic circuitry used with condenser microphones contains either (1) a polarization voltage or (2) a carrier frequency. Ordinarily the substantial part of the microphone electronics is located in a common housing with the microphone cartridge in order to avoid loss of sensitivity due to cable capacitance In the present application, however, such an arrangement is not possible, for the hostile operational environment necessitates that the microphone be separated from its supporting electronics by means of a cable roughly 6 m (20 ft) in length The use of a polarization voltage, then, is out of the question because of severe loading by the cable capacitance. In a carrier system, on the other hand, the effect of cable capacitance can be minimized by operation of the cable as a half-wavelength transmission line This is the approach pursued in the present research.

D. Objectives of the Present Research

The objective of NASA Grant NSG 1039 is to modify an existing microphone AM carrier system, developed under two previous NASA Contracts (refs. 3, 4), to meet the specifications listed in table 1. By nature the research lends itself to logical partition into three basic problems

(1) Design and construction of the condenser microphone The goal of this phase of the research is to advance the currently inadequate theory of condenser microphones to the point where the response of a particular design is readily

predictable, and to utilize the theoretical results in the design and construction of a prototype microphone.

(2) Design and fabrication of the high-temperature cable There are two major tasks associated with the cable. (a) to study the feasibility of operating the cable as a half-wavelength transmission line, and (b) to fabricate a cable capable of withstanding the severe environmental conditions at the microphone.

(3) Modification of the existing carrier electronics. The specifications of the existing AM carrier system, listed below in table 2, are seen to be compatible with the requirements of the present application. The presence of the cable necessitates two modifications (a) replacing the fixed-frequency local oscillator by a variable-frequency external oscillator to extend the tuning range of the converter, and (b) redesigning the automatic tuning control system to accommodate wide variations in carrier frequency.

Table 2. Specifications of existing microphone carrier system.*

Microphone	12.7 mm (1/2 in.)
Cable	2 conductor shielded
Termination network	None
Carrier frequency	10 MHz
Polarization voltage	None
Frequency response (-3 dB)	2 Hz - 20 kHz
Noise floor (22 4 Hz - 22.4 kHz)	55 dB
Dynamic range	72 dB

* Developed under NASA Grant NGR 36-028-004 and NASA Contract NAS1-11707-29.

Moreover, an attendant problem consists of devising the means of testing the completed system against the specifications of table 1 at both room and elevated temperatures.

II THE MICROPHONE PROBLEM

A Description of Condenser Microphone Operation

Figure 2 shows a cross section of a conventional condenser microphone Incident sound excites motion of the membrane, which compresses and expands the air in the gap, and creates a "reaction pressure," which opposes the motion of the membrane. The reaction pressure is partially relieved by the flow of air through the openings in the backplate, and these determine the damping of the coupled membrane-air system. The backplate may contain one or more "rings" of holes and nearly always a slot around its periphery The prototype cartridge used in the present research has a single ring of four evenly spaced holes in the backplate, as shown in figure 3.

Even upon excitation at rather intense sound pressure levels, the membrane displacement η remains small compared to the static gap distance h. Under this condition the variation in microphone capacitance (between the membrane and backplate) is practically linear with membrane displacement The function of the microphone supporting electronics is to produce an output voltage proportional to the instantaneous variation in microphone capacitance, and thus to the instantaneous membrane displacement and incident sound pressure

B. Theoretical Analysis

1 Past Work An extensive search of the literature has revealed that a theoretical analysis describing the response of a condenser microphone in terms of geometry, materials, and related physical properties is not yet available The strong coupling between the motions of the membrane and underlying air layer, together with the difficult and unusual boundary conditions at the backplate, render the exact solution to the problem so complex as to be of little use to the designer A firm theoretical basis for condenser microphone design was deemed essential for two reasons· (1) to eliminate time-consuming "trial and error" procedures as a means of obtaining satisfactory design goals, and (2) to provide the capability of predicting microphone behavior at elevated temperatures One of the objectives of the present investigation is to overcome the theoretical difficulties through realistic, physically sound assumptions, and ultimately to express the microphone

sensitivity (membrane displacement over incident acoustical sound pressure) in terms of the parameters mentioned above.

Robey was the first to solve the related fluid dynamical problem (ref 5), but an unrealistic microphone model makes his results of limited applicability to actual microphone design. In two papers, Petritskaya (refs. 6, 7) gives an exact solution to the coupled problem, even for the case of an arbitrary arrangement of openings in the backplate,[1] but his results are of such complexity that he does not give the membrane eigenfunctions and only presents numerical results for a particular microphone design. A numerical method by Warren, Brzezinski, and Hamilton does not allow for an angular dependence of the reaction pressure and is thus confined to cases where the backplate openings are in the form of annular slots (ref. 8); again, their results are presented only in numerical form for several particular microphone designs.

2. Derivation of the coupled fluid-membrane equations. To derive the fluid dynamical equations we express the particle velocity $\vec{v}$ in terms of a scalar potential ϕ and a vector potential $\vec{A}$,

$$\vec{v} = -\nabla\phi + \vec{A} \tag{2-1a}$$

and insert these into the Navier-Stokes, continuity, and state equations to arrive at the following.[2]

$$\nabla^2\phi + k^2\phi = 0 \tag{2-1b}$$

$$\nabla^2\vec{A} + L^2\vec{A} = 0 \ . \tag{2-1c}$$

Equation (2-1c) is true if we impose the additional condition that $\vec{A}$ be solenoidal

[1] Provided the openings have small radial dimensions, e.g , holes or annular slots

[2] A list of symbols appears in part IIF Several symbols in equation (2-8), taken from reference 6, are not used in the text and therefore do not appear in the list

$$\nabla \cdot \vec{A} = 0$$

We write the boundary conditions in terms of the radial and axial components of particle velocity (see figures 2 and 3)

$$v_r(r = a) = v_r(z = 0) = v_r(z = h) = 0 \qquad (2\text{-}2a,b,c)$$

$$v_z(z = 0) = i\omega\eta(r,\theta) \ , \quad v_z(z = h) = f(r,\theta) \qquad (2\text{-}2d,e)$$

The function $f(r,\theta)$, introduced by Petritskaya, describes the vertical component of the particle velocity at the backplate, and is shown at the bottom of figure 2. Each opening in the backplate is assigned a number $k = 1, 2, \ldots, q$, where q is the number of openings. The vertical velocity is zero on the solid region of the backplate, and is assumed equal to a constant f_k over the area of the kth opening Each of the f_k's is an unknown to be determined by the boundary condition (2-2e). Petritskaya assumes that the velocity f_k depends only upon the potential ϕ_k at the kth opening.[3]

$$f_k = \frac{i\omega\rho_o\phi_k}{z_k s_k} \ . \qquad (2\text{-}3)$$

Because ϕ_k , in turn, depends upon all the f_k's the latter are coupled through a set of q simultaneous equations in q unknowns Equation (2-3) neglects the fact that the volume velocities associated with the openings are coupled in the backchamber Figure 4 shows an equivalent circuit of the backplate and backchamber. As shown in Appendix A, solution to the circuit problem yields the result

$$f_k = \frac{i\omega\rho_o}{s_k} \sum_{\ell} Y_{k\ell}\phi_\ell \ , \qquad (2\text{-}4)$$

where $Y_{k\ell}$ is an element of an acoustical admittance matrix

---

[3] The acoustical impedance z_k is the ratio of the acoustic pressure $P_k = i\omega\rho_o\phi_k$ to the volume velocity $U_k = f_k s_k$.

Thus the f_k's are coupled below as well as above the backplate, for each ϕ_ℓ, as before, still depends upon all the f_k's. Equation (2-4) will lead to a more accurate prediction of the microphone response than equation (2-3).

The membrane equation contains two forcing terms, due to the incident sound and the reaction pressure at the membrane respectively.

$$\nabla^2\eta(r,\theta) + K^2\eta(r,\theta) = -\frac{F_o}{T} + \frac{p(r,\theta,0)}{T} , \tag{2-5}$$

where the reaction pressure depends only upon the scalar potential.

$$p(r,\theta,0) = i\omega\rho_o\phi(r,\theta,0) . \tag{2-6}$$

The membrane displacement must satisfy the following boundary conditions:

$$\eta(a,\theta) = 0 \tag{2-7a}$$

$$\eta(0,\theta) \text{ is finite} \tag{2-7b}$$

The solution to be presented here differs from that of Petritskaya in three respects the boundary condition at the backplate employs the more exact expression (2-4), and two key assumptions simplify the analysis to such an extent as to allow a simple solution in closed form.

3 Solution to the coupled fluid-membrane equations. The solutions to equations (2-1b) and (2-1c) are standard solutions to the Helmholz equation in cylindrical coordinates. We need both the scalar and vector potential functions to satisfy the boundary conditions (2-2). We shall restrict the analysis to cases where symmetry in the θ-direction is even--a restriction which will hardly affect the generality of our results. Petritskaya's solution for the scalar potential function at the surface of the membrane (ref. 6) becomes

$$\phi(r,\theta,0) = \sum_{m,n=0}^{\infty} \left[i\omega\eta_{n,m} + \sum_{k=1}^{q} f_k R_{k,n,m} \Gamma_{n,m} \frac{s_k}{\alpha_k} \right] \times \frac{J_n(\xi_{n,m} r) \cos(n\theta)}{T_{n,m} P_{n,m}} \tag{2-8}$$

where

$$\eta_{n,m} = \int_0^{2\pi} \int_0^a \eta(r,\theta)\, J_n(\xi_{n,m} r) \cos(n\theta)\, r\, dr\, d\theta \tag{2-9}$$

and the remaining symbols in (2-8), defined in Petritskaya's paper, will appear later in simplified form.[4] According to equation (2-6) we need only the scalar potential to find the reaction pressure.

If we attempt to solve the membrane equation (2-5) by expanding F_o and $\phi(r,\theta,0)$ in terms of the membrane eigenfunctions, then equations (2-5), (2-8), and (2-9) lead to an infinite set of simultaneous equations in an infinite number of unknowns. A "self-consistent" approach has been suggested to overcome these difficulties (ref. 9) The analysis is based upon the following simplifying assumptions

(a) The membrane displacement η is assumed independent of θ The effect of local variations in reaction pressure due to the openings in the backplate is assumed to be smoothed out by the membrane tension This assumption leads to the removal of the index n in equation (2-8) and permits us to set $n = 0$ wherever it appears as a factor.

---

[4] The factors $\Gamma_{n,m} \frac{s_k}{\alpha_k}$, where

$$\Gamma_{n,m} = \frac{\sin(k_{n,m}h) + \gamma_{n,m} \sin(L_{n,m}h)}{\sin(k_{n,m}h) \cos(L_{n,m}h) + \gamma_{n,m} \cos(k_{n,m}h) \sin(L_{n,m}h)}$$

do not appear in Petritskaya's expression See reference 6, equation (4)

(b) The reaction pressure is assumed relatively insensitive to the details of the shape of the membrane. In equation (2-9) η will be represented by a simple trial expression, which consists of a single unknown η_o and which retains the basic features of the membrane displacement below the first membrane resonant frequency (extremum at the center, zero on the periphery)

First let us examine the consequences of assumption (a). Equation (2-8) can be rewritten

$$\phi(r,\theta,0) = \sum_{m=0}^{\infty} \left[-i\omega\eta_m + \sum_{k=1}^{q} f_k R_{k,m} \Gamma_m \frac{s_k}{\alpha_k} \right] \frac{J_o(\xi_m r)}{T_m P_m} , \qquad (2\text{-}10)$$

wherein

$$\eta_m = 2\pi \int_o^a \eta(r)\, J_o(\xi_m r)\, r\, dr \qquad (2\text{-}11a)$$

$$R_{k,m} = \alpha_k\, J_o(\xi_m a_k) \qquad (2\text{-}11b)$$

$$\Gamma_m = \frac{\sin(k_m h) + \gamma_m \sin(L_m h)}{\sin(k_m h)\cos(L_m h) + \gamma_m \cos(k_m h)\sin(L_m h)} \qquad (2\text{-}11c)$$

$$T_m = \frac{k_m\{2[1 - \cos(k_m h)\cos(L_m h)] + (\gamma_m + \gamma_m^{-1})\sin(k_m h)\sin(L_m h)\}}{\sin(k_m h)\cos(L_m h) + \gamma_m \cos(k_m h)\sin(L_m h)} \qquad (2\text{-}11d)$$

$$P_m = \pi a^2 J_o^{\,2}(\xi_m a) \qquad (2\text{-}11e)$$

$$k_m^{\,2} = k^2 - \xi_m^{\,2} \qquad (2\text{-}11f)$$

$$L_m^{\,2} = L^2 - \xi_m^{\,2} \qquad (2\text{-}11g)$$

$$\gamma_m = k_m L_m / \xi_m^{\,2} . \qquad (2\text{-}11h)$$

When we employ the expressions (2-11) in (2-1a) and the boundary condition (2-2e), and use (2-10) to relate the ϕ_k's to the f_k's, we obtain the following set of equations, written in matrix form:

$$(\underline{I} + \underline{A})\underline{F} = \underline{B} , \tag{2-12}$$

where $\underline{I}$ $(q \times q)$ is the identity matrix and $\underline{F}$ $(q \times 1)$ a column matrix,

$$\underline{I} = \begin{pmatrix} 1 & & & & \\ & 1 & & & \\ & & \cdot & & \\ & & & \cdot & \\ & & & & 1 \end{pmatrix}, \quad \underline{F} = \begin{pmatrix} f_1 \\ f_2 \\ \cdot \\ \cdot \\ f_q \end{pmatrix} \tag{2-13a,b}$$

and A $(q \times q)$ and B $(q \times 1)$ contain the following elements [5]

$$a_{ks} = - \frac{i\omega\rho_o s_s}{s_k} \sum_{\ell=1}^{q} \sum_{m=0}^{\infty} \frac{J_o(\xi_m a_s)\, J_o(\xi_m a_\ell)\, Y_{k\ell}}{P_m T_m} , \tag{2-13c}$$

$$b_k = \frac{\rho_o \omega^2}{s_k} \left[\sum_{\ell=1}^{q} \sum_{m=0}^{\infty} \frac{\eta_m \Gamma_m\, J_o(\xi_m a_\ell)\, Y_{k\ell}}{P_m T_m} \right] . \tag{2-13d}$$

Upon solving (2-12) for the f_k's, we substitute the results into (2-10) to find $\phi(r,\theta,0)$ The solution is incomplete because the unknown displacement $\eta(r)$, contained in the integral η_m (2-11a), is still present in equations (2-10) and (2-13d). In order to resolve this difficulty we turn to assumption (b) and represent $\eta(r)$ by a trial expression in equation (2-11a). Actually three different trial expressions have been investigated

[5] Petritskaya excludes the factors $\frac{s_k s_s}{\alpha_k^2}$ and $\frac{s_k}{\alpha_k}$ in his expressions for a_{ks} and b_k respectively

(1) Constant $\eta(r) = \eta_o$. Here we assume that the reaction pressure depends only upon the average value of the displacement, but not its shape (ref. 10).

(2) Parabolic: $\eta(r) = \eta_o(1 - r^2/a^2)$ This is the simplest polynomial fulfilling the requirements at the center and periphery

(3) Bessel· $\eta(r) = \eta_o[J_o(Kr)/J_o(Ka) - 1]$. Here we assume that the effect of the reaction pressure is to change the amplitude, but not the shape, of the membrane displacement.

Substitution of a trial expression into equation (2-11a) permits a straightforward solution for η in equation (2-5) in terms of the single unknown η_o , which we eliminate by requiring that the average value of η , as obtained from equation (2-5), be equal to that obtained from the trial expression. We express the latter in terms of η_o and a "shape" factor B ·

$$\langle\eta(r)\rangle = B\eta_o \tag{2-14}$$

where

$$B = 1 \quad \text{for case (1) (constant)} \tag{2-15a}$$

$$= 1/2 \quad \text{for case (2) (parabolic)} \tag{2-15b}$$

$$= J_2(Ka)/J_o(Ka) \quad \text{for case (3) (Bessel)} \; . \tag{2-15c}$$

We express the integral (2-11a), as well, in terms of the unknown constant η_o

$$\eta_m = \pi a^2 \eta_o \delta(m) \quad \text{for case (1)} \tag{2-16a}$$

$$= \frac{\pi a^2}{2} \eta_o \delta(m) - 4\pi\eta_o \frac{J_o(\xi_m a)}{\xi_m{}^2} [1 - \delta(m)] \quad \text{for case (2)} \tag{2-16b}$$

$$= 2\pi\eta_o \left[\frac{Ka\, J_o(\xi_m a)\, J_1(Ka)}{(K^2 - \xi_m^2)\, J_o(Ka)} - \frac{a^2}{2}\,\delta(m) \right] \quad \text{for case (3)} , \qquad (2\text{-}16c)$$

where $\delta(m) = 1$ if $m = 0$ or 0 if $m \neq 0$. Because η_m is proportional to η_o, it follows that the constants b_k and f_k are also proportional to η_o, as we see from equations (2-13) and (2-12). We shall find it convenient to define a new integral

$$\theta_m = \eta_m/\eta_o \qquad (2\text{-}17)$$

and new matrices

$$\underline{T} = \underline{F}/\eta_o , \quad \underline{\beta} = \underline{B}/\eta_o , \qquad (2\text{-}18a,b)$$

with elements $T_s = f_s/\eta_o$ and $\beta_s = b_s/\eta_o$ $(s = 1, 2, \ldots, q)$, so that we may rewrite equation (2-12) in terms of $\underline{T}$ and $\underline{\beta}$.

$$(\underline{I} + \underline{A})\underline{T} = \underline{\beta} . \qquad (2\text{-}19)$$

The solution to equation (2-5) is the following

$$\eta(r) = \frac{F_o}{TK^2} \left[\frac{J_o(Kr)}{J_o(Ka)} - 1 \right] - \frac{12\omega\rho_o\eta_o}{T_a} \times \sum_{p=1}^{\infty} \sum_{m=0}^{\infty} \left[-12\omega\theta_m + \sum_{s=1}^{q} T_s s_s \Gamma_m J_o(\xi_m a_s) \right] \times \frac{\lambda_p J_o(\xi_m a)\, J_o(\lambda_p r)}{(\lambda_p^2 - \xi_m^2)(\lambda_p^2 - K^2) T_m P_m J_1(\lambda_p a)} . \qquad (2\text{-}20)$$

Equation (2-20) is found with the aid of the Fourier-Bessel series expansion

$$J_o(\xi_m r) = \frac{2}{a} \sum_{p=1}^{\infty} \frac{\lambda_p\, J_o(\xi_m a)\, J_o(\lambda_p r)}{(\lambda_p^2 - \xi_m^2)\, J_1(\lambda_p a)} ,$$

where

$$J_o(\lambda_p a) = J_1(\xi_m a) = 0$$

From (2-20) we find the average value of the displacement $\eta(r)$.

$$\langle \eta(r) \rangle = \frac{2}{a^2} \int_o^a \eta(r)\, r\, dr$$

$$= \frac{F_o}{TK^2} \frac{J_2(Ka)}{J_o(Ka)} - \frac{i4\omega\rho_o \eta_o}{\pi T} \sum_{m=0}^{\infty} \left[-i\omega\theta_m + \sum_{s=1}^{q} T_s s_s \Gamma_m J_o(\xi_m a_s) \right]$$

$$\times \frac{1}{T_m J_o(\xi_m a)} \left\{ \frac{1}{4K^2 a^2} \frac{J_2(Ka)}{J_o(Ka)} \delta(m) + \frac{J_1(Ka)[1 - \delta(m)]}{2K(K^2 - \xi_m^2)\, J_o(Ka)} \right\} . \quad (2\text{-}21)$$

In equation (2-21) the p-summation is evaluated in closed form:

$$\sum_{p=1}^{\infty} \frac{1}{(\lambda_p^2 - \xi_m^2)(\lambda_p^2 - K^2)} = \frac{a^2}{4K^2} \frac{J_2(Ka)}{J_o(Ka)} \delta(m) + \frac{aJ_1(Ka)[1 - \delta(m)]}{2K(K^2 - \xi_m^2)\, J_o(Ka)} . \quad (2\text{-}22)$$

Proof of equation (2-22) is given in Appendix B. Upon comparing equation (2-21) with (2-14) we eliminate the unknown η_o and write the average membrane displacement in terms of the microphone parameters.

$$\langle \eta(r) \rangle = \frac{F_o}{TK^2} \cdot \frac{J_2(Ka)}{J_2(Ka) + D} , \quad (2\text{-}23)$$

where

$$D = \frac{i4\omega\rho_o}{\pi TB} \sum_{m=0}^{\infty} \left[-i\omega\theta_m + \sum_{s=1}^{q} T_s s_s J_o(\xi_m a_s) \right] \frac{1}{T_m J_o(\xi_m a)} \times \left\{ \frac{J_2(Ka)}{4K^2a^2}\delta(m) + \frac{J_1(Ka)[1 - \delta(m)]}{2Ka(K^2a^2 - \xi_m{}^2a^2)} \right\} . \tag{2-24}$$

In equation (2-24) we obtain θ_m from equations (2-16) and (2-17), and T_s from (2-13), (2-18), and (2-19).

The frequency dependence of the average membrane displacement amplitude, computed from equations (2-23) and (2-24) for the prototype microphone cartridge described below in table 3, is shown for each of the trial expressions in figure 5.[6] We note that η = constant [case (1)] tends to underestimate the damping, and that the parabolic and Bessel expressions [cases (2) and (3)] show excellent agreement with one another right through the first membrane resonance. Hereafter, in the remainder of this report, we shall use the Bessel expression [case (3)] in all theoretical analyses of condenser microphone response.

We could insert the known expression for η_o [from (2-14) and (2-21)] back into (2-20) to find a better approximation to the integral (2-11a), however, continued iterations of this sort have not been pursued.

4. Lumped-parameter model. We can write the expression (2-23) for $\langle\eta(r)\rangle$ in the following familiar form (ref. 10)

$$\langle\eta(r)\rangle = \frac{\pi a^2 F_o}{i\omega z_M} , \tag{2-25}$$

where z_M is the mechanical impedance of the membrane-air layer system

$$z_M = \frac{\pi a^2 TK^2}{i\omega} \left[\frac{J_o(Ka)}{J_2(Ka)} + D \right] \tag{2-26}$$

[6] The summations over m are carried to 10 terms.

Table 3. Parameters of prototype microphone cartridge.

a	membrane radius	4.7625×10^{-3} m
t	membrane thickness	5.588×10^{-6} m
ρ'_M	membrane density	7.9×10^{3} kg/m^3
σ	membrane surface density	4.4145×10^{-2} kg/m^2
ρ_o	air density	1.21 kg/m^3
η_A	air viscosity coefficient	1.86×10^{-5} N sec/m^2
c	air sound velocity (isothermal)	2.8735×10^{2} m/sec
a_{BP}	backplate radius	4.5720×10^{-3} m
b_1	number of holes in backplate	4
a_1	hole location	2.6924×10^{-3} m
r_1	hole radius	3.969×10^{-4} m
ℓ_1	hole depth	6.604×10^{-4} m
a_2	slot center line location	4.667×10^{-3} m
t_2	slot width	9.525×10^{-5} m
ℓ_2	slot depth	6.604×10^{-4} m
V	volume of backchamber	1.4878×10^{-7} m^3
Adjustable	h air gap T membrane tension	

At frequencies well below the first membrane resonance $\omega << 2\ 408\ c_M/a$ the Bessel functions in equations (2-23) and (2-26) can be approximated by the first few leading terms in their power series expansions. The acoustical impedance becomes

$$Z_M = \frac{z_M}{(\pi a^2)^2} = i\omega\frac{4}{3}\frac{\sigma}{\pi a^2} + \frac{8\pi T}{i\omega(\pi a^2)^2} + \frac{8\pi T}{i\omega(\pi a^2)^2}(D_1 + D_2 + D_3 + D_4)\ , \tag{2-27}$$

in which $\sigma = \frac{T}{c_M^2} = \frac{TK^2}{\omega^2}$. The first and second terms represent the membrane mass M and compliance C_M, where

$$M = \frac{4}{3}\frac{\sigma}{\pi a^2}\ ,\quad C_M = \frac{(\pi a^2)^2}{8\pi T}\ , \tag{2-28a,b}$$

and the D's are obtained from equation (2-24)

$$D = D_1 + D_2 + D_3 + D_4 \tag{2-29}$$

$$D_1 = \frac{\rho_o\omega^2 J_2(Ka)}{Tk^2K^2h} \approx \frac{\rho_o c^2 a^2}{8Th} \tag{2-30a}$$

$$D_2 = \frac{i\rho_o\omega J_2(Ka)}{\pi TBk^2K^2a^2h}\sum_{s=1}^{q} T_s s_s \approx \frac{i\rho_o\omega}{8\pi TBk^2h}\sum_{s=1}^{q} T_s s_s \tag{2-30b}$$

$$D_3 = \frac{2\rho_o\omega^2 J_1(Ka)}{\pi TBKa}\sum_{m=1}^{\infty}\frac{\theta_m}{T_m(K^2a^2 - \xi_m^2a^2)\ J_o(\xi_m a)} \tag{2-30c}$$

$$\approx \frac{\rho_o\omega^2}{\pi TB}\sum_{m=1}^{\infty}\frac{\theta_m}{T_m(K^2a^2 - \xi_m^2a^2)\ J_o(\xi_m a)}$$

$$D_4 = \frac{12\rho_o \omega J_1(Ka)}{\pi TBKa} \sum_{m=1}^{\infty} \sum_{s=1}^{q} \frac{T_s s_s \Gamma_m J_o(\xi_m r_s)}{T_m (K^2a^2 - \xi_m{}^2 a^2)\, J_o(\xi_m a)}$$

$$\approx \frac{1\rho_o \omega}{\pi TB} \sum_{m=1}^{\infty} \sum_{s=1}^{q} \frac{T_s s_s \Gamma_m J_o(\xi_m r_s)}{T_m (K^2a^2 - \xi_m{}^2 a^2)\, J_o(\xi_m a)} \quad . \qquad (2\text{-}30d)$$

The D's have the following physical meanings:

D_1 = air compliance term,

D_2 = term accounting for motion of air through the openings in the backplate,

D_3 = correction to D_1 accounting for curvature of the membrane,

D_4 = correction to D_2 accounting for curvature of the membrane,

From equations (2-27) and (2-30) we find the air compliance C_A

$$C_A = \frac{(\pi a^2)^2}{8\pi T \mathrm{Re}\{D\}} \quad . \qquad (2\text{-}31a)$$

A resistive element R , which accounts for the microphone damping, consists of the real terms of equation (2-27).

$$R = \frac{8\pi T}{\omega (\pi a^2)^2} \mathrm{Im}\{D\} \quad . \qquad (2\text{-}31b)$$

The representation (2-27) suggests the lumped-parameter equivalent circuit of figure 6, which is valid below the first membrane resonance. The expression for the air compliance (2-31a) yields substantially greater values than the corresponding expression for a closed cavity C_A' because of the openings in the backplate

$$C_A >> C_A' = \frac{(\pi a^2)^2}{8\pi T \mathrm{Re}\{D_1\}} \approx \frac{\pi a^2 h}{\rho_o c^2} .$$

In the expression (2-31b) for the resistance R, D_1 makes no contribution since it has no imaginary part, furthermore the imaginary parts of D_2 and D_4 are proportional to ω, so that the major contribution to the frequency dependence of R orginates in the D_3 term, which is small at low frequencies. The quality factor of the microphone is given by the elementary formula

$$Q = \frac{1}{R}\sqrt{\frac{M(C_M + C_A)}{C_M C_A}} \quad . \tag{2-32}$$

Figure 7 shows the theoretical frequency dependence of C_A, R, and Q, all computed for case (3) Beyond 2 kHz the lumped-parameter approximation breaks down, but the Q given by equation (2-32) is still indicative of the height of the microphone resonant peak. We take the values at 1 kHz as representative of the microphone. For the prototype described in table 3 and figure 5, equations (2-28), (2-31), and (2-32) yield the following values for the lumped parameters.

membrane mass	$M = 826$ kg/m^4
membrane compliance	$C_M = 6.82 \times 10^{-14}$ m^5/N
air compliance	$C_A = 1.60 \times 10^{-12}$ m^5/N
air resistance	$R = 1.32 \times 10^7$ N sec/m^5
quality factor	$Q = 8.52$

C. Comparison with Experiment

The preceding theory has been used as the basis for design of the prototype high-temperature microphone. Figure 8 shows a block diagram of the instrumentation used to measure the frequency response of the microphone by the electrostatic actuator technique The microphone membrane was excited into vibration at a selected frequency by an ac signal originating at the oscillator, amplified by the power amplifier, superimposed upon an 800 V polarization voltage in the microphone

calibration apparatus, and applied to the electrostatic actuator. Motion of the membrane was detected by the converter-zero drive system, which produces an output voltage proportional to the instantaneous membrane displacement This system is described in detail in references 3 and 4 Because the short connection between the microphone and converter is unavoidably unshielded in this experiment, the spurious electrical pickup, which proved to be considerable, required filtering. The highpass and lowpass sections of the filter were adjusted at each frequency to provide a third-octave bandwidth After some amplification by the oscilloscope plug-in unit, the magnitude of the response was measured on a true rms voltmeter; with the output of the power amplifier serving as a reference, the phase was measured at the output of the filter. For the purpose of determining the attenuation and phase shift of the filter alone, measurements were taken with a reference signal switched directly from the oscillator to the input of the filter after each change in frequency. The automatic counter was used to measure the oscillator frequency. Identification of all the instruments in the system is included in the caption of figure 8

The response of several prototype microphones, fabricated in the Instrument Development Section, Langley Research Center, has been measured for comparison with theoretical predictions. The values of the parameters entering equations (2-23) and (2-24) are listed in table 3. Two of the parameters readily permitted adjustment the gap distance by means of a threaded shaft supporting the back-plate; and the membrane tension by means of a threaded ring, which applies pressure to a tension ring (see figure 12 to follow). The gap distance h was determined by measurement of the static capacitance C between the membrane and backplate:

$$h = \frac{a_{BP}^2}{36 \times 10^9 \, C} \quad , \tag{2-33}$$

where a_{BP} is the radius of the backplate. The membrane tension T was determined by measurement of the first vacuum resonant frequency f_{R1} (for which the experimental arrangement of figure 8 was also used)

$$T = 6.825 \, a^2 f_{R1}^2 \rho_o t \quad . \tag{2-34}$$

Figure 9 shows the theoretical and experimental microphone frequency response for two different gap distances. Because of the difficulty in obtaining an absolute calibration of the membrane displacement, the experimental data for each microphone were multiplied by a constant calibration factor to fit the theory at a frequency of 10 Hz The figure shows that the theory accurately predicts the height of the membrane resonance peak for both gap and distances as well as the shift in peak location with respect to that of the vacuum resonance (no damping). The increase in damping with decreasing gap distance is expected in view of the role of viscosity in the flow between the membrane and backplate

Figure 10 shows the response for two different membrane tensions at constant gap distance Again both the height of the resonance peak and the shift in peak location show good agreement between theory and experiment. The change in membrane tension has two effects, both apparent in the figure: first the resonant frequency increases as the square root of the tension, secondly the sensitivity below resonance decreases with tension. The peak height does not change with tension because the latter has but negligible effect upon the damping.

Figure 11 shows the frequency dependence of the phase angle between applied driving force and membrane displacement Theory accurately predicts the frequency at which the phase goes through the resonance step. The high experimental values on the high-frequency side of resonance are believed to contain a contribution from the zero drive amplifier, which produces some phase shift at frequencies approaching 20 kHz

The theoretical and experimental results presented here lead to two conclusions

(a) The close agreement between the theoretical curves of those trial functions which satisfy the boundary requirements [cases (2) and (3)] supports assumption (b), i e., that the reaction pressure is relatively insensitive to the details of the shape of the membrane

(b) Accurate prediction of the relative microphone response, and changes therein with changes in parameters, substantiates the self-consistent approach and the assumptions upon which it is based

D Practical Construction of a High-Temperature Condenser Microphone

A cross section of the prototype microphone cartridge is shown in figure 12. All parts are made of 300-series stainless steel, except the backplate B and insulator F, which are made of type 17-4 PH stainless steel and macor[7] machinable glass ceramic respectively. The membrane A is stretched over the top face of the case E and clamped in place by means of the membrane retaining ring D, which overlaps the case to facilitate membrane replacement. The macor insulator F supports the backplate B, which serves as the fixed electrode; a 4-40 thread provides for adjustment of the gap between the backplate and membrane. Four holes in the backplate, in addition to the peripheral slot, permit the flow of air between the gap and the backchamber concomitant with the membrane motion. The threaded ring G is used to adjust the vertical position of the insulator and tension ring C, and thus provides the means of adjusting the tension in the membrane. The insulator contains a keyed slot to prevent rotation and a 0.000508 m (20 mil) vent hole for pressure equalization (neither shown on the figure). The locking tube H holds the backplate firmly in place, once the gap and tension adjustments are completed, and terminates with a slotted-shell contact to engage the pin of the mating cable connector (part C, figure 19). The flange at the bottom of the case contains four screw holes for attachment to the test panel as well as to various adapters used in laboratory tests

The choice of macor as the material for the insulator F, as well as for the insulating pieces in the cable connectors, is based upon two outstanding properties· (1) machinability, which permits fabrication of small pieces with conventional tools and equipment, and (2) excellent stability of its mechanical and electrical properties at elevated temperatures.

In the prototype cartridge shown in figure 12 the force exerted by the threaded ring G upon the tension ring C is transmitted through the insulator F In order to relieve the insulator of this force, an alternative design was studied which features two tightening rings. a membrane tightening ring directly below the tension ring C, and a second tightening ring below the

[7] TM Corning Glass Works.

insulator F solely to hold the latter in place. However, inferior microphone response at elevated temperatures led to abandonment of this design.

E. Design Considerations

The choice of microphone design parameters is based upon three fundamental considerations sensitivity, bandwidth, and maximum allowable membrane tension. The sensitivity S is defined as the capacitance change δC per unit incident sound pressure F_o. At frequencies well below the first membrane resonance, where membrane stiffness predominates over the inertial and damping forces, we neglect D in equation (2-23), approximate the Bessel functions by their leading terms, and arrive at the following approximate expression for average membrane displacement

$$\langle \eta(r) \rangle \approx \frac{F_o a^2}{8T} . \tag{2-35}$$

The capacitance change is related to the average displacement according to the familiar relation

$$\delta C = -\langle \eta(r) \rangle \frac{C}{h} \approx - \frac{\varepsilon_o A_{BP} a^2 F_o}{8Th^2} , \tag{2-36}$$

where A_{BP} is the area of the backplate. From equations (2-35) and (2-36) we find the microphone sensitivity.

$$S = \left| \frac{\delta C}{F_o} \right| = \frac{\varepsilon_o A_{BP} a^2}{8Th^2} \tag{2-37}$$

The bandwidth will depend upon the first membrane resonant frequency,

$$f_{R1} = \left(\frac{T}{6.285\ \rho_M t a^2} \right)^{1/2} \tag{2-38}$$

and the maximum allowable membrane tension upon the tensile strength σ_T of the membrane material,

$$T < T_{max} = \sigma_T t \quad . \tag{2-39}$$

We have four basic design parameters--membrane radius a, tension T, thickness t, and gap h --to satisfy the requirements of equations (2-37), (2-38), and (2-39). A summary of these requirements appears qualitatively in table 4.

Table 4. Requirements of microphone design parameters

Parameter	Requirement for	
	High Sensitivity	Large Bandwidth
Membrane radius a	large	small
Membrane tension T	small	large
Membrane thickness t	---	small
Gap h	small	---

It is clear from equation (2-37) that, independently of the values we assign the other parameters, we can adjust the gap h to yield any desired sensitivity (limited only by the supporting electronics) The bandwidth, on the other hand, is limited by the tensile strength of the membrane material, as indicated by equations (2-38) and (2-39).

In view of the requirements regarding dynamic range and frequency response, the prototype microphone cartridge, as specified in table 3, is dimensioned roughly after the commercial 12.7 mm (1/2 in.) microphone. Its case, however, is larger and sturdier for better adaption to the hostile operational environment The choice of membrane material is based upon three criteria

(1) high strength at elevated temperatures,

(2) good corrosion resistance at elevated temperatures,

(3) sufficient ductility to form a smooth membrane.

Three different foils, listed in table 5, were examined as possible membrane materials.

Table 5 Properties of membrane foils.

Material	Thickness	Tensile strength* (ref 11)
304 S/S	5.588×10^{-6} m (0.00022 inch)	5.861×10^{8} N/m^2 (85000 psi)
302 S/S	7.112×10^{-6} m (0.00028 inch)	6.205×10^{8} N/m^2 (90000 psi)
K-Monel	7.874×10^{-6} m (0 00031 inch)	6.205×10^{8} N/m^2 (90000 psi)

* Annealed condition

Because the K-Monel membranes consistently showed a tendency to produce cracks under tension, they were abandoned, subsequent testing was restricted to the other two foils.

With the thicknesses listed above and the values of ρ_o and a given in table 3, we use equations (2-38) and (2-39) to find the membrane tension and stress necessary to produce a membrane resonant frequency of 20 kHz For the type 304 and 302 stainless steel foils T = 2733.5 and 3479.0 N/m respectively. The corresponding stress in the membrane in both cases amounts to $4\ 89 \times 10^{8}$ N/m^2 (71000 psi), which is safely below the tensile strengths given above However, a certain margin of safety is needed for operation at elevated temperatures, owing to the decrease in tensile strength with increasing temperature

The backplate is designed to produce a slightly underdamped membrane motion, a situation corresponding to curve 2 of figure 9 We notice that the -3 dB point on the high-frequency flank of the resonant peak roughly coincides with the membrane vacuum resonance, so that equation (2-38) is a good criterion for the bandwidth The choice of type 17-4 PH stainless steel for the backplate material is based upon a favorable thermal expansion coefficient, as will be explained in Part VC The effect of temperature upon other microphone parameters and subsequent microphone operation will be discussed there as well.

F. List of Symbols Used in Part II

Numbers in parentheses refer to defining equations.

$\vec{A}$	vector velocity potential (2-1a)
$\underline{A}$	see (2-12) and (2-13c)
A_{BP}	area of backplate [m^2]
a	radius of membrane [m]
a_k	location of kth hole [m] (fig. 3)
a_{ks}	element of matrix $\underline{A}$
a_{BP}	radius of backplate [m]
B	shape factor (2-15)
$\underline{B}$	see (2-12) and (2-13d)
b_k	element of matrix $\underline{B}$
b_1	number of holes in backplate of prototype microphone (table 3)
C	static capacitance between membrane and backplate [pF]
C_A	air compliance [m^5/N] (2-31a)
C_A'	air compliance for the case of no openings in backplate [m^5/N]
C_M	membrane compliance [m^5/N] (2-28b)
c	isothermal sound velocity in air = $(P_o/\rho_o)^{1/2}$ [m/sec]
c_M	sound velocity in membrane = $(T/\sigma_M)^{1/2}$ [m/sec]
$D = D_1 + D_2 + D_3 + D_4$	contributions to mechanical impedance from air layer (2-23) and (2-24)
D_1 , D_2 , D_3 , D_4	see (2-30)
$\underline{F}$	see (2-12) and (2-13b)
F_o	incident acoustic sound pressure [N/m^2]

f_k	vertical velocity at kth opening in backplate [m/sec]
$f(r,\theta)$	vertical velocity at backplate (2-2e)
f_{R1}	first membrane resonant frequency in vacuum [Hz] (2-38)
h	gap distance between membrane and backplate [m]
$\underline{I}$	identity matrix (2-13a)
$J_n(x)$	Bessel function of the first kind of order n and argument x
K	wave number of sound in membrane $= 2\pi\omega/c_M$ $[m^{-1}]$
k	wave number of sound in air $= 2\pi\omega/c$ $[m^{-1}]$ index to enumerate openings in backplate
k_m	see (2-11f)
L	wave number for vector potential $= (-i\omega/\nu)^{1/2}$ $[m^{-1}]$
L_m	see (2-11g)
ℓ	index used with admittance matrix $Y_{k\ell}$
ℓ_k	depth of kth opening in backplate [m] (A-4, A-5)
M	membrane mass $[kg/m^4]$ (2-28a)
m	index used with air layer eigenfunctions
n	index used with air layer eigenfunctions
$\underline{P}$	acoustical pressure matrix (A-1)
P_k	acoustical pressure at kth hole $[N/m^2]$ (A-2a)
P_m	see (2-11e)
p	index used with membrane eigenfunctions
$p(r,\theta,z)$	reaction pressure $[N/m^2]$ (2-5)
Q	quality factor of microphone (2-32)
q	number of openings in backplate (including slot)
R	equivalent microphone resistance $[Nsec/m^5]$ (2-31b)

$R_{k,m}$	see (2-11b)
r	radial coordinate (fig. 3)
r_k	radius of the kth hole in backplate [m] (A-4)
s	index to enumerate openings in backplate
s_k	area of kth opening in backplate [m^2]
T	tension of membrane [N/m]
T_m	see (2-11d)
t	thickness of membrane [m]
t_k	width of kth opening if a slot [m] (A-5)
$\underline{U}$	volume velocity matrix [m^3/sec] (A-1)
U_k	volume velocity at kth opening in backplate [m^3/sec] (A-2b)
V	volume of backchamber [m^3]
$\vec{v}$	acoustical particle velocity [m/sec] (2-1a)
v_r	radial component of $\vec{v}$ [m/sec]
v_z	axial component of $\vec{v}$ [m/sec]
w_k	length of kth opening if a slot [m] (A-5)
$\underline{Y}$	acoustical admittance matrix = $\underline{Z}^{-1}$ [m^5/Nsec] (A-8)
$Y_{k\ell}$	element of matrix $\underline{Y}$ [m^5/Nsec]
$\underline{Z}$	acoustical impendance matrix [Nsec/m^5] (A-2c)
Z_c	acoustical impedance of backchamber [Nsec/m^5] (A-3)
Z_M	acoustical impedance of microphone [Nsec/m^5] (2-27)
Z_k	acoustical impedance of kth opening in backplate [Nsec/m^5] (A-4) or (A-5)
z	axial coordinate
z_k	mechanical impedance of kth opening in backplate [Nsec/m] (2-3)

z_M	mechanical impedance of membrane-air layer system [Nsec/m] (2-26)
α_k	angle subtended by kth opening in backplate (fig. 3)
$\underline{\beta}$	$= \underline{B}/\eta_o$ (2-18b)
β_s	$= b_s/\eta_o$
Γ_m	see (2-11c)
γ_m	see (2-11h)
$\delta(m)$	Dirac delta function
ε_o	dielectric permittivity in air [Farad/m] (2-36)
η , $\eta(r)$, $\eta(r,\theta)$	displacement of membrane [m]
η_A	viscosity coefficient of air [Nsec/m^2]
η_m	see (2-11a)
η_o	unknown in trial expression for membrane displacement [m]
θ	angular coordinate
θ_m	$= \eta_m/\eta_o$
λ_p	used to designate roots of Bessel function $J_o(\lambda_p a) = 0$ (2-20)
ν	kinematic viscosity of air $= \eta_A/\rho_o$ [m^2/sec]
ξ_m	used to designate roots of Bessel function $J_1(\xi_m a) = 0$ (2-20)
ρ_o	static density of air [kg/m^3]
ρ_M	density of membrane material [kg/m^3]
σ	surface density of membrane $= \rho_M t$ [kg/m^2]
σ_T	tensile strength of membrane material [N/m^2] (2-39)
$\underline{T}$	$= \underline{F}/\eta_o$
T_s	$= f_s/\eta_o$

ϕ , $\phi(r,\theta,z)$	acoustical scalar potential (2-1a)
ϕ_k	acoustical scalar potential at kth opening in backplate (2-3) and (2-4)
ω	angular frequency of incident sound [sec^{-1}]

III. THE CABLE PROBLEM

A. Role of the Cable

Figure 13 shows a block diagram of the microphone carrier system. Pressure fluctuations produce capacitance changes in the condenser microphone, which amplitude-modulate a carrier voltage provided by the carrier electronics The detected output signal is measured or recorded on an output device. A cable of length $\ell \approx 6$ m (20 ft) separates the carrier electronics from the microphone.

The carrier electronics consists of a converter and a zero drive amplifier described in detail in references 3 and 4. The function of the converter, for which a circuit diagram appears in figure 14, is to produce an output current at terminal A proportional to the instantaneous sound pressure at the microphone C. In brief, the central component is the 3N202 dual-gate FET, which serves as a mixer. An RF oscillator, connected to terminal L, drives gate G_2 and produces a drain current at the carrier frequency. A tank circuit consisting of the condenser microphone C, the cable, the 1N5463 varactor diodes, and the 9μH inductor is connected to gate G_1 and tuned to the carrier frequency by either of two methods. (1) by applying a control voltage at terminal E to control the capacitance of the varactor diodes, or (2) by controlling the frequency of the RF oscillator As result of drain-to-gate capacitive coupling, a small fraction of the drain current leaks into the tank circuit and produces a voltage at gate G_1 . Because the transconductance with respect to gate G_1--that is, the ratio of drain current to voltage at gate G_1--is highly sensitive to the voltage applied to gate G_2, the signal at gate G_1 mixes with that at gate G_2 to generate a direct drain current component (over and above the quiescent current) A change in capacitance C changes the level of this direct current component, consequently a periodic change in C, as caused by the presence of sound in the microphone, produces a periodic drain current at the frequency of the sound. The circuit

components to the right of the FET serve the functions of amplification, detection, and reduction of output impedance.

The zero drive amplifier, connected to terminals A-B, has three functions

(1) to provide a constant 22 V at the converter terminals A-B Normally an intermediate device, a "line driver," is connected between the signal source and the zero drive amplifier Elimination of the line driver permits use of the 22 V on the line as the supply voltage of the converter.

(2) to amplify the converter signal for recording on an output device. While maintaining a stiff voltage between terminals A-B, the zero drive amplifier senses changes in the converter line current (entering point A) and provides a proportional output voltage

(3) to provide a reference voltage for automatic tuning control The zero drive amplifier contains an internal voltage which is indicative of the status of converter tuning. This voltage is used to fulfill an automatic tuning control function, as will be described in part IV

In the original converter circuit, for comparison, a local oscillator with a fixed frequency of 10 MHz provides the carrier voltage at gate G_2 The microphone is connected to gate G_1 without an intervening cable, and optimal tuning is achieved by means of the control voltage applied to terminal E.

The circuit of figure 14 was used in the present cable studies as well as several laboratory tests of the microphone carrier system. The tuning frequencies are determined essentially by the cable resonances and are only slightly affected by the original tank circuit. The frequency of the external oscillator connected to terminal L is adjusted for initial tuning, and the voltage at terminal E is used for subsequent automatic tuning control.

In the final version of the converter circuit, a voltage-controlled oscillator (VCO) provides the carrier frequency at terminal L. Now the control voltage is used to control the oscillator frequency The inductor and varactor diodes are removed altogether, and optimal tuning occurs very close to the cable resonances Details are given in part IV.

A half-wavelength[8] lossless cable would reflect the condenser microphone directly to the input terminals of the converter The losses in a real cable, however, lead to a substantial reduction in system sensitivity In this phase of the research we investigate the operation of the cable as a half-wavelength transmission line and seek criteria for holding its detrimental effects to a minimum.

B. Theoretical Analysis

The analysis presented in this section[9] yields an expression for the output voltage of the system with the cable relative to that without the cable. This expression enables us to predict the signal attenuation due to the presence of the cable and to compare performance with different cables.

A circuit diagram of the "front end" of the converter (elements connected to gate G_1) is shown in figure 15a. Elements L, C_o, and R represent the tank circuit, C as before the condenser microphone, and Z_S and Z_R the impedance at the sending and receiving ends of the cable, respectively. The admittance Y_T between gate G_1 and common is the following:

$$Y_T = \frac{1}{j\omega L} + j\omega C_o + \frac{1}{R} + \frac{1}{Z_S} \quad , \tag{3-1}$$

where ω is the carrier angular frequency. If the losses of the cable are small, the admittance Y_S looking into the sending end of the cable can be approximated as follows (ref. 12)

$$Y_S = \frac{1}{Z_S} = \frac{1}{R_o} \left[\frac{\alpha\ell(1 - \omega CR_o \tan \omega\tau) + j(\omega CR_o + \tan \omega\tau)}{(1 - \omega CR_o \tan \omega\tau) + j\alpha\ell(\omega CR_o + \tan \omega\tau)} \right] , \tag{3-2}$$

where

[8] Or integral multiple thereof

[9] Some symbols have a different meaning from that in Part II A list of symbols for Part III appears in Part IIIE

α = attenuation constant of the cable [neper/m]

$\tau = \ell/c$ = transit time from one end of the cable to the other [sec]

c = velocity of propagation [m/sec]

R_o = characteristic impedance of the cable [Ω]

Near the resonant frequencies of the cable it will always be true that

$$|\omega C R_o \tan \omega\tau| << 1 \ . \tag{3-3}$$

Using the inequality (3-3) and substituting equation (3-2) into (3-1), we obtain an approximate expression for Y_T near the resonant frequencies of the cable:

$$Y_T \approx j \left[-\frac{1}{\omega L} + \omega(C_o + C) + \frac{\tan \omega\tau}{R_o} \right] + \frac{1}{R} + \frac{\alpha\ell}{R_o} \left[1 + (\omega C R_o + \tan \omega\tau)^2 \right] \tag{3-4}$$

Resonance occurs when the imaginary part of equation (3-4) vanishes

$$-\frac{1}{\omega L} + \omega(C_o + C) + \frac{\tan \omega\tau}{R_o} = 0 \tag{3-5}$$

By applying Newton's Rule we obtain an approximate solution for the resonant angular frequencies ω_R.

$$\omega_R \approx \frac{n\pi}{\tau} + \frac{R_o}{n\pi L} \frac{(1 - n^2\pi^2/\omega_o^2\tau^2)}{[1 + (R_o/\omega_o^2 L\tau)(1 + \omega_o^2 \tau^2/n^2\pi^2)]} \ , \tag{3-6}$$

$$(n = 1, 2, 3, \ldots) \ ,$$

where $\omega_o = [L(C_o + C)]^{-1/2}$ = resonant angular frequency of the isolated tank circuit with the microphone Hence the coupling between the cable and the tank circuit renders the sequence of frequencies anharmonic. If both the tank circuit

and the cable, in its fundamental mode, are tuned to the carrier frequency, it follows that:

$$\omega_o \tau = \pi \quad . \tag{3-7}$$

In practice, equation (3-7) is only approximately fulfilled owing to imprecision in cutting the cable and to the effect of the cable connectors. In the present application it is true that

$$R_o/\pi L << \pi/\tau \quad . \tag{3-8}$$

In view of expressions (3-7) and (3-8), the anharmonicity becomes greater with increasing n but remains small for the first several values of n

It will be found convenient to represent the cable by an equivalent parallel tank circuit, as shown in figure 15b, which will be valid near the cable resonances The last term in equation (3-4) represents the equivalent parallel resistance R_ℓ

$$\frac{1}{R_\ell} = \frac{\alpha \ell}{R_o} \left[1 + (\omega C R_o + \tan \omega\tau)^2\right] \quad . \tag{3-9}$$

The equivalent capacitance C_ℓ and inductance L_ℓ , when isolated, must yield the resonances of the isolated cable.

$$L_\ell C_\ell = \tau^2/n^2\pi^2 \quad . \tag{3-10}$$

Furthermore, the circuit of figure 15b must yield the resonant frequencies given by equation (3-6).

$$\left(\frac{LL_\ell}{L + L_\ell}\right) (C + C_o + C_\ell) = \frac{1}{\omega_R^2} \quad . \tag{3-11}$$

Equations (3-10) and (3-11) yield the following expressions for C_ℓ and L_ℓ

$$C_\ell = \frac{\tau}{2R_o}\left[1 - \frac{R_o}{\omega_o^2 L\tau}\left(1 - \frac{\omega_o^2\tau^2}{n^2\pi^2}\right)\right] \quad , \tag{3-12a}$$

$$L_\ell = \frac{2R_o\tau}{n^2\pi^2\left[1 - \frac{R_o}{\omega_o^2 L\tau}\left(1 - \frac{\omega_o^2\tau^2}{n^2\pi^2}\right)\right]} \quad . \tag{3-12b}$$

The admittance of the circuit shown in figure 15b may be written

$$Y_T = j\left[-\frac{1}{\omega}\left(\frac{1}{L} + \frac{1}{L_\ell}\right) + \omega(C + C_o + C_\ell)\right] + \frac{1}{R} + \frac{1}{R_\ell} \quad . \tag{3-13}$$

According to equations (12) and (18) of reference 3 the conversion gain s of the carrier electronics (output voltage per unit pressure amplitude) can be written in the form

$$s = K[Q/(C + C_o + C_\ell)]^2 \tag{3-14}$$

where K depends upon parameters of the electronic circuit and Q is the quality factor of the circuit of figure 15b

$$Q = \omega_R(C + C_o + C_\ell)\left(\frac{RR_\ell}{R + R_\ell}\right) \tag{3-15}$$

Substituting for Q in equation (3-14) we find

$$s = K\left(\frac{\omega_R RR_\ell}{R + R_\ell}\right)^2 \tag{3-16}$$

The conversion gain without the cable is

$$s_o = K\omega_o^2 R_1^2 \quad , \tag{3-17}$$

where R_1 = equivalent parallel resistance of the isolated tank circuit at its resonance. Then the output voltage with the cable, relative to that without the cable, is given by the following expression:

$$\begin{aligned} \text{Output voltage [dB]} &= 20 \log (s/s_o) \\ &= 40 \log [\omega_R R R_\ell / \omega_o R_1 (R + R_\ell)] \quad . \end{aligned} \tag{3-18}$$

Near the resonant frequencies we may neglect $\tan \omega\tau$ in equation (3-9) and then substitute the resulting approximate expression for R_1 into equation (3-18):

$$\begin{aligned} \text{Output voltage [dB]} = 40 \log \{&\omega_R R_o R / \omega_o R_1 (R_o + R\alpha\ell \\ &\times (1 + \omega_R^2 C^2 R_o^2)]\} \quad . \end{aligned} \tag{3-19}$$

Under the conditions of the present experiments $R_o << R\alpha\ell$. Thus

$$\text{Output voltage [dB]} \approx 40 \log [\omega_R R_o / \omega_o R_1 \alpha\ell (1 + \omega_R^2 C^2 R_o^2)] \quad . \tag{3-20}$$

Equation (3-20) shows that a high output voltage is favored by a high value of the ratio $R_o/\alpha\ell$, i.e., high characteristic impedance and, of course, low cable losses. This ratio at some fixed frequency may be regarded as a figure of merit for the cable.

C. Comparison with Experiment

Examination of equation (3-19) reveals that we must know the equivalent parallel resistance R of the original tank circuit as well as the cable attenuation α in order to compare experimental results with theory. Both quantities are, in general, frequency dependent.

The equivalent parallel resistance R was determined by the method suggested by equation (16) of reference 3 (utilizing the difference in frequencies

at the positive and negative peaks of the converter transfer function). Varying the capacitance of the varactor diodes and adding external capacitance permitted determination of R over the frequency range 8 to 14 MHz The data fit the expression

$$R = 43754\ f^{-0.73}\ [\Omega]\ (f \text{ in MHz}),$$

which was used over the entire frequency range investigated (7 to 50 MHz)

The frequency dependence of the attenuation coefficient α was determined from measurements on a Hewlett-Packard Model 4815A Vector Impedance Meter The α values were found slightly higher than those listed in reference 13, probably as a result of connector losses, but agreement was generally good The attenuation values for all the cables tested, shown in figure 16, fit expressions of the form

$$\alpha = Df^{A}\ (f \text{ in MHz})$$

Values of D and A , as well as the characteristic impedance R_o , length ℓ , and figure of merit at 10 MHz $R_o/\alpha_{10}\ell$ are listed in table 6 on the following page Other parameters entering equation (3-19) have the following values.

$$\omega_o = 70.0890 \times 10^6 \text{ radian/sec}$$

$$C = 17\ 7 \text{ pf}$$

A block diagram of the instrumentation used to test the system sensitivity with various cables is shown in figure 17 The microphone was excited by means of an acoustic calibrator, driven externally by the test oscillator-power amplifier combination The test cable connected the microphone to gate G_1 of the FET in the converter. The converter-zero drive system was the same as that described in references 3 and 4 except for the chassis, a conventional minibox in place of the stainless steel tube, which contains jacks for connecting the cable and an external carrier voltage to drive gate G_2 of the FET The rf signal generator provided the carrier voltage, and a digital true rms voltmeter measured the output voltage Both the acoustical and carrier frequencies were monitored on electronic counters.

Table 6. Coaxial cable parameters.

Cable	Characteristic Impedance	Attenuation Parameters		Length	Figure of Merit
	R_o	D	A	ℓ	$R_o/\alpha_{10}\ell$*
	Ω	neper/m		m	
G03233H**	76	1.66×10^{-3}	0.53	10 75	1257
RG 62 A/U	95	1.13×10^{-3}	0.53	15.11	1642
RG 58 C/U	51	1.66×10^{-3}	0.53	11.10	817
RG 11 A/U	76	9.44×10^{-4}	0.53	11.19	2123
RG 59 B/U	76	1.36×10^{-3}	0.53	11.14	1480

* α_{10} = attenuation constant at 10 MHz.

** Video cable.

The level of acoustical excitation was adjusted for 132 dB at 1 kHz for all measurements. The rf signal generator was tuned to a resonant frequency of the coupled tank circuit-cable system, and the output voltage of the zero drive amplifier recorded, this procedure was repeated to obtain data for the first six resonant frequencies. A measurement was also made with the microphone connected directly to the converter in order to establish the output reference voltage $V_{REF} = 7.53$ V. Then, if V_{OUT} is the system output voltage with the cable, we have

$$\text{Output voltage [dB]} = 20 \log (V_{OUT}/V_{REF}) . \qquad (3\text{-}21)$$

Figure 18 shows the theoretical [equation (3-19)] and experimental [equation (3-21)] output voltages versus carrier frequency for the five coaxial cables investigated. The theoretical curves are plotted with no adjustable parameters. The roll-off of the experimental points beyond 31.6 MHz is attributed to the deterioration of the quality factor of the inductor at high frequencies and is, in fact, displaced to higher frequencies when the inductor is removed. In view of the wide range of test frequencies and cable properties involved, agreement between theory and experiment is considered excellent.

Tests on two-wire, 300 ohm antenna cables, both shielded and unshielded, showed that these are unsuited for the present application because of high sensitivity to vibration, high electrical pickup, and erratic behavior of the cable parameters with varying carrier frequency.

The results presented in figure 18 enable us to draw the following conclusions:

(1) Because the response of the system has a direct correspondence with the cable figure of merit, $R_o/\alpha\ell$, the latter should be as high as possible for the cable used in the system (see table 6). For this reason RG11 A/U is chosen as the system cable type.

(2) System sensitivity increases with carrier frequency. It is desirable to use a higher carrier frequency than the 10 MHz in the original converter. In fact, upon removal of the inductor, which is not needed in normal system

operation, the optimal carrier frequency is found to lie in the vicinity of 48 MHz, for which the electronic system is ultimately designed.

(3) The use of a high-quality cable, together with a high carrier frequency, confines the loss of system sensitivity to about 20 dB. This would appear to raise the noise floor of the system from 55 to 75 dB (see table 2), however, two additional contributions further elevate the noise floor. (1) noise generated in the cable itself, and (2) reduced microphone sensitivity, as is required to accommodate high sound pressure levels. Thus a cable with the highest possible figure of merit is needed to meet the system dynamic range specifications.

D. Practical Construction of a High-Temperature Cable Connector

The function of the high-temperature cable connector, shown in figure 19, is to transmit the modulated carrier signal between the high-temperature environment of the microphone and the cooler environment of the RG 11 A/U cable A 7.5 cm (~ 3 inch) connector length is deemed sufficient to protect the cable.

The microphone connector consists of case A, spacer B, and contact pin C The contact pin, silver-soldered to the center conductor G, engages the slotted shell of the microphone locking tube (part H in figure 12) A small piece of brass foil wrapped around the contact pin promotes good electrical contact to the shell. An external stainless steel ring between case A and the microphone case insures proper contact pressure. Two macor spacers E prevent motion of the center conductor with respect to the copper tube D, the outer conductor. The cable connector consists of the cap H and a TNC straight coaxial jack (General Fittings Part No. 4025-005), which is screwed onto the external threads of the cap. The original jack insulators are replaced with identical macor insulators. The internal threads of the cap are used to adjust the tension in the center conductor, whereafter the cap is spot-soldered to the tube.

A 1.22 m (4 ft) rigid cable, similar in design, was constructed for the purpose of high temperature testing in the laboratory This cable was used as an intermediate connection between the microphone and RG 11 A/U cable when the former was tested in an oven. As before, all insulating parts subjected to elevated temperatures were made of macor.

E. List of Symbols Used in Part III

Numbers in parentheses refer to defining equations

A	exponent in expression for frequency dependence of cable attenuation
c	velocity of propogation in cable [m/sec]
C	condenser microphone capacitance [pF]
C_ℓ	equivalent capacitance of cable near resonance (3-10) [pF]
C_o	tank circuit capacitance without condenser microphone [pF]
D	coefficient in expression for frequency dependence of cable attenuation
f	frequency [MHz]
K	coefficient in expression for conversion gain (3-16)
ℓ	cable length [m]
L	tank circuit inductance [μH]
L_ℓ	equivalent cable inductance near resonance (3-16) [μH]
n	cable harmonic number (= 1, 2, 3, . .)
Q	quality factor of front end of converter
R_ℓ	equivalent cable resistance (3-9) [Ω]
R_o	characteristic impedance of cable [Ω]
R	equivalent parallel resistance of isolated tank circuit [Ω]
R_1	value of R at resonant frequency of isolated tank circuit (3-17) [Ω]
s	conversion gain of electronic system with cable (3-14) [Vm^2/N]

S_o	conversion gain of electronic system without cable (3-16) [Vm^2/N]
V_{OUT}	converter output voltage with cable (3-21) [V]
V_{REF}	converter output voltage without cable (3-21) [V]
Y_S	admittance looking into sending end of cable (3-2) [mho]
Y_T	admittance looking into front end of converter (3-1) [mho]
Z_R	impedance at receiving end of cable [Ω]
Z_S	$= Y_S^{-1}$ impedance looking into sending end of cable (3-1) [Ω]
α	cable attenuation constant [neper/m]
α_{10}	cable attenuation constant at 10 MHz [neper/m]
τ	$= \ell/c$ one-way transit time along cable [sec]
ω	angular frequency [rad/sec]
ω_o	resonant angular frequency of isolated tank circuit [rad/sec]
ω_R	resonant angular frequency of front end of converter (3-6) [rad/sec]

IV. THE ELECTRONICS PROBLEM

When the inductor and varactor diodes are removed from the front end of the converter, the nth resonant frequency of the cable terminated by the microphone is obtained by letting $C_o = 0$, $L \to \infty$ in equation (3-6)

$$f_n \approx \frac{n}{2\tau}\left(1 - \frac{R_o C}{\tau}\right) , \qquad (R_o C << \tau) ,$$

where τ is the one-way transit time along the cable, R_o the characteristic impedance of the cable, and C the static capacitance of the microphone. Changes

in microphone capacitance C resulting from changes in temperature will thus lead to a shift in the resonant frequency, detuning of the converter, and reduction in conversion gain. An automatic tuning control system is needed to compensate continuously for changes in static microphone capacitance.

Figure 20 shows a block diagram of the microphone carrier system with automatic tuning The voltage-controlled oscillator (VCO) supplies the carrier voltage to the converter. There are two modes of operation, "open-loop" and "closed-loop," corresponding to operation without and with automatic tuning control, respectively. In the open-loop mode the differential amplifier-filter is disconnected from the system by means of mode switch S. Tuning of the converter is accomplished directly through adjustment of open-loop reference voltage V_{R4} , which controls the VCO frequency.

The system is switched to the closed-loop mode of operation to maintain a fixed converter tuning point The zero drive amplifier contains an internal voltage, located at a circuit point called "test point 3," which is highly sensitive to the state of tuning of the converter The difference between the test point 3 voltage v_3 and the closed-loop reference voltage V_{R3} provides the error voltage v_4 at the output of the differential amplifier-filter, which is used to correct the frequency of the VCO. Under optimal tuning the test point 3 voltage v_3 matches the closed-loop reference voltage V_{R3} , the error voltage v_4 is zero, and the open-loop reference voltage V_{R4} alone determines the VCO frequency. A change in static microphone capacitance C produces corresponding changes in v_3 and v_4 ; the latter causes the control voltage v_5 and the VCO frequency to change in such a manner as to compensate for the change in C.

When sound is applied to the microphone, the corresponding variation in v_3 , too, would normally produce a differential amplifier output, which would cause changes in VCO frequency to compensate for changes in C To avoid cancellation of the acoustical signal, low-pass filtering is built into the differential amplifier stage The relatively high acoustical frequencies are blocked, but the slow variations associated with changes in static microphone capacitance pass through the differential filter to complete the control loop The upper cutoff frequency is selected to be 1 Hz, corresponding to a control system time constant of 0 16 sec

The circuit diagrams of the differential amplifier-filter and summing amplifier are identical to those shown in reference 4 with one exception voltage v_4 is applied here to the noninverting input of the summing amplifier instead of the inverting input, because of the direction in which the VCO frequency changes with control voltage.[1] Both stages are located physically within the zero drive amplifier chassis.

In order to calibrate the system an electrical signal v_C is applied at the inverting input of the summing amplifier. The calibration signal frequency-modulates the VCO and produces variations in converter output voltage similar to those produced by acoustical excitation of the microphone.

The procedure for adjusting the control system for optimal tuning is straightforward and simple. First one switches the system to the open-loop mode, applies either an acoustical or electrical calibration signal, and tunes the converter by adjusting V_{R4} to obtain a maximum output voltage v_o Then he switches to the closed-loop mode and repeats the procedure with an adjustment of V_{R3} . The system is then ready for operation.

The VCO is a Hope Electronics Model VCO-100A, having a center frequency of 48 MHz, controllable to within ±5 percent, and an output power of 100 mW into a 50 Ω load.

Modifications to the front end of the converter are shown on the insert of figure 20 The 47Ω-110 pF parallel network is required to provide the proper load to the VCO; the 470 pF capacitor isolates the VCO from the gate G_2 bias voltage. The 100 kΩ resistor reduces the impedance from gate G_1 to ground, thus improving converter stability and lowering the noise floor A type 3N212 is used to replace the type 3N202 because of superior conversion gain. The connections to gate G_2, drain D , and source S are otherwise the same as in figure 14.

The tuning controls, which include the potentiometers for control voltages V_{R3} and V_{R4} and the feedback mode switch, as well as the calibration jack and gain switches, in steps of 2 dB and 10 dB, are located on the front panel of the zero drive amplifier. No other controls are needed for adjustment of the system.

---

[1] The VCO frequency increases with increasing control voltage

The development of the VCO system took place in the closing stages of the research grant. For this reason much of the system testing had been undertaken with the varactor diode system, employing an external signal generator and the converter of figure 14 Although both systems were found to show similar performance, the VCO system is preferred for its lower cost, considerably less bulk, and better adaptability for field service

V RESULTS OF LABORATORY TESTS

A Description of Systems Tested

A series of laboratory tests was conducted to compare system performance against the specifications listed in table 1. The VCO system of figure 20 was used for the dynamic range and vibration sensitivity tests, the varactor diode system, in which the rf signal generator replaces the VCO, was used for the frequency response and thermal shock tests Two prototype microphones with different membrane thicknesses were prepared, whose properties are summarized in table 3 and table 7 below [1]

Table 7. Some properties of prototype microphones used in laboratory tests.

	Microphone 1	Microphone 2
Membrane thickness [m]	$5\ 588 \times 10^{-6}$	7.112×10^{-6}
Membrane tension [N/m]	2893.1	4487.2
Static capacitance [pF]	15 6	13.6
Gap [m]	$3\ 72 \times 10^{-5}$	4.30×10^{-5}

The cable was a 5.718 m length of RG11A/U with a type N coaxial connector and TNC adapter The system was always switched to the closed-loop control mode for all the tests.

[1] Exceptions are noted in the text

B. Dynamic Range

1. Definitions. The "dynamic range" of the microphone system is defined to extend from 5 dB above the noise floor to the sound pressure level (SPL) at 4 percent distortion. The "noise floor" is taken to be the internal system noise within the frequency band 22.4 Hz to 22.4 kHz, corresponding to the "linear" band of the third-octave analyzer used in the measurements. The definition of "percent distortion" is based upon the response of the system to excitation by a pure tone. If the system is excited at some fundamental frequency to an amplitude A_1 and if the output amplitude at the ith harmonic frequency is A_i ($i = 1, 2, 3, \ldots$), then the percent distortion is obtained from the following formula.

$$\text{percent distortion} = \left(\frac{A_2^2 + A_3^2 + \ldots}{A_1^2 + A_2^2 + A_3^2 + \ldots} \right)^{1/2} \times 100 \ . \qquad (5\text{-}1)$$

As before, all measured amplitudes, when expressed in dB, are referred to 2×10^{-5} N/m^2 .

2. Experimental method Figure 21 shows the experimental arrangement used to measure the harmonic distortion The microphone was excited by means of a calibrated sound source at known frequency and sound pressure level. The output amplitudes at the fundamental frequency and the next three harmonics were measured on the third-octave analyzer; harmonics higher than the fourth were found to contribute practically nothing and were neglected.

Two different sound sources were employed a Model PC-125 Acoustic Calibrator of Photocon Research Products, and a Model 901D Microphone Calibrator of BB&N, Inc. Each source contains an inherent distortion, which we call "chamber distortion" and which was determined through measurements on a system known to have negligible distortion over the applicable amplitude ranges a B&K microphone, type 2615 preamplifier, and type 2801 microphone power supply. Pertinent information regarding the sound sources and their calibration is given in table 8. In view of the specifications regarding the B&K microphones it is felt that the latter made no significant contribution to the distortion at the SPL's used in the tests The measured values of chamber distortion at

Table 8 Calibrated sound sources.

Sound Source	Photocon PC-125	BB&N 901D/Module 40-70
Driving mechanism	acoustic driver	pistonphone
Output adjustments		
Sound pressure levels [dB]	110, 120, 130, 140, 150	140, 150, 160, 170
Operating frequency [Hz]	1000	80
B&K microphone used to measure chamber distortion		
Type	4134	4136
Size	12 7 mm (1/2 inch)	6.35 mm (1/4 inch)
Distortion specification	4% @ >164 dB	3% @ >172 dB

each SPL are summarized in table 9. The relatively high second harmonic content of the BB&N 901D lies in the nature of the driving mechanism. The substantial frequency drift of this unit precluded use of a distortion analyzer for the distortion measurements.

The distortion tests were conducted at the frequencies and SPL's listed in table 8. The sound sources themselves provided reference levels to calibrate the third-octave analyzer 130 dB at 1 kHz for the PC-125 and 140 dB at 80 Hz for the 901D. The noise level in each applicable third-octave band was also measured on the third-octave analyzer The true harmonic amplitudes were evaluated according to the following formula·

$$A_i = (M_1^2 - N_1^2)^{1/2} - C_1 \quad , \tag{5-2}$$

where

A_1 = true amplitude of the ith harmonic

M_1 = measured amplitude

N_1 = noise amplitude

C_1 = chamber distortion amplitude

All quantities entering equations (5-1) and (5-2), of course, were converted from dB levels to absolute amplitudes.

3. Results. Figure 22 shows the percent distortion versus sound pressure level for both microphones Below 160 dB the distortion is attributed to electrical noise and imprecise compensation for chamber distortion, at 160 dB the microphone system distortion becomes noticeable; and at 170 dB, the highest SPL for which measurements could be conducted, it remains well below the 4 percent limit.

Because the distortion originates predominantly from saturation of the carrier electronics, and not nonlinearity of the membrane deflection, it depends

Table 9. Chamber distortion of calibrated sound sources

A Photocon Research Products PC-125

Input SPL at	Output SPL at							
1000 Hz	1000 Hz		2000 Hz		3000 Hz		4000 Hz	
[dB]	[dB]	[%]	[dB]	[%]	[dB]	[%]	[dB]	[%]
110	110.0	100	55.8	0.19	51.6	0 12	*	-
120	120.0	100	65.8	0.19	60.6	0.11	*	-
130	130.0	100	76.2	0.20	71.6	0 12	*	-
140	140.0	100	94.6	0.54	84 6	0.17	*	-
150	150.0	100	114.4	1.66	100.2	0.32	*	-

* Less than 50 0 dB.

B. BB&N 901D/Module 40-70

Input SPL at	Output SPL at							
80 Hz	80 Hz		160 Hz		240 Hz		320 Hz	
[dB]	[dB]	[%]	[dB]	[%]	[dB]	[%]	[dB]	[%]
140	140.0	100	117.8	7.7	103.2	1.4	102.2	1 3
150	149 8	100	127 6	7 7	113 4	1.5	107 6	0.8
160	159.8	100	139.2	9.3	124 6	1 7	113 6	0 5
170	169.6	100	152.6	14.0	137.8	2 5	124.8	0.6

Note [%] refers to percent of fundamental amplitude.

upon all the factors which affect the system gain, including the range setting of the zero drive amplifier, membrane-backplate gap, and membrane tension. The lowest zero drive amplifier range for which a reasonable noise floor could be obtained was the 10 dB range for microphone 1 and the 20 dB range for microphone 2, and these were selected for measurement of the system dynamic range. Several tests revealed that the distortion increases with decreasing gap and decreasing tension, a trend which correlates with increasing system gain A gap near 40 μm, corresponding to a static capacitance of about 14 pF, appears to be an optimal choice, for a smaller gap will tend to increase the distortion beyond specification and a larger gap to produce too high a noise floor

The dynamic range data, including both noise floor and percent distortion, are summarized in table 10

Table 10. Dynamic range of microphones 1 and 2.

Microphone	Zero Drive Range [dB]	Noise Floor[1] [dB]	Percent Distortion at 170 dB SPL	Dynamic Range[2] [dB]
1	10	105 4	1.4%	>60
2	20	109.4	1.5%	>55

[1] Bandwidth. 22.4 Hz to 22.4 kHz.

[2] From 5 dB above noise floor to SPL at 4 percent distortion. Output voltage of the zero drive amplifier at 170 dB is approximately 5V P-P.

C. Frequency Response at Room and Elevated Temperatures

1. Experimental method. For the purpose of testing microphone frequency response at room and elevated temperatures, a high-temperature electrostatic actuator (ref 14) was constructed, consisting of a stainless steel electrode, macor insulator, and three standoffs to seat the actuator on the microphone. Each standoff was made of a macor pin pressed axially into a stainless steel set screw By means of the latter the separation between the actuator electrode and microphone membrane was adjusted to 4.572×10^{-4} m (0 018 inch) This was the only feasible means of conducting tests at elevated temperatures

Figure 23 shows the experimental arrangement for measuring the frequency response. The microphone and electrostatic actuator were placed in an oven with automatic temperature control The bare copper leads to the electrostatic actuator entered the oven through ceramic tubing The 1 22 m (4 ft) rigid cable described at the end of part IIID, terminating with a BNC connector containing macor insulators, furnished the electrical connection to the microphone The excitation instrumentation--the oscillator, power amplifier, and microphone calibration apparatus--appears in the upper portion of the figure, and the microphone response instrumentation--the converter, zero drive amplifier, and third-octave analyzer, etc.--appears in the lower portion of the figure. The equivalent sound pressure p exerted on the membrane is found from the well-known formula (ref. 15)

$$p = 8\ 85 \times 10^{-12} \frac{E_o e}{d_1^2} \ [N/m^2] \ . \qquad (5\text{-}3)$$

With a polarization voltage E_o = 800V , ac excitation voltage e = 20V rms , and spacing $d_1 = 4.572 \times 10^{-4}$ m , we obtain p = 0.6774 N/m^2 rms , which corresponds to a sound pressure level of 90 6 dB. The rf signal generator was tuned to the fundamental resonant frequency of the coaxial cable-rigid cable combination (approximately 15 MHz), where the response was slightly better than at any of the higher resonances, the carrier voltage was adjusted to 2.2 V rms Furthermore, because of the weak excitation of the electrostatic actuator the range setting of the zero drive amplifier was increased to 30 dB

Throughout a temperature run the converter automatic tuning control remained operative, the system was never retuned manually--by means of neither the carrier frequency nor the control voltage At each temperature the microphone frequency response, temperature, control voltage, and microphone resonant frequency were measured. These measurements were performed during both heating and cooling at temperatures of 21°C (70°F), 93°C (200°F), 204°C (400°F), 316°C (600°F), and 427°C (800°F) Prior to measurement the microphone was allowed to remain at the set temperature for one hour, a sufficient time to insure thermal equilibrium. The temperature was read directly from the controller The microphone frequency response measurements were later corrected for noise, which was in most cases insignificant.

Voltmeter 1 was used to monitor the varactor diode control voltage, from which the gap (membrane-backplate separation) could be inferred. The automatic tuning control system strives to keep constant the sum $C_T = C + C_V$ of the microphone and varactor diode capacitances. Using the known relationship between C_V and control voltage V_C (ref 4), we relate the microphone capacitance to the control voltage.

$$C = C_T - C_V = C_T - \frac{11}{\left(1 + \frac{V_c}{0.6}\right)^{0\ 44}} \text{ [pf]} , \quad (V_C \text{ in volts}) . \tag{5-4}$$

The total capacitance C_T is known from the known values of microphone capacitance and control voltage at room temperature (see table 7). In the present tests V_C was adjusted to 5.6 volts at room temperature, corresponding to a varactor diode capacitance of 3.94 pf.

Voltmeter 2 was used to determine the microphone resonant frequency and hence the membrane tension. As the oscillator was tuned to the membrane resonant frequency, the reading on voltmeter 2 reached a maximum. The filter served to bandpass frequencies in the neighborhood of the microphone resonance. With the aid of figure 6 we find the membrane compliance C_M in terms of the membrane resonant frequency f_R

$$C_M = \frac{C_{MO}}{1 + 4\pi^2 M C_{MO} (f_R - f_{RO})} \text{ [m}^5\text{/N]} , \tag{5-5}$$

where C_{MO} and f_{RO} are known room-temperature values. The membrane mass is known from equation (2-28a). Since the membrane compliance varies inversely with membrane tension T [see equation (2-28b)], we find the tension at any temperature from the relationship

$$T = C_{MO}\ T_O/C_M , \tag{5-6}$$

where T_O is the room-temperature value of membrane tension.

2. Results. Figure 24 shows the frequency response of microphone 1 at the selected frequencies during both heating and cooling. After an initial microphone failure at elevated temperature the membrane had to be replaced, for this reason the membrane tension and gap, given in the figure caption, differ from those given in table 7. The height of the resonant peak reveals lower membrane damping than desired. This is the result of an increase in gap needed to maintain good linearity at high SPL's.

The theoretical considerations of part II facilitate the interpretation of the frequency response curves The three predominant effects of temperature changes are changes in the gap, membrane tension, and air viscosity Of primary interest is the temperature dependence over the flat region of the frequency response. Because the air viscosity has but negligible effect over this region, even at elevated temperatures, only the other two parameters need be considered

Figure 25a shows the temperature dependence of the microphone response at 1000 Hz, representative of the microphone sensitivity. During heating up to 316°C (600°F) the response remains nearly constant. Between 316°C and 427°C (800°F) an irreversible change in the microphone takes place, which enhances the microphone sensitivity by about 2.5 dB. Upon cooling from 316°C the microphone sensitivity drops steadily to a new room temperature value 2 dB below the original room temperature value

Figures 25b and 25c show the temperature dependence of the membrane tension and gap, computed from equations (2-38), (5-4), (5-5), and (5-6) During heating the gap remains nearly constant, but the microphone tension shows a sharp drop between 316°C and 427°C, which accounts for the rise in microphone sensitivity. During cooling the situation is reversed, the membrane tension remains nearly constant, and the loss of microphone sensitivity is attributable to an irreversible widening of the gap. Fortunately, the decrease in membrane tension and increase in gap have compensating effects upon the microphone sensitivity, in fact the compensation at 204°C during cooling is nearly perfect

For comparison, the temperature dependence of the same parameters is shown in figures 26 and 27 for microphone 1 with reduced membrane tension and gap. In contrast to figure 25a, figure 27a reveals relative insensitivity of the microphone response to temperature changes The trend of increasing gap with

temperature is compensated for by a steady decrease in membrane tension, at least for measurements following those at 204°C of the heating portion of the thermal cycle. Furthermore this microphone shows no permanent geometric changes as a result of the thermal cycle--only a small decrease in membrane tension, which accounts for the 1.8 dB increase in gain upon cooling.

Figure 28 shows the results of some early measurements on a microphone with a backplate made of type 347 S/S, for which the thermal expansion coefficient closely matches that of the case material, type 304 S/S The strong reduction in gap with increasing temperature leads to an unacceptably rapid increase in microphone sensitivity For this reason the backplate material was changed to type 17-4PH S/S, which not only reverses the temperature dependence of the gap but closely matches the macor insulator with regard to thermal expansion, as illustrated in table 11.

Table 11. Thermal expansion coefficient α of microphone materials

Material	Microphone part	α [$°C^{-1}$] at 20°C	Remarks
304 S/S	case	17.3×10^{-6}	
347 S/S	backplate	16.7×10^{-6}	Abandoned
17-4PH S/S	backplate	10.8×10^{-6}	Close match to macor
Macor	insulator	9.4×10^{-6}	

D. Vibration Sensitivity

1. Experimental method The experimental arrangement of figure 29 was used to measure the vibration sensitivity, that is, the response of the microphone to external vibrations A B&K type 4809 Vibration Exciter served as a source of axial vibrations, whose amplitude and frequency were controlled by adjustments of the test oscillator. The microphone acceleration was measured with a BB&N type 501-159 accelerometer, bonded to the microphone, and the microphone output was measured on a third-octave analyzer.

Initially the microphone carrier system was calibrated at 1000 Hz with the aid of a PC-125 acoustic calibrator. Then the microphone was mounted in the vibration exciter adapter and subjected to sinusoidal vibrations at frequencies of 20, 50, 100, 200, 500, 1000, 2000, and 5000 Hz The cable was clamped rigidly to a support on the workbench at a point about 60 cm from the microphone to suppress triboelectric noise At each frequency the test oscillator output level was adjusted to produce an accelerometer output corresponding to 0.5 g, the highest level showing a linear response at all frequencies. The vibration sensitivity levels--output volts per unit acceleration--were measured on the third-octave analyzer and later corrected for electrical noise.

2. Results. The vibration sensitivity spectra for microphones 1 and 2 are shown in figure 30 The response of each microphone lies below the specified limit of 0.6895 $N/m^2/g$ (horizontal line) at all frequencies. For comparison the vibration sensitivity specifications for two commercial transducers are given below:

B&K type 4134 12.7 mm (1/2 inch) condenser microphone· 0.5 $N/m^2/g$
Kulite type BQH-1100-5 solid state pressure sensor 1.38 $N/m^2/g$.

These values apply to the entire operating frequency range.

According to reference 16 the vibration sensitivity at 1 g should equal σg , where σ is the membrane surface density and g the acceleration of gravity For microphones 1 and 2 these values are 0.433 and 0 551 $N/m^2/g$ respectively, decidedly above the measured values Apparently vibrations applied to the flange of the microphone case are damped along the path to the membrane

The maximum allowable vibration sensitivity per specification corresponds to a noise level of 91 dB at 1 g Since the system noise floor exceeds 100 dB, vibration sensitivity will not be the limiting factor regarding the lowest measurable dynamic pressure levels

E. Thermal Shock

1 Definition "Thermal shock" refers to a rapid change in microphone temperature [about 167°C (300°F) per minute], during which time the response of

the microphone to a steady acoustical excitation is monitored. The purpose of the test is to study the stability of the microphone under dynamic thermal conditions.

2. Experimental method. Refer to figure 31. The microphone and electrostatic actuator were mounted on a stand, which rested upon a flat side of an aluminum cable drum The hole through the center of the drum and the two wooden spacers on which it was supported provided clearance for the microphone cable. The electronic systems for exciting the electrostatic actuator and measuring microphone response were essentially the same as those used in the static temperature tests (figure 23). In the absence of the rigid cable, however, the rf signal generator was adjusted for a carrier frequency near 48 MHz and an output of 2.2 V. The polarization voltage applied to the electrostatic actuator, furthermore, was reduced to about 400 V to prevent arcing at high temperatures The test was conducted at a single acoustical frequency of 2000 Hz, for which third-octave band the electrical noise was lowest. The HP model 3403C True RMS Voltmeter provided an output proportional to the logarithm of the input; this was used to monitor the output level of the microphone in dB on one channel of the strip chart recorder. Despite the low-level excitation by the electrostatic actuator, the signal-to-noise ratio on the 2000 Hz third-octave band amounted to 27.4 dB

The microphone was heated simply by means of an acetylene flame applied by hand. A blower, Master Appliance Corp. HG 301 Heat Gun (switched to "cool"), provided means of rapid, forced-air cooling A copper-constantan thermocouple, screwed onto the electrostatic actuator near the microphone, together with a reference thermocouple at ambient temperature, 20°C, provided the temperature signal on the remaining channel of the strip chart recorder.

The microphone remained excited at 2000 Hz and fixed amplitude all during the test. The acetylene flame was applied to the microphone, as uniformly as possible around its periphery, until the recorder indicated a thermocouple output corresponding to at least 370°C. Then the flame was removed and the microphone temperature permitted to decrease slowly, when it reached 340°C the blower was switched on, and the thermocouple and microphone outputs were recorded simultaneously on the strip chart recorder

3 Results The test result for microphone 2 is shown in figure 32. The average cooling rate of the microphone over the first minute is found to be 162°C per minute, very close to the 167°C per minute required by the specifications. After an initial negative spike following activation of the blower, the microphone response remains well within a 2 dB band over the entire cooling interval. The fluctuations in the microphone response are of aerodynamic origin; because of their broad frequency spectrum, it was necessary to insert a filter which passed only those frequencies within the 2000 Hz third-octave band. Figure 32 is typical of repeated dynamic temperature tests of microphone 2 as well as microphone 1. From these tests we conclude that microphone stability under rapid temperature changes is satisfactory.

VI. CONCLUSIONS

A. Review of Work Accomplished Toward Achievement of Research Objectives

The objectives of the three basic research problems--microphone, cable, and electronics--have been for the most part satisfactorily achieved. The self-consistent theory of part IIB, by which one can predict the frequency response, quality factor, air compliance, air resistance, and other parameters in terms of the physical properties of the microphone, has been substantiated by experiment, and has proved useful as a basis for condenser microphone design. The prototype microphone-cartridge of figure 12, which has operated successfully at temperatures up to 427°C (800°F), contains two new design features not found in conventional microphones First, the choice of a backplate material (type 17-4PH stainless steel) with a lower thermal expansion coefficient than that of the case has alleviated problems concerning rapid changes of the microphone gap with changes in temperature, secondly, the slotted-shell contact on the locking tube H, mated to the contact pin C of figure 19 (with a brass foil in between), has maintained reliable electrical continuity at elevated temperatures

Operation of the 6 m (20 ft) cable in figure 13 as a half-wavelength transmission line has been demonstrated in part III as a practical and effective means of separating the microphone from the carrier electronics To minimize cable losses it was determined that the cable should have the

highest possible figure of merit $R_o/\alpha\ell$, where R_o, α, and ℓ are the cable characteristic impedance, attenuation constant, and length, and that the system should operate at the highest possible carrier frequency The cable losses of the prototype carrier system, operating with an RG11A/U cable at 48 MHz (third cable resonance), have been limited to about 20 dB

The use of a voltage-controlled oscillator (VCO), in place of the varactor diodes, have proved an effective means of achieving automatic tuning control of the converter, as described in part V. A possible improvement in the electronics system would be the addition of automatic gain control, which would keep overall system gain constant despite variations in static microphone capacitance One such system, developed under a previous grant (ref 17), utilizes an insertion voltage in a feedback loop to detect and compensate for changes in system gain.

B. Analysis of Laboratory Test Results

The laboratory test results of part VC clearly suggest that the microphone cartridge must be modified to improve the frequency response of the system. Two considerations are of primary interest First, the present microphone has a much lower damping than desired; the resonant peak, shown in figure 24, is in fact so high as to render the microphone useful at frequencies up to only 10 kHz In the original design of the microphone it was intended that the gap be adjusted to about 29 μm, corresponding to a static capacitance of 20 pf. With such a small gap setting, however, it was learned that the harmonic distortion at 170 dB exceeded specification and could not be reduced to an acceptable level until the gap was increased to about 40 μm. The increase in gap consequently reduced the microphone damping to the detriment of its frequency response. Secondly, the membrane tension required to extend the microphone frequency response to 20 kHz is excessively high and thus excessively sensitive to temperature. Figures 25b and 27d show that the membrane with lower tension (2733 N/m) is less affected by exposure to elevated temperatures than the membrane with higher tension (4288 N/m), hence the desirability of a reduced membrane tension

The dual goals of lowering the sensitivity to reduce harmonic distortion and of extending the bandwidth can both be realized through a reduction in the radius of the membrane, in which case the microphone could operate at reduced values of gap and membrane tension. The reduced gap would increase the damping and, together with proper backplate design, would suppress the resonant peak and

extend the bandwidth, the reduced tension would render the membrane less sensitive to temperature cycling and thus enhance microphone stability

The present system has achieved its best performance under the following operating conditions

membrane tension ≈ 4000 N/m

gap ≈ 40 μm

carrier frequency ≈ 48 MHz (third resonance of a 5 7 m length of RG11A/U)

zero drive range = 10 for microphone 1
= 20 for microphone 2 .

Microphone 1 (membrane thickness = 5.588 μm) showed somewhat better specifications than microphone 2 (membrane thickness = 7.112 μm), but the latter may prove more durable in field tests. A summary of the specifications achieved with the two microphones appears in table 12.

Table 12. Summary of achieved specifications.

Specification	Microphone 1[1]	Microphone 2[2]
Harmonic distortion at 170 dB SPL	1.4%	1.5%
Noise floor (22 4 Hz to 22 4 kHz)	105 dB	109 dB
Frequency response (±2 dB)	20 Hz to 10 kHz	
Maximum operating temperature	>427°C (800°F) (continuous duty)	
Thermal shock	<2 dB change in sensitivity during cooling at rate of 162°C/min (292°F/min)	
Vibration sensitivity	<0.5 $N/m^2/g$ (7.25×10^{-5} psi/g)	

[1] Membrane thickness = 5.588 μm (0.00022 in).

[2] Membrane thickness = 7.112 μm (0.00028 in)

The noise floor of both microphones is somewhat higher than desired, but that of microphone 1 is acceptable for measurements at SPL's above 110 dB. The

upper limit of the dynamic range can only be estimated, for no means of testing above 170 dB was available. Nevertheless extrapolation of the curves of figure 22 suggests that the harmonic distortion may not exceed 4 percent at 180 dB. The upper limiting frequency of 10 kHz falls shy of the desired 20 kHz, as explained above, and the frequency response below 20 Hz was not measured. The specification on thermal shock is acceptable if a 2 dB change in sensitivity is permitted. The vibration sensitivity meets specifications, even without external vibration damping or compensation.

C. Effect of Temperature Upon Condenser Microphone Operation

It was pointed out in part VC that the three predominant effects of temperature changes are changes in gap, membrane tension, and air viscosity. The effect upon the gap, related to the thermal expansion coefficients of the backplate and case materials, was discussed previously.

The effect upon the membrane tension warrants a more complex interpretation, for there are contributions from two different physical effects. thermal expansion, which tends to stiffen the membrane with increasing temperature, and the temperature dependence of the tensile strength, which tends to soften it. As seen in figure 27b, thermal expansion prevails up to 204°C of the heating portion of the thermal cycle, but the reduction in tensile strength prevails at all temperatures thereafter. In the static test of figure 27, where the microphone was held at each temperature for one hour, a permanent reduction in membrane tension after the test is evident In the dynamic test of figure 32, on the other hand, where the microphone was exposed to elevated temperatures for only a few minutes, a permanent change in microphone sensitivity, and thus membrane tension, is lacking. A permanent reduction in membrane tension may be attributable to creep of the membrane material upon prolonged exposure to elevated temperatures, and may possibly not appear in field tests of relatively short duration. In any case, the membrane can easily be retightened or even replaced after a temperature run.

Viscosity affects the frequency response significantly only near the microphone resonance. The increase in viscosity with increasing temperature tends to lower the resonant peak, as is evident in figure 26, and is but a secondary consideration.

The present microphone was designed such that the change in gap and membrane tension will have compensating effects upon the microphone sensitivity

D. Public Disclosure

During the course of the research several aspects of the microphone system have been presented at scientific conferences.

1 N. V Cohen, "Analytical and Experimental Studies of Capacitance Microphones," Virginia Academy of Sciences, 53rd Annual Meeting, May 1975

2. A. J. Zuckerwar, "Self-consistent Approach to the Problem of Fluid-Membrane Coupling in Condenser Microphones," 90th Meeting of the Acoustical Society of America, November 1975 (J. Acoust. Soc. Am. 58, Suppl 1, S45, 1975).

3 A. J. Zuckerwar, "Operation of a Condenser Microphone as the Terminal Element of a Half-wavelength Transmission Line in an AM Carrier System," 91st Meeting of the Acoustical Society of America, April 1976 (J Acoust. Soc. Am 59, Suppl. 1, S62, 1976).

4. A. J. Zuckerwar, "Performance of a Condenser Microphone Designed for Operation at Elevated Temperatures," to be presented at the 93rd Meeting of the Acoustical Society of America, June 1977.

Descriptions of the self-consistent theory of condenser microphones and the high-temperature microphone carrier system will be submitted for publication in scientific journals A Disclosure of Invention (NASA Form 235), describing the microphone system, will be submitted to the Office of Patent Counsel, Langley Research Center.

ACKNOWLEDGMENTS

Mr. Norman V. Cohen, graduate research assistant in the Department of Physics and Geophysical Sciences at Old Dominion University during the academic year 1974-1975, designed and dimensioned the microphone cartridge of figure 12 and conducted the initial frequency response tests described in part IIC

Over the two-year period of this research grant the principal investigator often required, and now gratefully acknowledges, the assistance of many individuals at NASA Langley Research Center. These include Mr H. K Holmes, for suggesting the analysis of part IIIB and the use of the electrostatic actuator as a means of testing microphones at elevated temperatures; Mr. W. Eugene Robbins, for fabricating the microphones and assisting in their design; Mr. W. N Branch and Mr R. H. Coultrip, for fabricating and assembling the high-temperature rigid cables and assisting in their design, Mr. A. M. Rackley and Mr. T. Vranas, for assistance in setting up the thermal shock test, Mr. J. W. Lynch and Mr. F. R. Batten for assistance in setting up the vibration sensitivity test; Mr. J M. Harris, for preparing the cables used in the tests of part IIIC; and Mr. C. E. Johnson, for providing the oven used in the tests of part VC. In addition, Mr R. Perry of Hampton Institute provided valuable assistance in setting up the harmonic distortion test.

Appendix A. The Boundary Condition at the Backplate.

We write the circuit equations of figure 4 in matrix form

$$\underline{P} = \underline{Z}\,\underline{U}\ , \tag{A-1}$$

where the pressure, volume velocity, and acoustic impedance matrices are defined as follows

$$\underline{P} = \begin{pmatrix} P_1 \\ P_2 \\ \cdot \\ \cdot \\ \cdot \\ P_q \end{pmatrix}\ , \qquad \underline{U} = \begin{pmatrix} U_1 \\ U_2 \\ \cdot \\ \cdot \\ \cdot \\ U_q \end{pmatrix}\ , \tag{A-2a,A-2b}$$

$$\underline{Z} = \begin{pmatrix} Z_1 + Z_C & Z_C & \cdot & \cdot & \cdot & Z_C \\ Z_C & Z_2 + Z_C & & & & \\ \cdot & & \cdot & & & \\ \cdot & & & \cdot & & \\ \cdot & & & & \cdot & \\ Z_C & & & & & Z_q + Z_C \end{pmatrix} \tag{A-2c}$$

In the matrix (A-2c) the impedance Z_C is just the acoustic impedance of the backchamber

$$Z_C = \frac{\rho_o c^2}{i\omega V} \tag{A-3}$$

and the impedance Z_k (k = 1, 2, ..) of the kth opening of the backplate is given by

$$Z_k = \frac{8\rho_o \nu \ell_k}{\pi r_k^4} + i\,\frac{4}{3}\,\frac{\rho_o \ell_k \omega}{\pi r_k^2} \tag{A-4}$$

if the opening is a hole of radius r_k and depth ℓ_k, or by

$$Z_k = \frac{12\rho_o \nu \ell_k}{t_k{}^3 w_k} + i\,\frac{6}{5}\,\frac{\rho_o \ell_k \omega}{t_k w_k}$$

if the opening is a narrow slot of length w_k, width t_k, and depth ℓ_k.

Upon using the relationships

$$P_k = i\omega\rho_o\phi_k \,, \tag{A-6a}$$

$$U_k = f_k s_k \,, \tag{A-6b}$$

and rewriting equation (A-1) in the form,

$$\underline{U} = \underline{Y}\,\underline{P} \,, \tag{A-7}$$

where

$$\underline{Y} = \underline{Z}^{-1} \,, \tag{A-8}$$

we find the following expression for the f_k's.

$$f_k = \frac{i\omega\rho_o}{s_k} \sum_{\ell} Y_{k\ell}\phi_\ell \,. \tag{A-9}$$

The matrix $\underline{Y}$, with elements $Y_{k\ell}$ in equation (2-4), is just the inverse of $\underline{Z}$, defined in equation (A-2c)

Appendix B. Proof of Equation (2-22).

First let us expand the summand S_p into partial fractions:

$$S_p = \frac{1}{(\lambda_p^2 - \xi_m^2)(\lambda_p^2 - K^2)} = \frac{a^4}{(\xi_m^2 a^2 - K^2 a^2)(\lambda_p^2 a^2 - \xi_m^2 a^2)} + \frac{a^4}{(K^2 a^2 - \xi_m^2 a^2)(\lambda_p^2 a^2 - K^2 a^2)} \tag{B-1}$$

Now, starting with the identity (ref. 18)

$$J_o(z) = \prod_{p=1}^{\infty} \left(\frac{\lambda_p^2 a^2 - z^2}{\lambda_p^2 a^2} \right) ,$$

taking the natural logarithm of both sides, and differentiating with respect to z, we obtain

$$\frac{J_1(z)}{2zJ_o(z)} = \sum_{p=1}^{\infty} \frac{1}{\lambda_p^2 a^2 - z^2} \tag{B-2}$$

Upon summing (B-1) over p and applying (B-2) we find

$$\sum_{p=1}^{\infty} S_p = \frac{a^4}{(\xi_m^2 a^2 - K^2 a^2)} \cdot \frac{J_1(\xi_m a)}{2\xi_m a J_o(\xi_m a)} + \frac{a^4}{(K^2 a^2 - \xi_m^2 a^2)} \cdot \frac{J_1(Ka)}{2KaJ_o(Ka)}$$

However,

$$\frac{J_1(\xi_m a)}{\xi_m a} = 0 \quad \text{if} \quad m \neq 0$$

$$= \frac{1}{2} \quad \text{if} \quad m = 0 ,$$

from which equation (2-22) follows.

REFERENCES

1. J S. Mixon, J A. Schoenster, and C. M. Willis, "Fluctuating Pressures on Aircraft Wing and Flap Surfaces Associated with Powered-lift Systems," AIAA Paper 75-472, March 1975.

2. J. C. Schneider and R. K Duke, "Development of a 1093°C (2000°F) Prototype Microphone Transducer," AFFDL-TR-73-62, February 1974

3. A. J. Zuckerwar and W. W. Shope, "A Solid-state Converter for Measurement of Aircraft Noise and Sonic Boom," IEEE Trans. Instrum. Meas., IM-23, 23-27, March 1974.

4. A. J. Zuckerwar and H. K. Holmes, "A Unified Acquisition System for Acoustic Data," NASA TN-D8327, to be published.

5. D. H. Robey, "Theory of the Effect of a Thin Air Film on the Vibrations of a Stretched Circular Membrane," J. Acoust. Soc. Am. 26, 740-745 (1954).

6. I. G. Petritskaya, "Impedance of a Thin Layer of Air in the Harmonic Vibrations of a Membrane," Soviet Phys.--Acoust. 12, 193-198 (1966)

7. I. G Petritskaya, "Vibrations of a Membrane Loaded with a Thin Layer of Air," Soviet Phys.--Acoust. 14, 105-106 (1968).

8. J. E. Warren, A. M. Brzezinski, and J. F. Hamilton, "Capacitance Microphone Dynamic Membrane Deflections," J Acoust. Soc. Am. 54, 1201-1213 (1973) .

9. A. J. Zuckerwar, "Self-consistent Approach to the Problem of Membrane-fluid Coupling in Condenser Microphones," J. Acoust. Soc. Am. 58, Suppl. 1, S45, Fall 1975

10. P. M Morse, Vibration and Sound, McGraw-Hill (1948), p. 200

11 T Baumeister and L. S. Marks, Standard Handbook for Mechanical Engineers, 7th Ed., p. 6-43, McGraw-Hill (1967)

12. J D Ryder, Networks, Lines, and Fields, Prentice-Hall (1955), p. 340.

13 Catalog ACD-5, Amphenol Corp Cable Division.

14. G Rasmussen, "The Free Field and Pressure Calibration of Condenser Microphones using Electrostatic Actuator," B&K Technical Review 1-1969

15 An excellent description of the principle of the electrostatic actuator appears in "Instrumentation and Applications, Microphone Calibration Apparatus Type 4142," Bruel & Kjaer, Reprint March 1967

16. E Rule, F J Sullentrop, and T A. Perls, "Vibration Sensitivity of Condenser Microphones," J. Acoust Soc Am. 32, 821-823 (1960)

17. A. J. Zuckerwar, Technical Report PGS-TR-PH-75-18, Old Dominion University Research Foundation, December 1975.

18. G. N. Watson, A Treatise on the Theory of Bessel Functions, Cambridge at the University Press, The Macmillan Company (1944), p. 500.

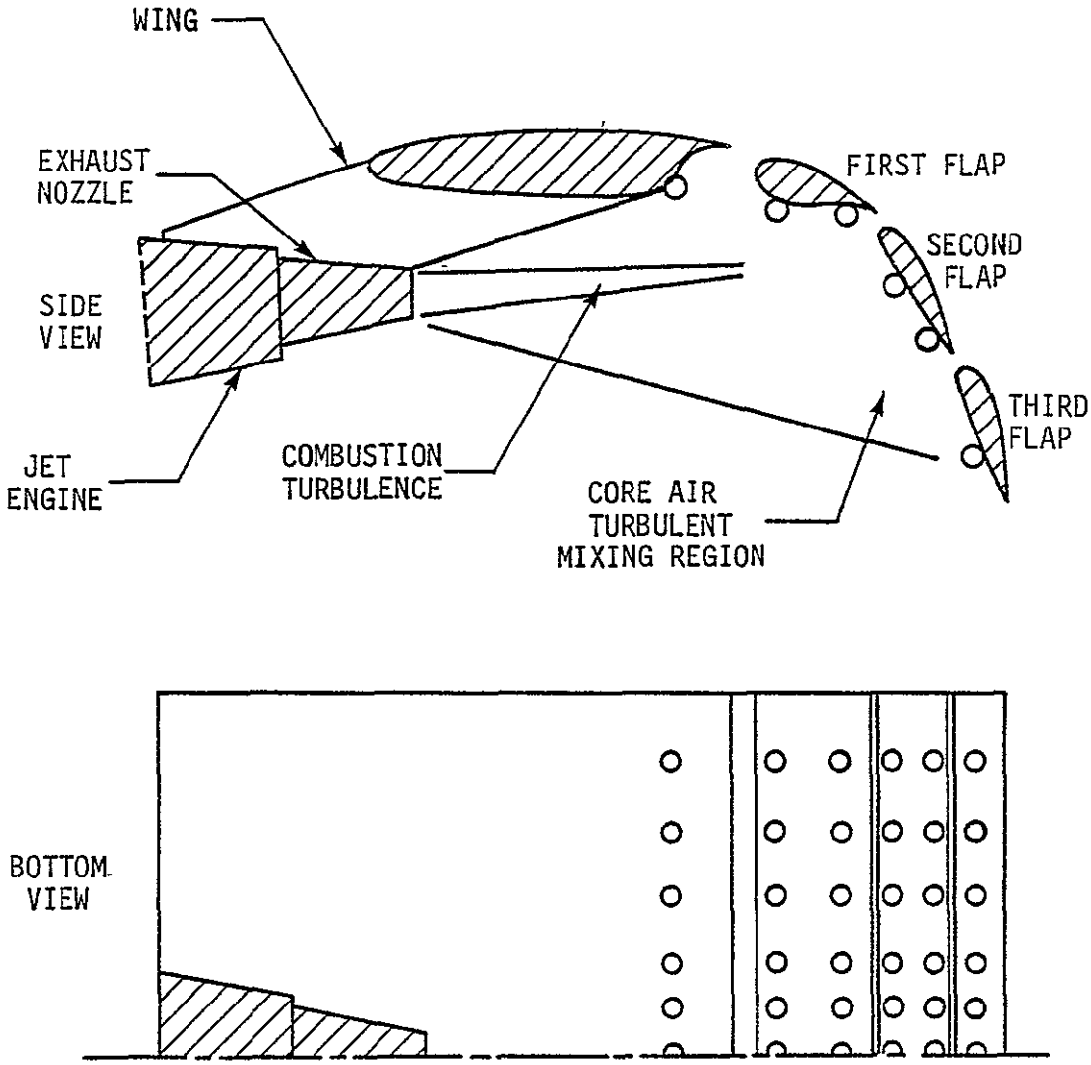

Figure 1. Typical experimental arrangement to measure pressure fluctuations on externally blown flaps.

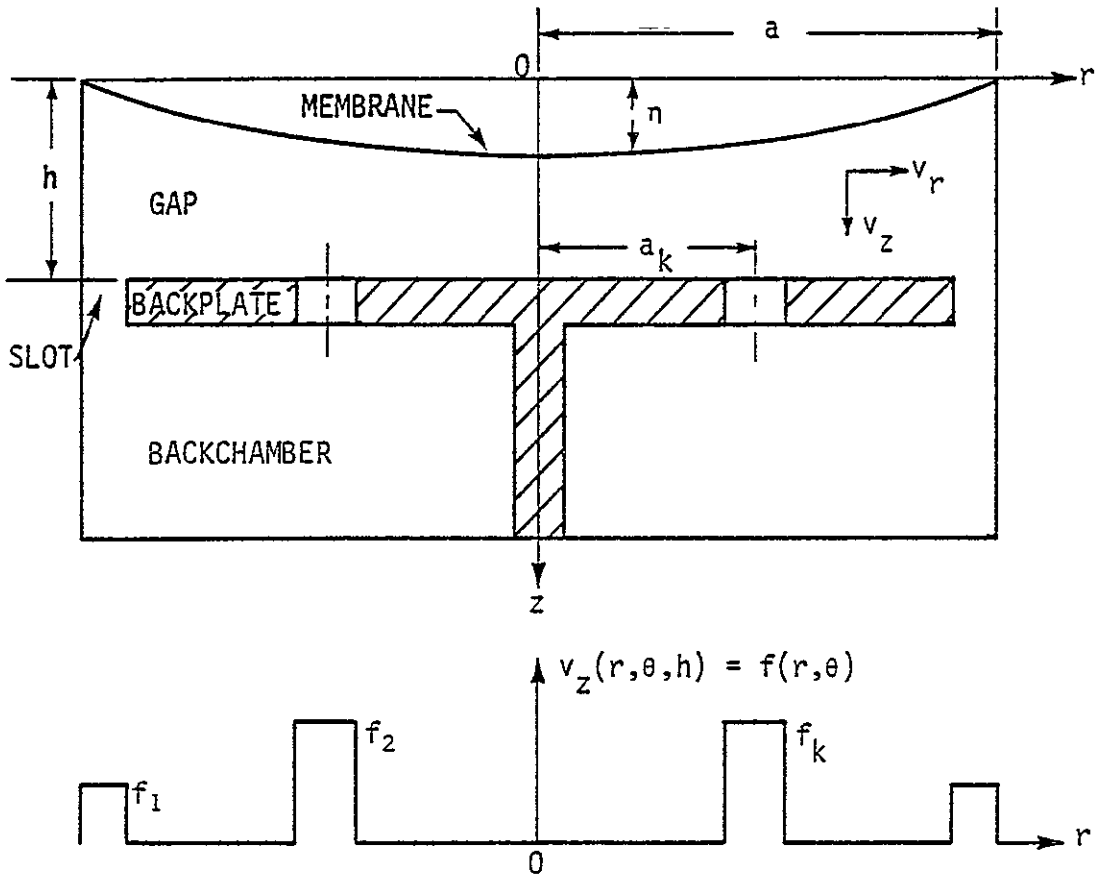

Figure 2. Cross section of prototype condenser microphone and profile of vertical velocity at backplate.

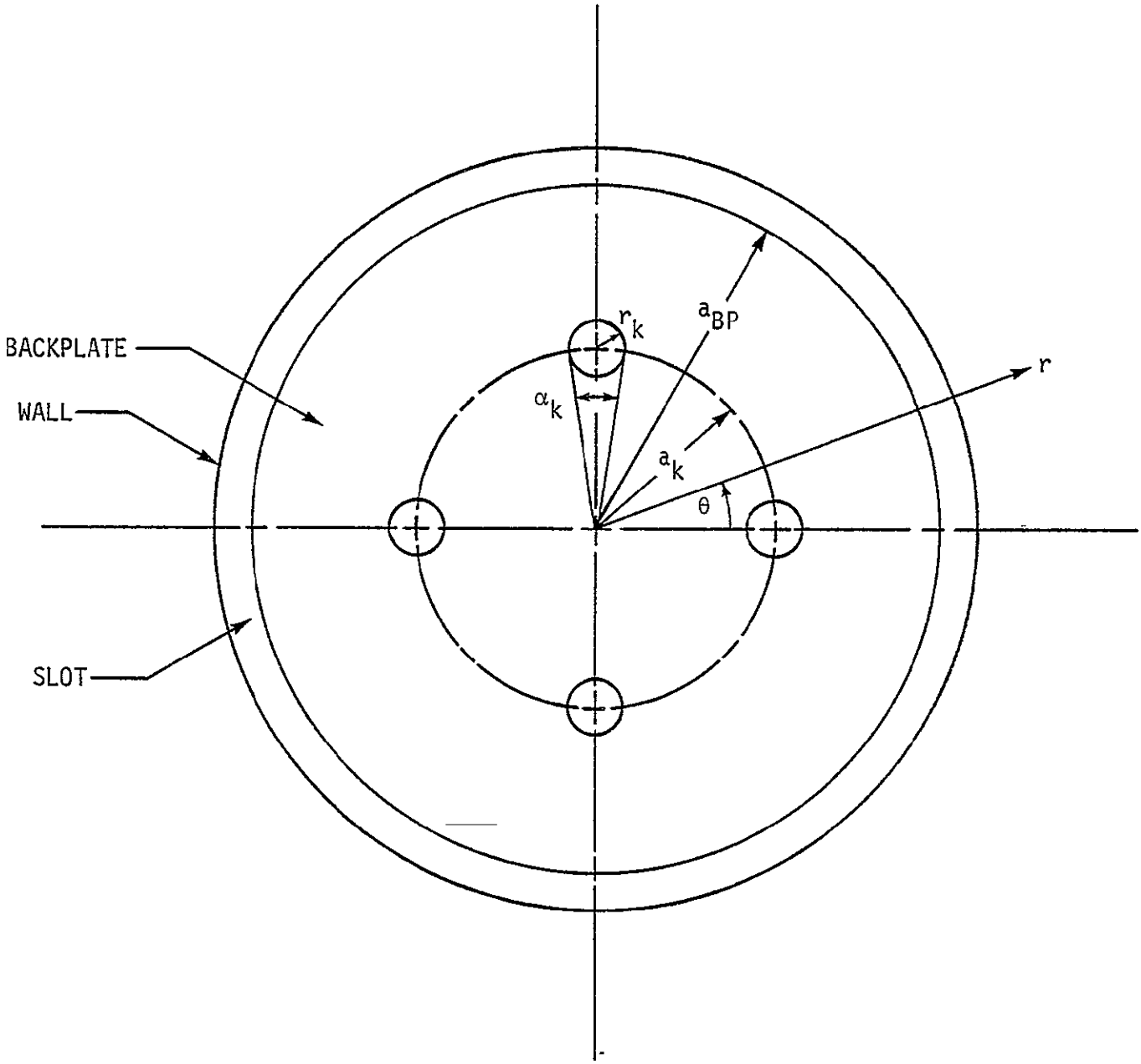

Figure 3 Arrangement of openings in backplate.

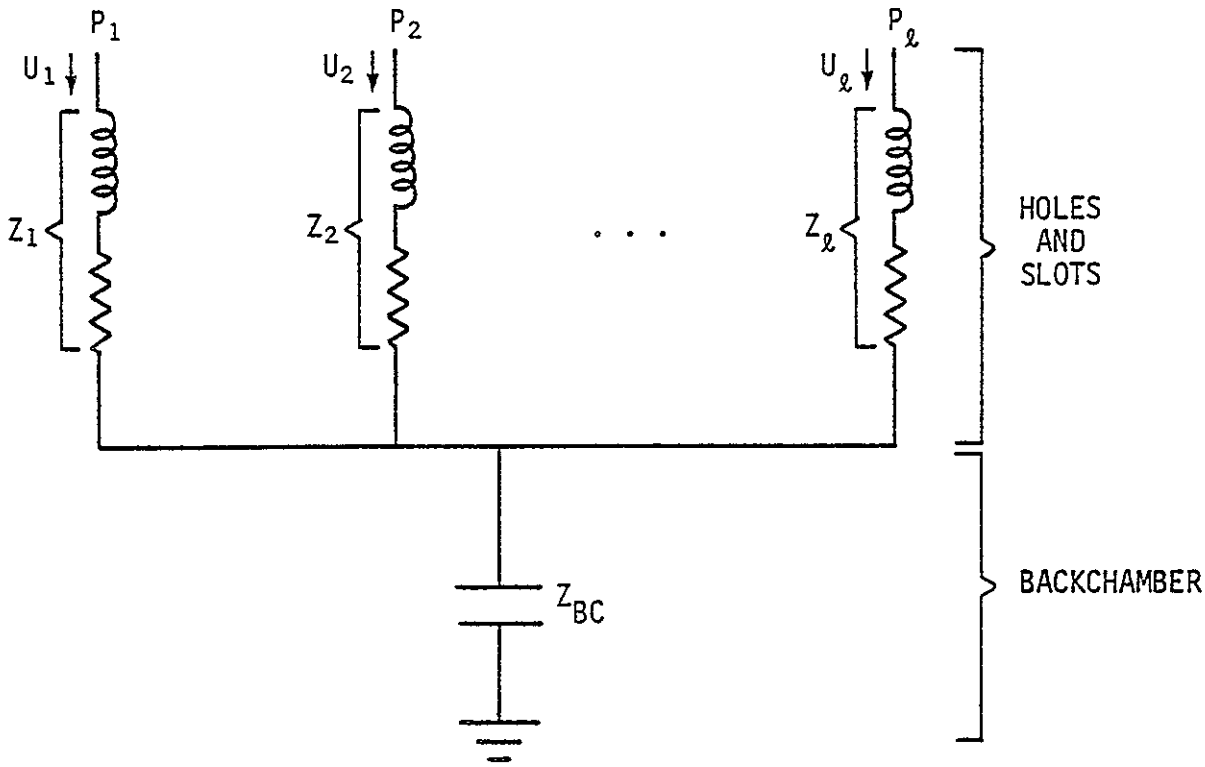

Figure 4 Equivalent circuit of backplate and backchamber.

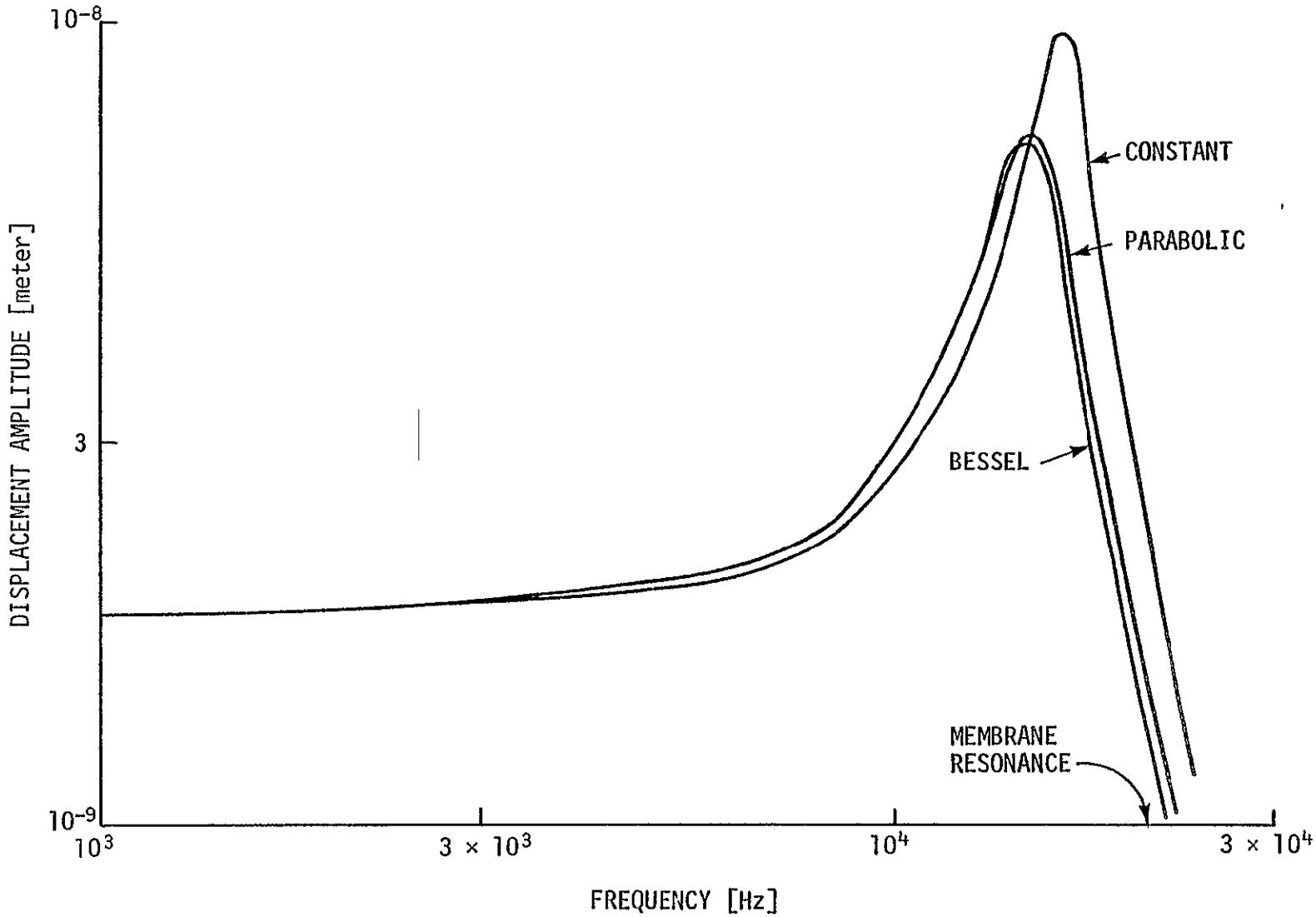

Figure 5 Frequency dependence of average membrane displacement for the constant [case (1)], parabolic [case (2)], and Bessel [case (3)] trial expressions entering equation (2-11a). Membrane tension = 2962 N/m. Air gap = 6.05×10^{-5} m. SPL = 1 N/m^2 (94 dB).

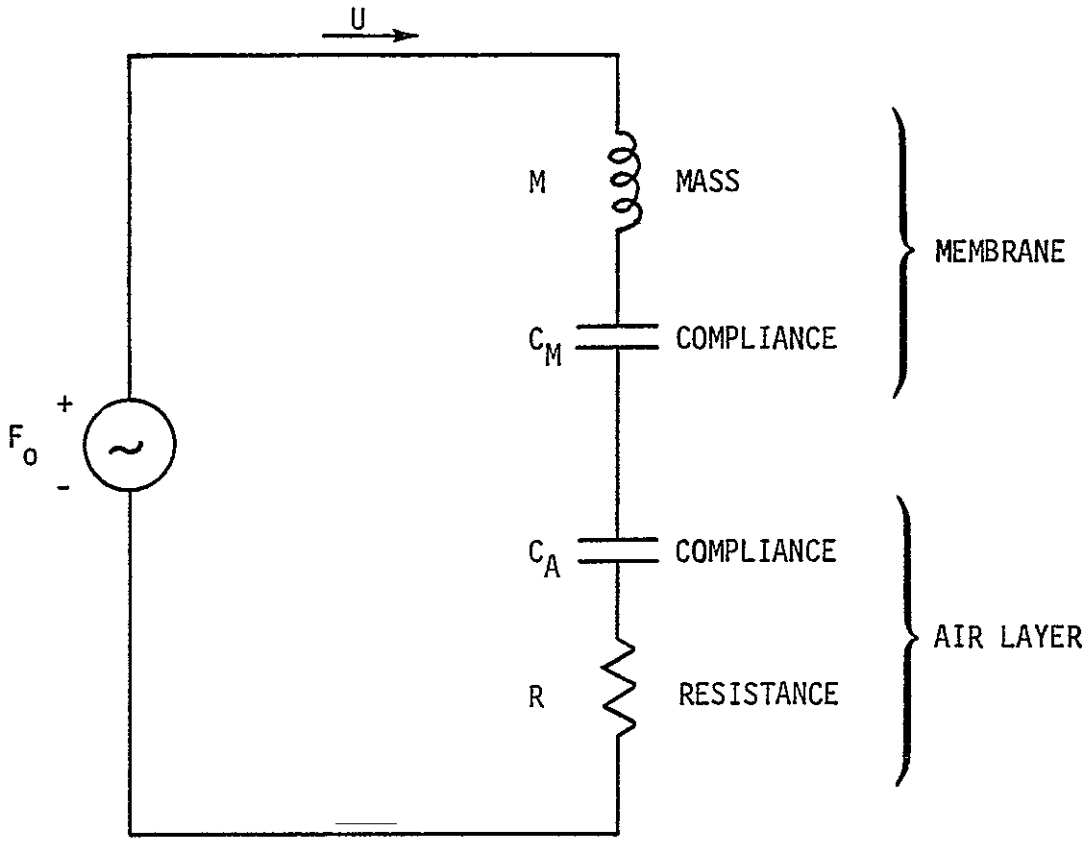

Figure 6 Equivalent circuit of microphone.

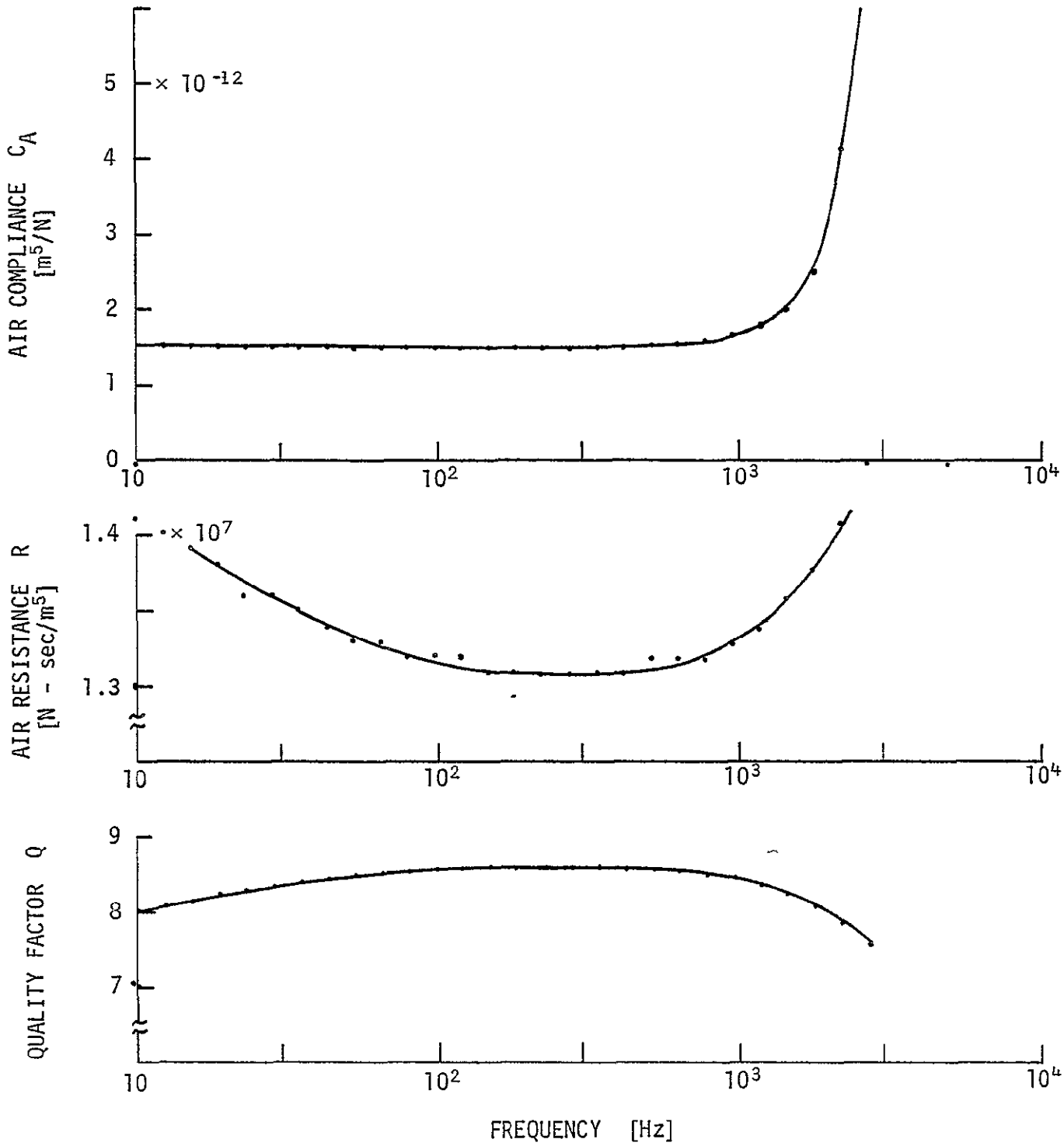

Figure 7. Frequency dependence of air compliance, resistance, and quality factor for the prototype microphone of figure 5.

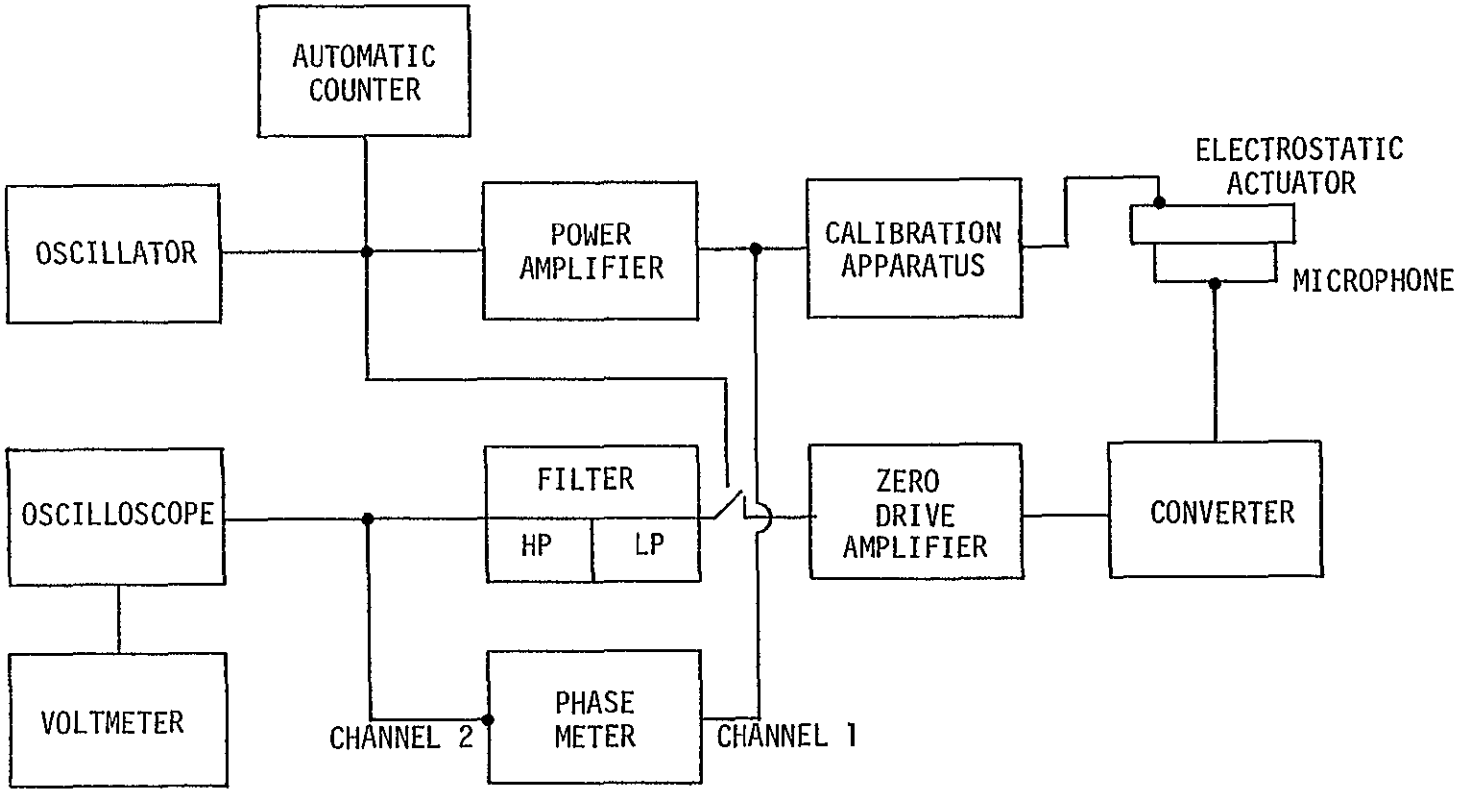

Figure 8. Instrumentation used to measure microphone frequency response. oscillator = HP model 651B, automatic counter = HP model 5323A; power amplifier = HP model 467A, calibration apparatus = B & K type 4142, converter (see reference 3); zero drive amplifier = MB Electronics type N461 with modifications (see reference 4); filter = Kronhite model 3202, oscilloscope = Tektronix type 549 with 1A7A plug-in, voltmeter = HP model 3403C, phase meter = Ad-Yu Electronics type 405L.

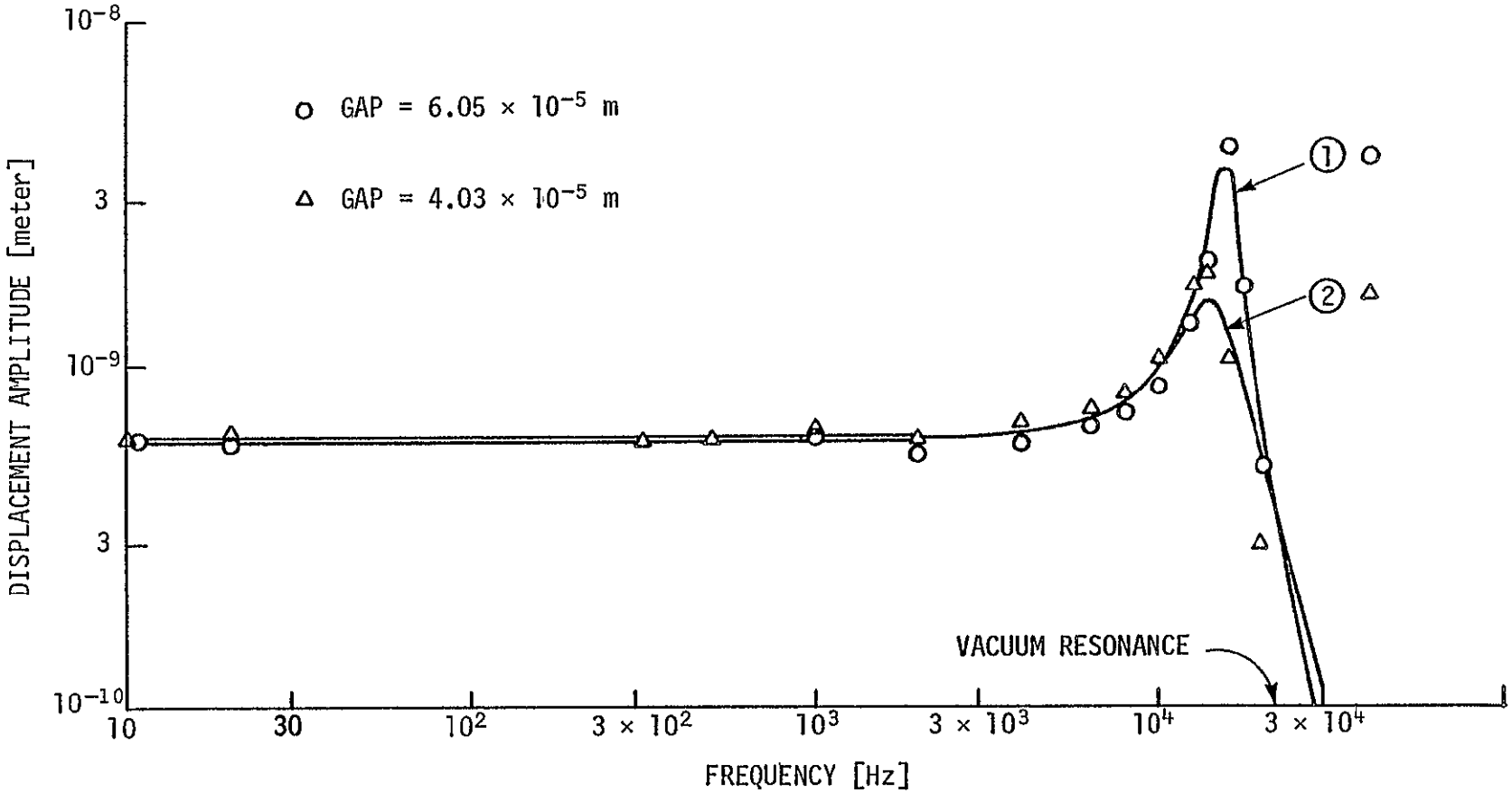

Figure 9. Frequency dependence of membrane displacement amplitude for two different gap distances. theoretical curve (case 3): ———, experimental points. o and Δ . Tension = 2962 N/m. Excitation = 0.6774 N/m^2 (90.6 dB)

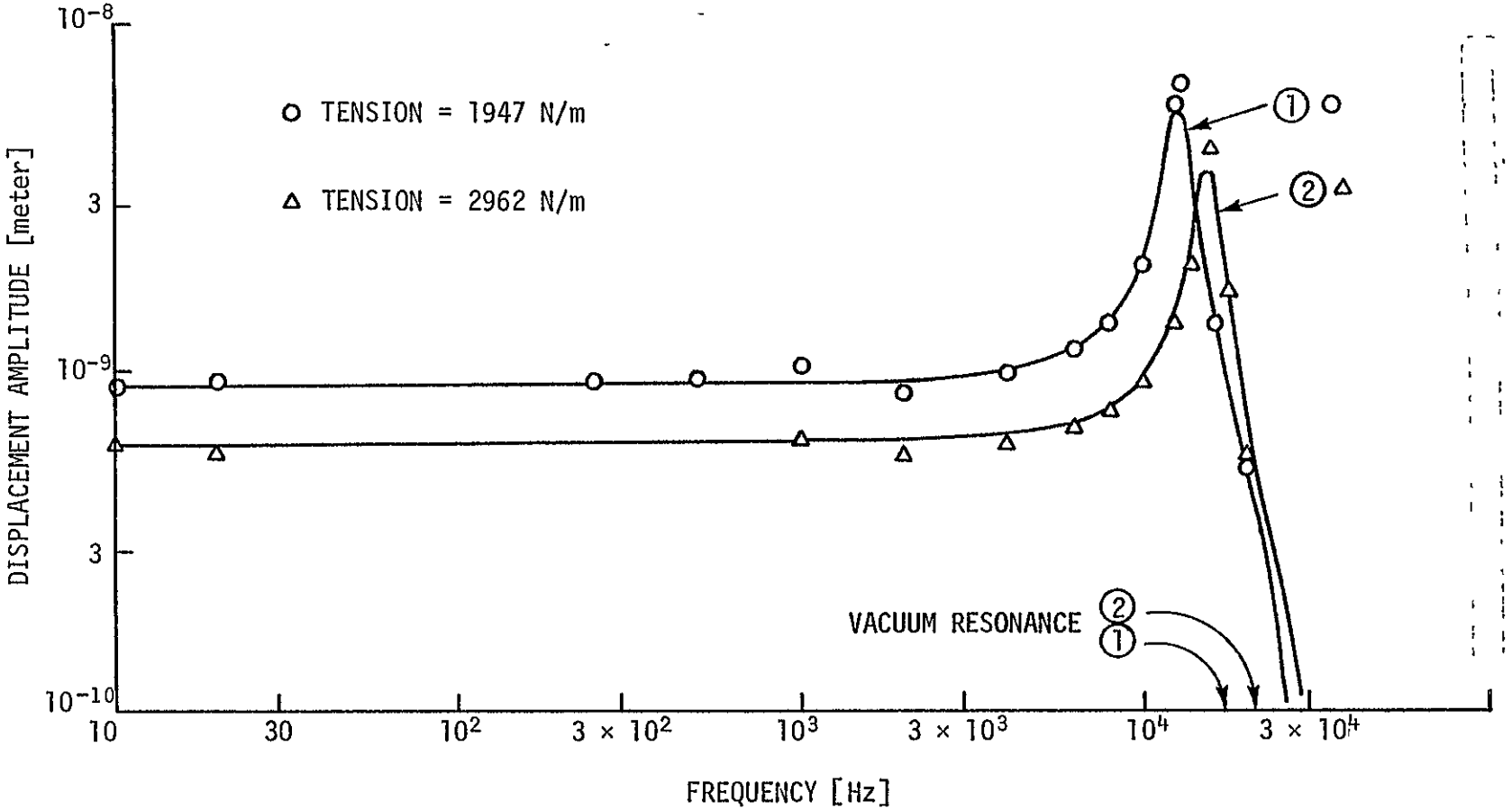

Figure 10. Frequency dependence of membrane displacement amplitude for two different values of membrane tension theoretical curve (case 3). ———, experimental points. o and Δ . Gap = 6.05×10^{-5} m. Excitation = 0.6774 N/m^2 (90 6 dB)

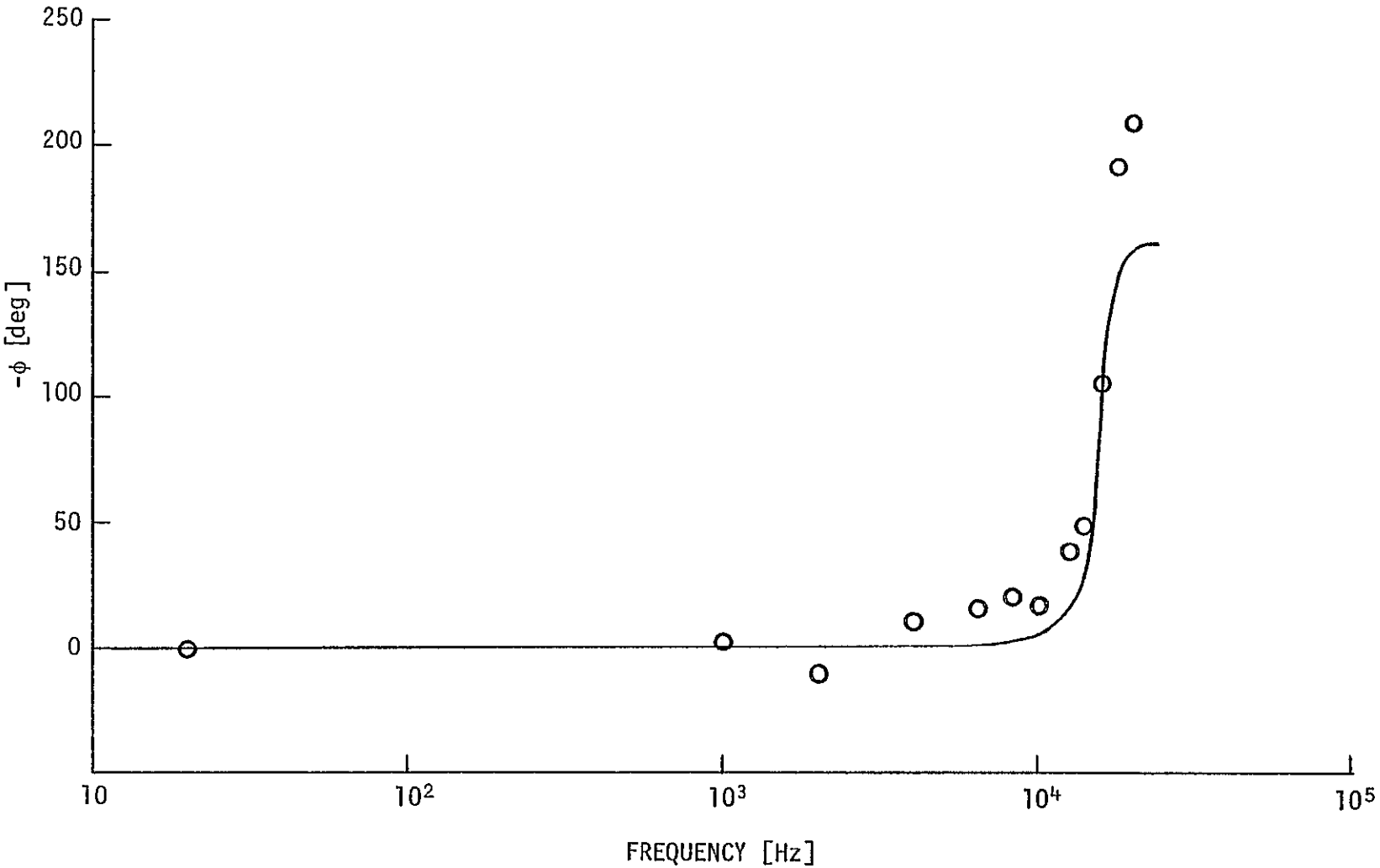

Figure 11 Frequency dependence of phase angle between incident pressure and membrane displacement corresponding to curve ① of figure 9.

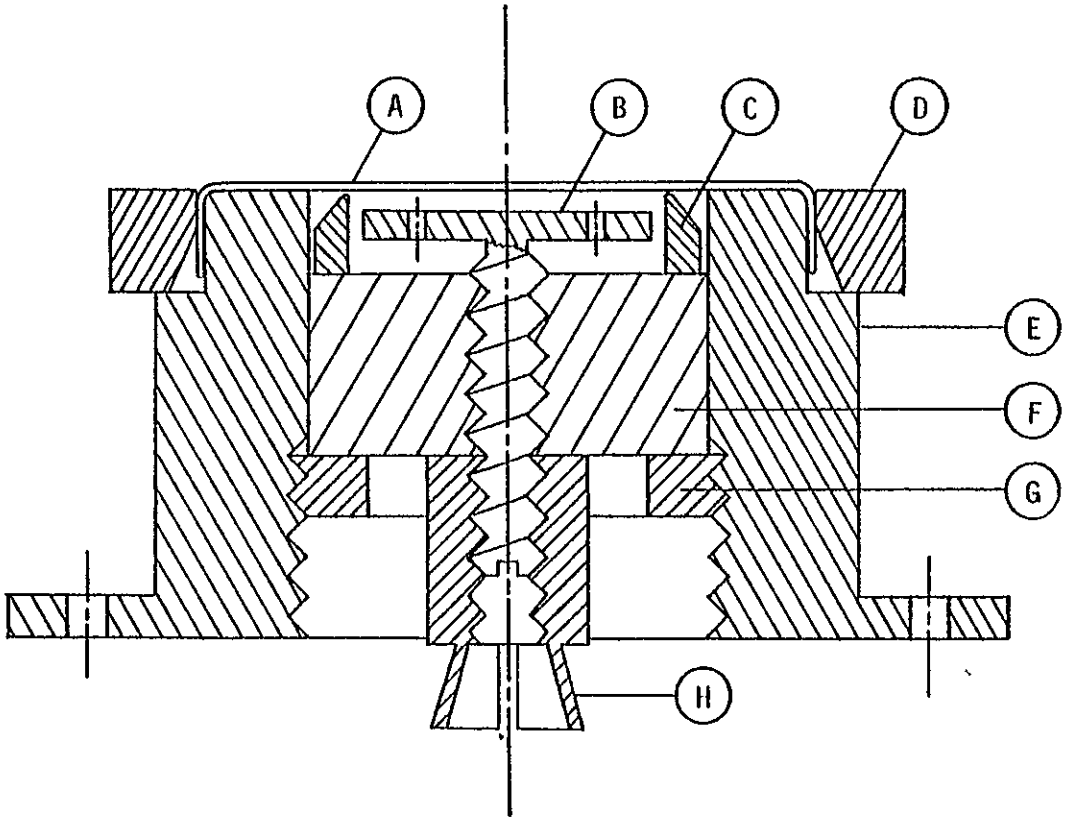

Figure 12. Assembly drawing of microphone cartridge. A membrane, B backplate, C tension ring, D membrane retaining ring, E case, F insulator, G threaded ring, H locking tube.

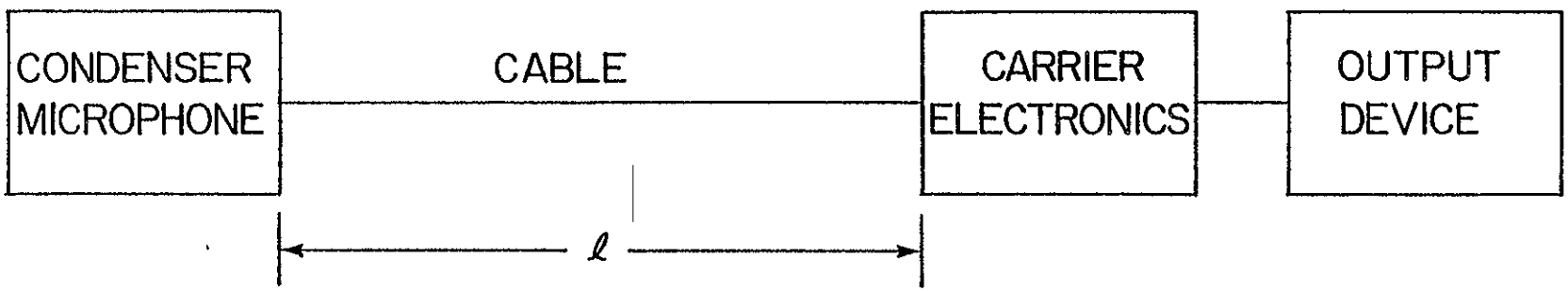

Figure 13. Block diagram of high-temperature microphone system

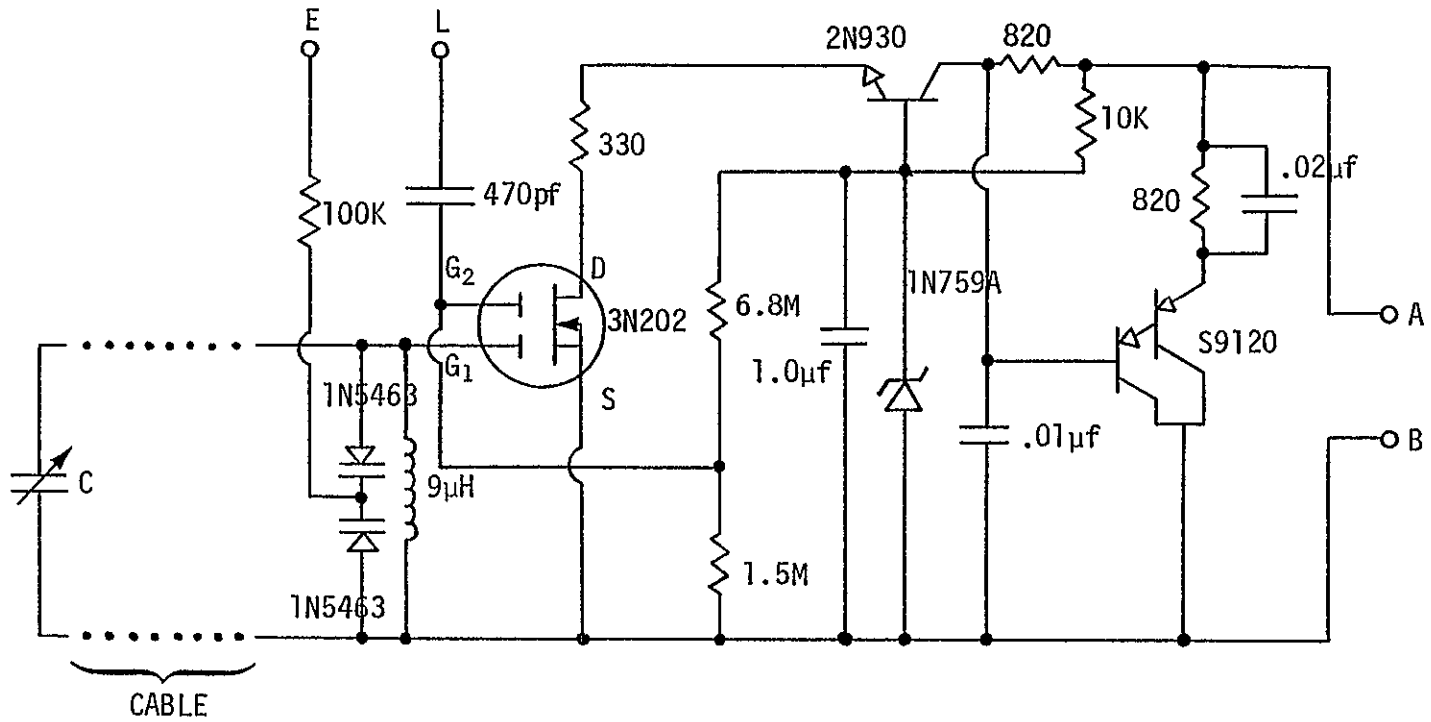

Figure 14. Circuit diagram of the converter containing varactor diodes for tuning control. Terminal connections. A zero drive amplifier input, B zero drive amplifier common, E zero drive amplifier control, L RF signal generator. C = condenser microphone.

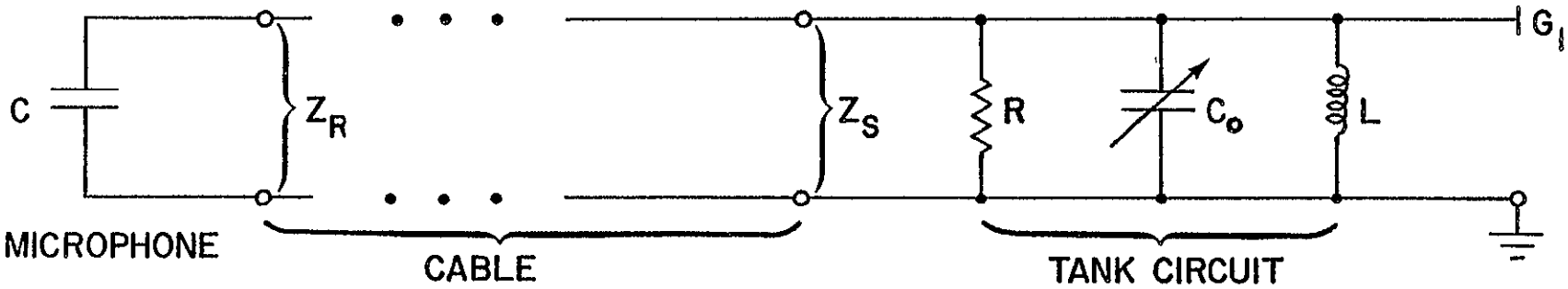

(a) ACTUAL CIRCUIT

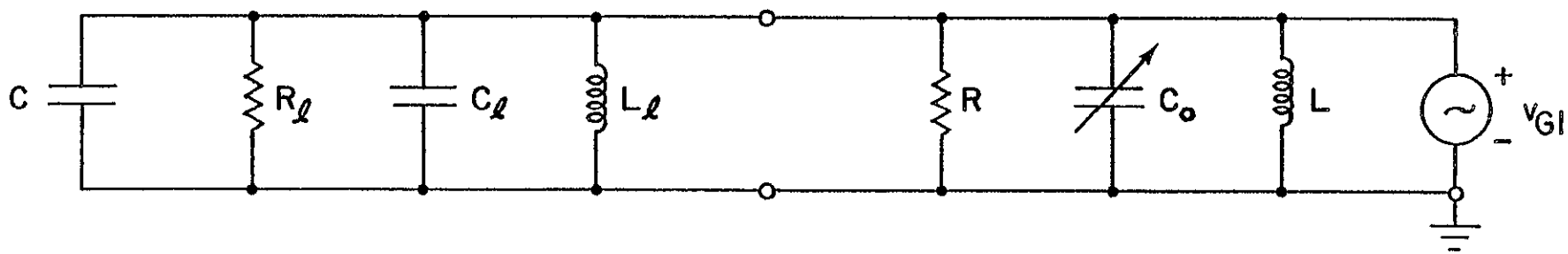

(b) EQUIVALENT CIRCUIT

Figure 15. Front end of the converter.

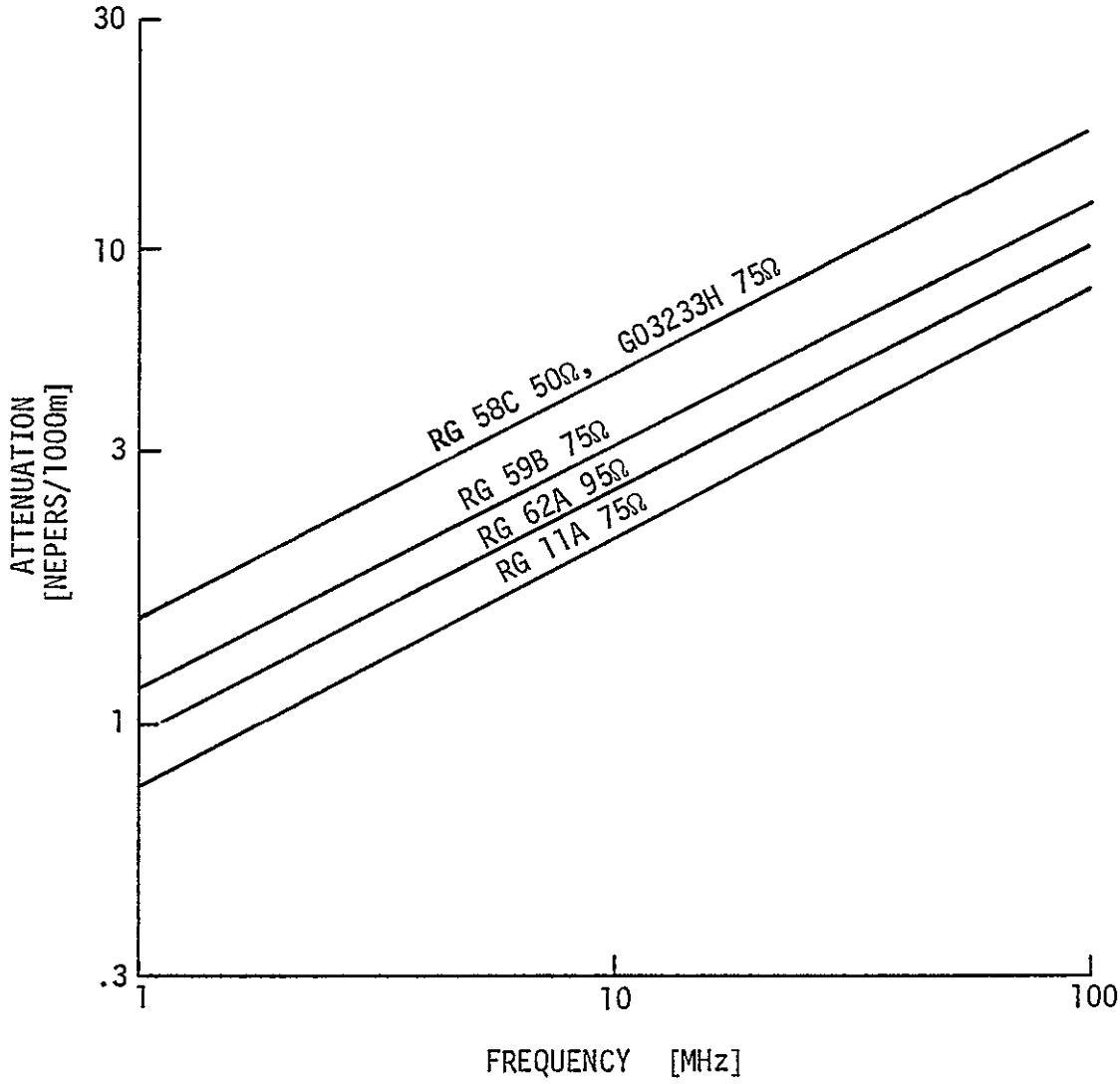

Figure 16. Measured cable attenuation versus frequency

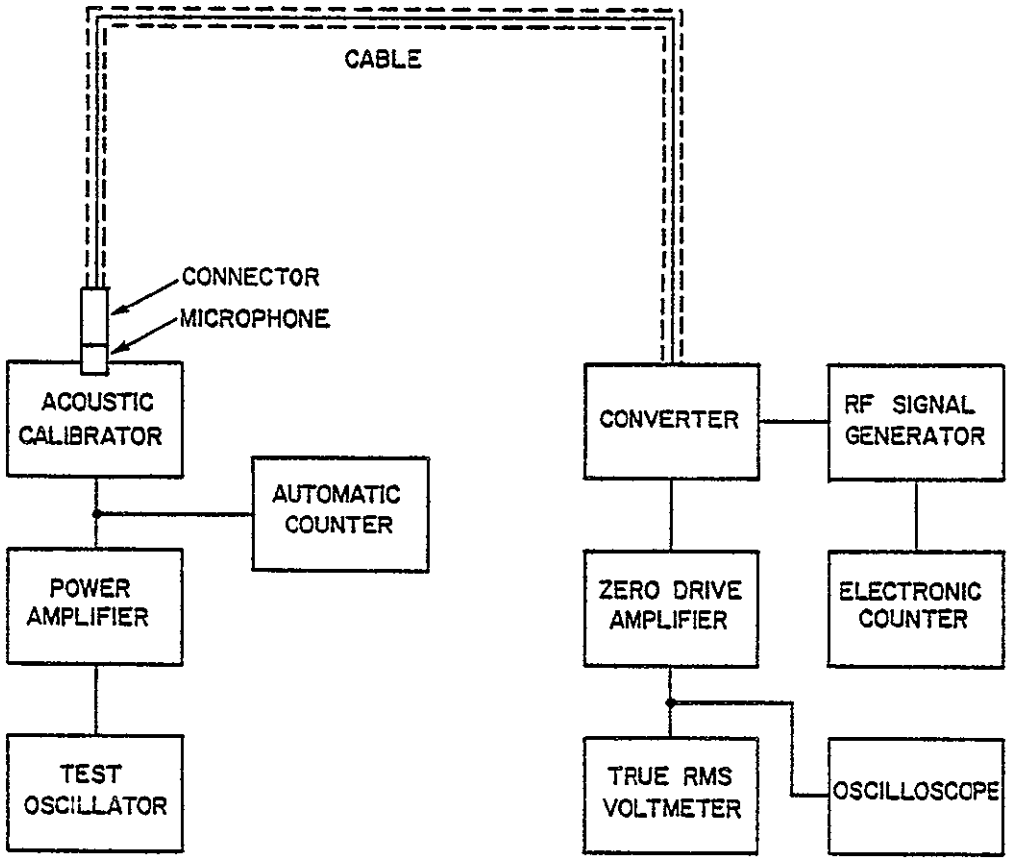

Figure 17 Instrumentation used to measure system sensitivity. Test oscillator = HP651B, power amplifier = HP467A, automatic counter = HP5323A, acoustic calibrator = Photocon PC-125, microphone = B&K 4134 (SN 489856), converter (see refs. 3 and 4), zero drive amplifier = Gilmore N461 (modified), true rms voltmeter = HP3403C, rf signal generator = HP606B; electronic counter = HP5245L, oscilloscope = Tektronix 549 with 1A1 plug-in.

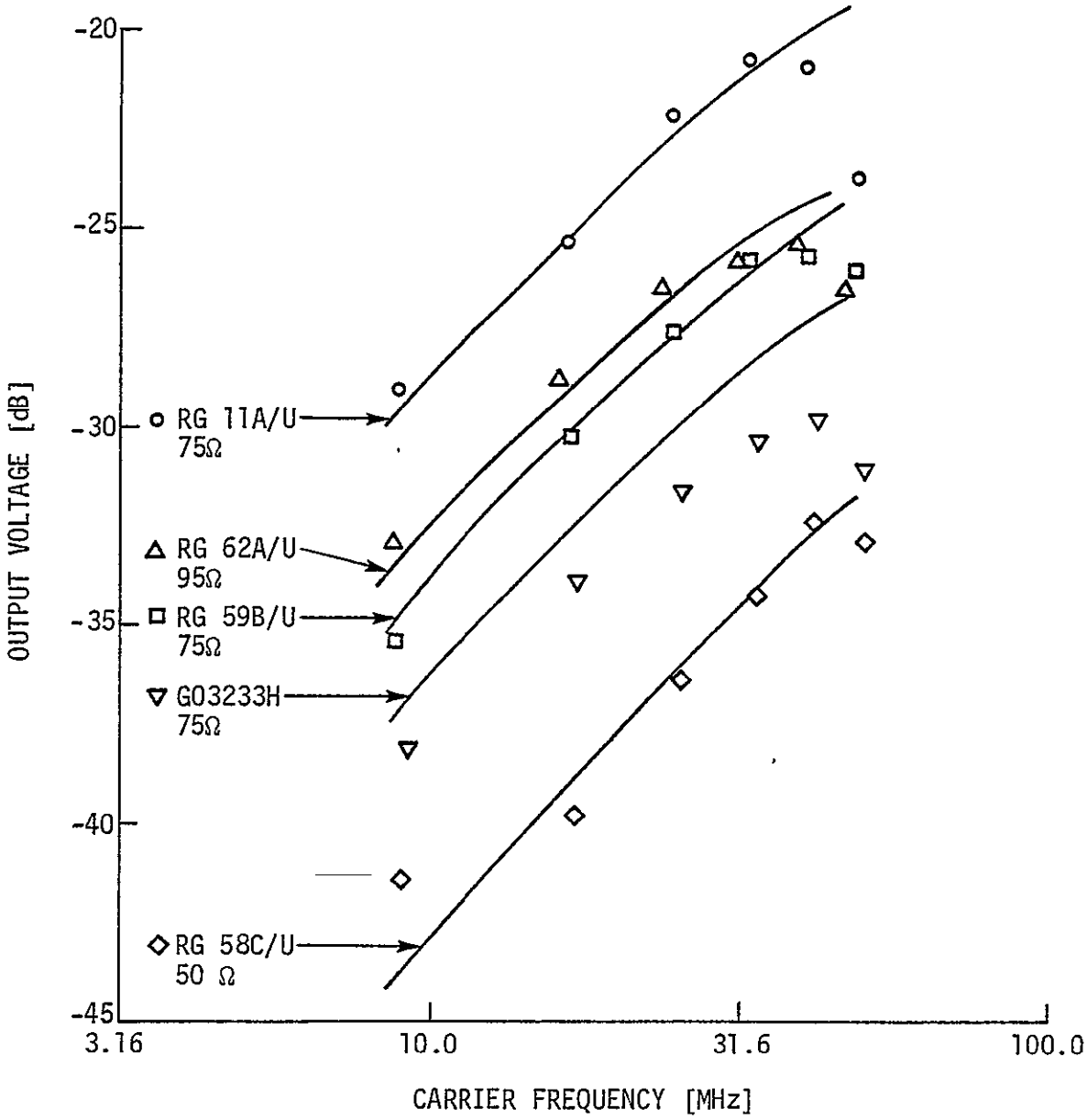

Figure 18 Relative sensitivity of system with various coaxial cables versus carrier frequency Output voltages are referred to system response with microphone connected directly to converter (no intervening cable). Solid curves: theoretical. Symbols: experimental data points.

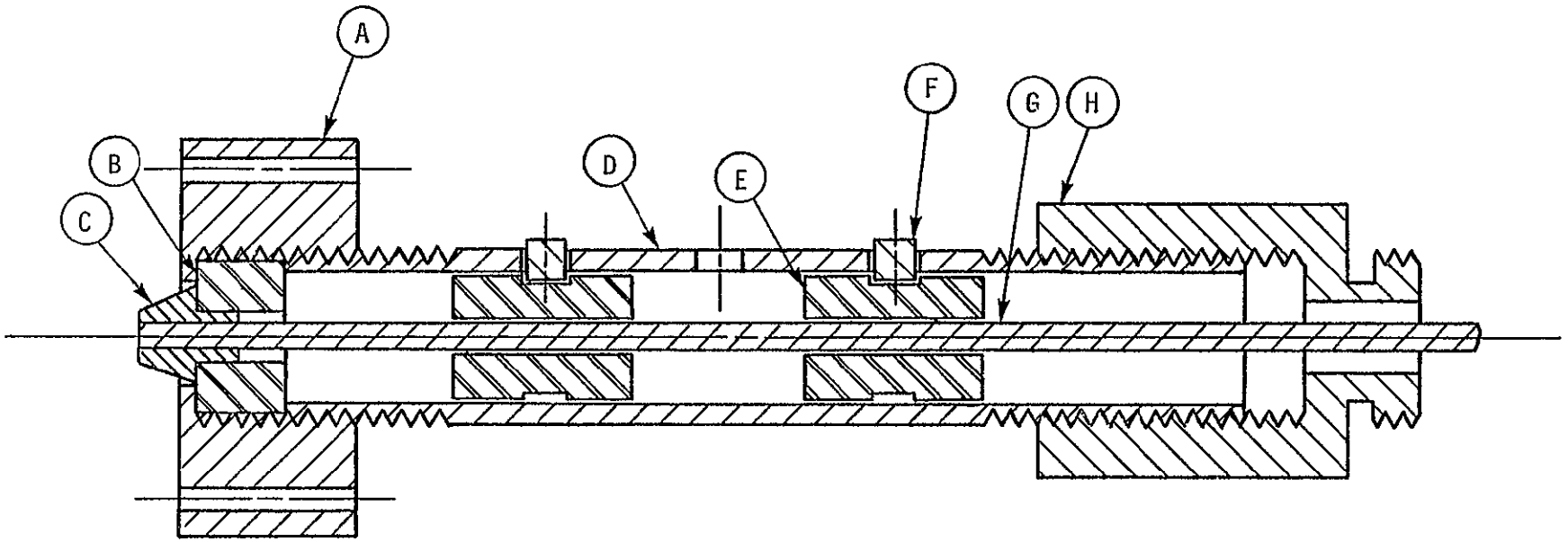

Figure 19. Microphone-cable connector assembly. Microphone connector parts A Case (stainless steel), B Spacer (macor), C Contact pin (stainless steel). Extension tube parts: D Tube (copper), E Spacer (macor), F Pin (copper), G Center conductor (copper). Cable connector parts H Cap (copper), plus parts of a TNC connector (not shown, see text). Scale: linear dimensions twice actual size, except for center conductor G, which is exaggerated.

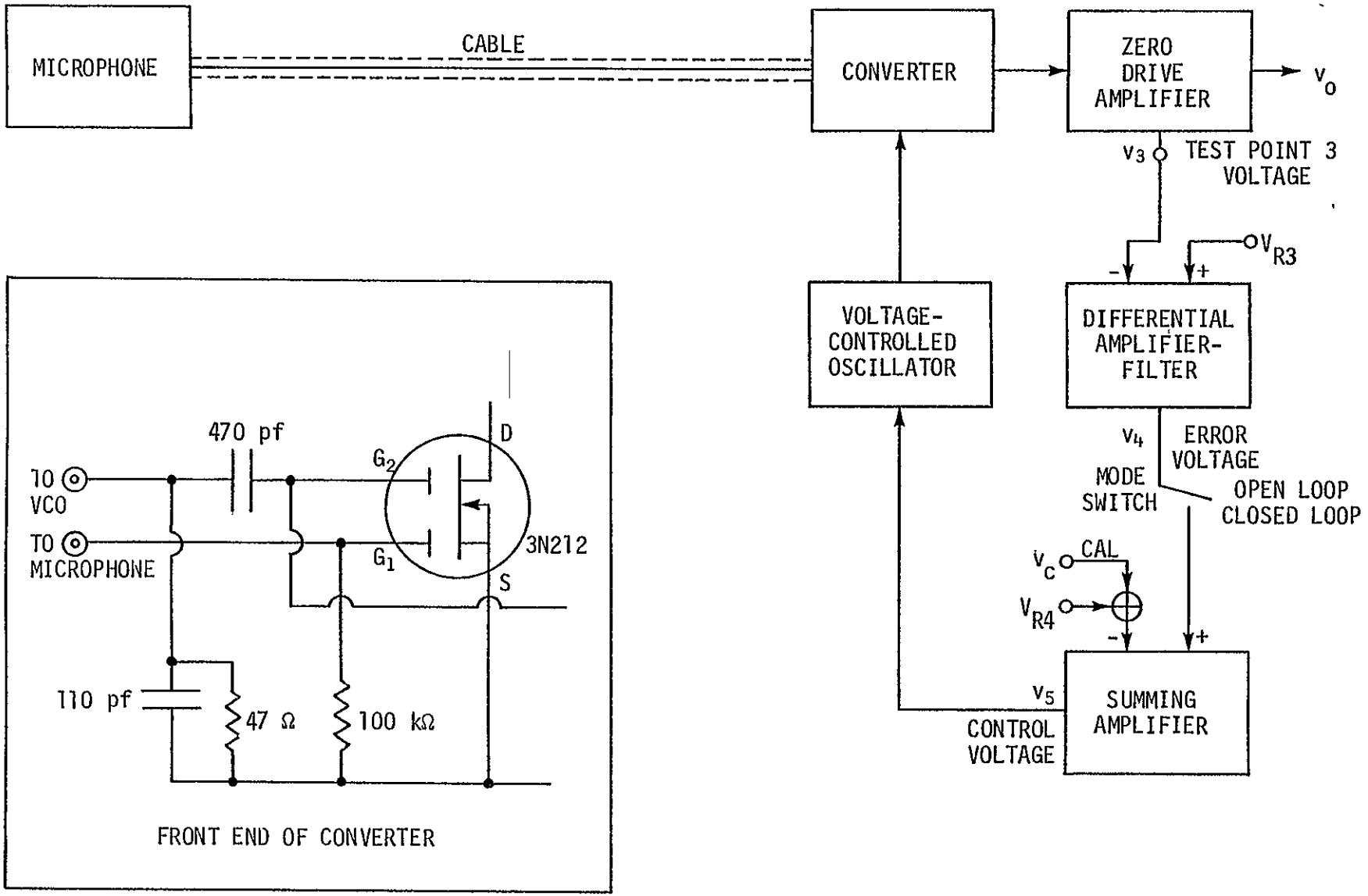

Figure 20 Block diagram of the VCO system with automatic tuning control. Insert shows details of the modified front end of the converter.

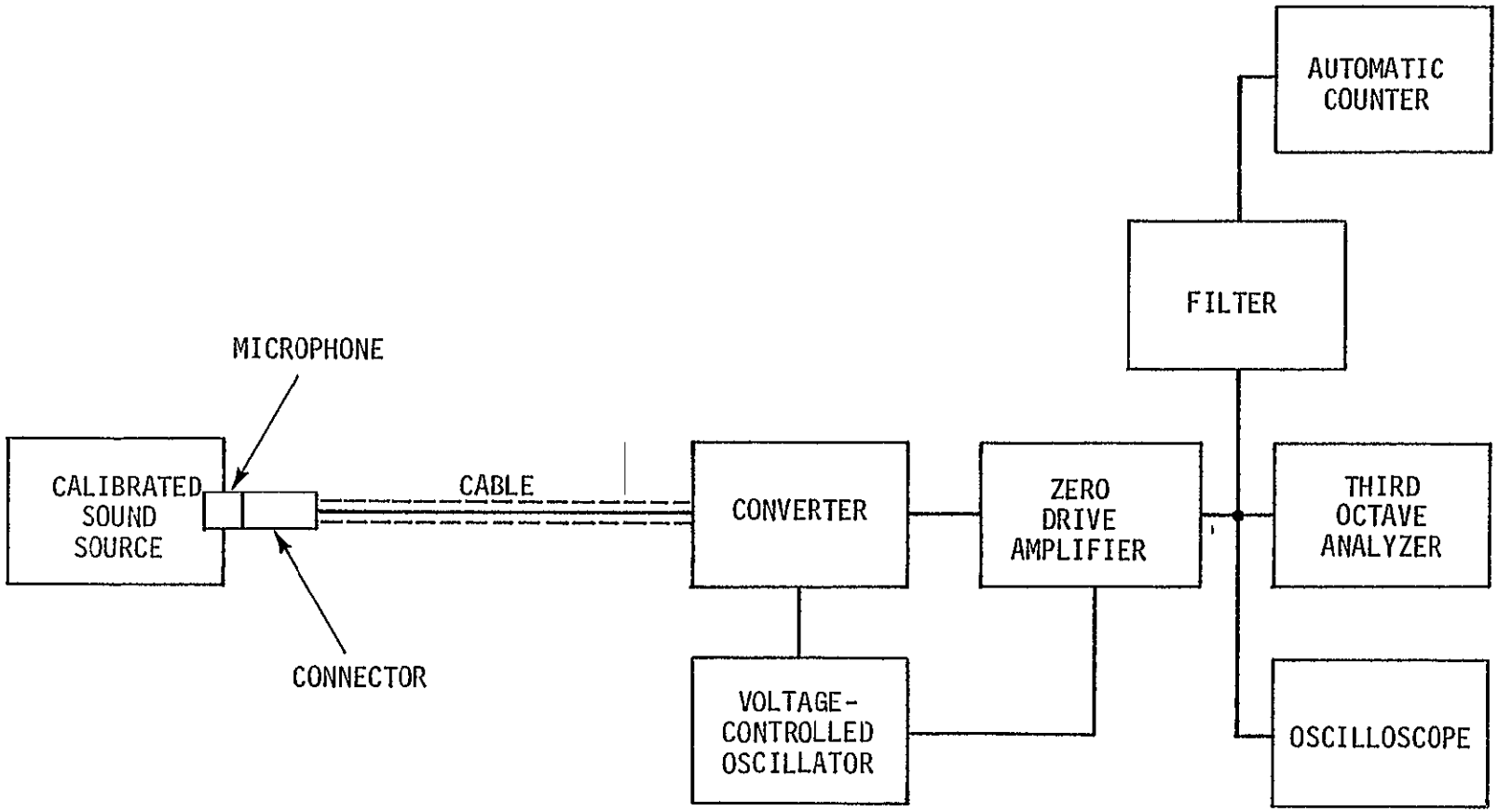

Figure 21. Experimental arrangement for measuring harmonic distortion. Calibrated sound source = Photocon PC-125 or BB&N 901D; third octave analyzer = B&K 3347; filter = HP5489A; cable = RG 11 A/U (5 72 m), voltage-controlled oscillator = Hope VCO-100A; remaining components are the same as those in figure 17.

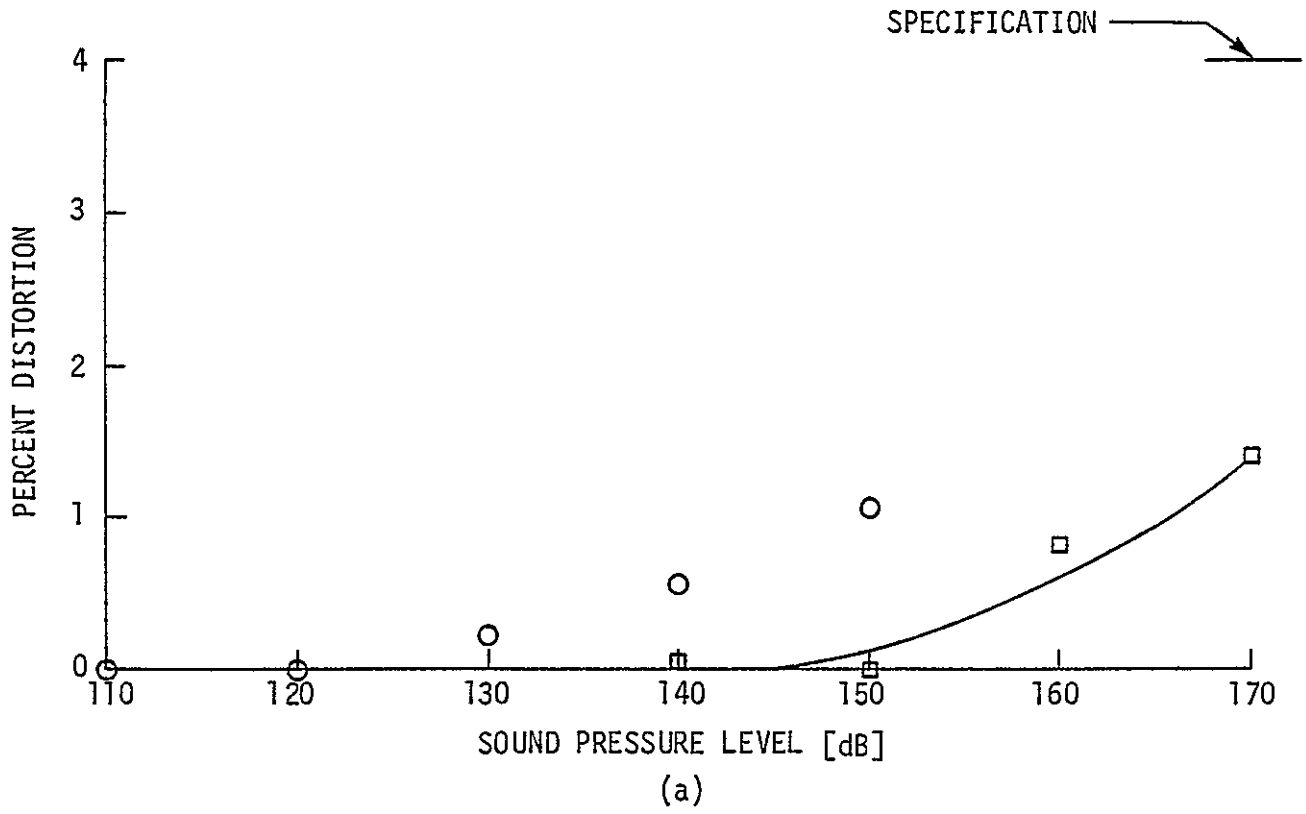

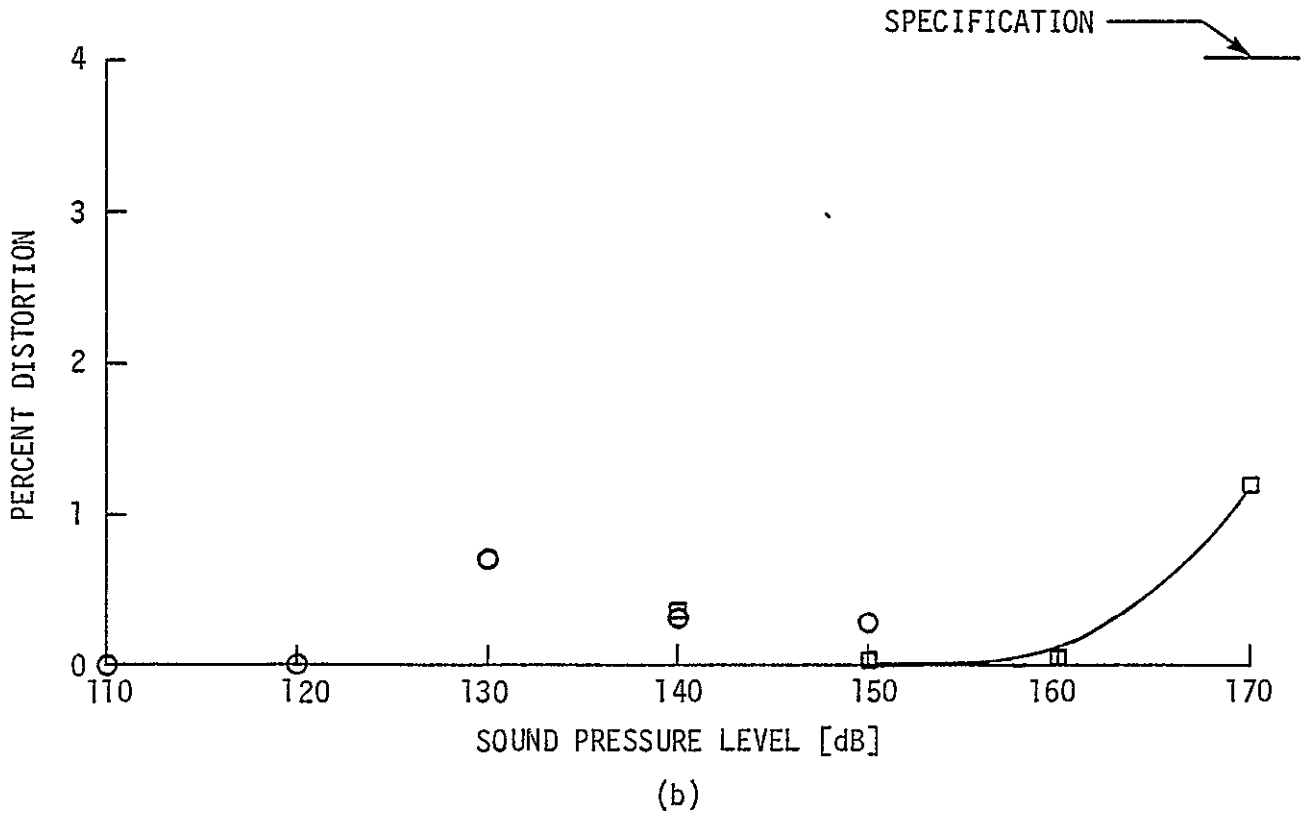

Figure 22. Harmonic distortion versus sound pressure level for (a) microphone 1 and (b) microphone 2, measured with O PC-125 at 1000 Hz, □ BB&N 901D at 80 Hz.

C.5

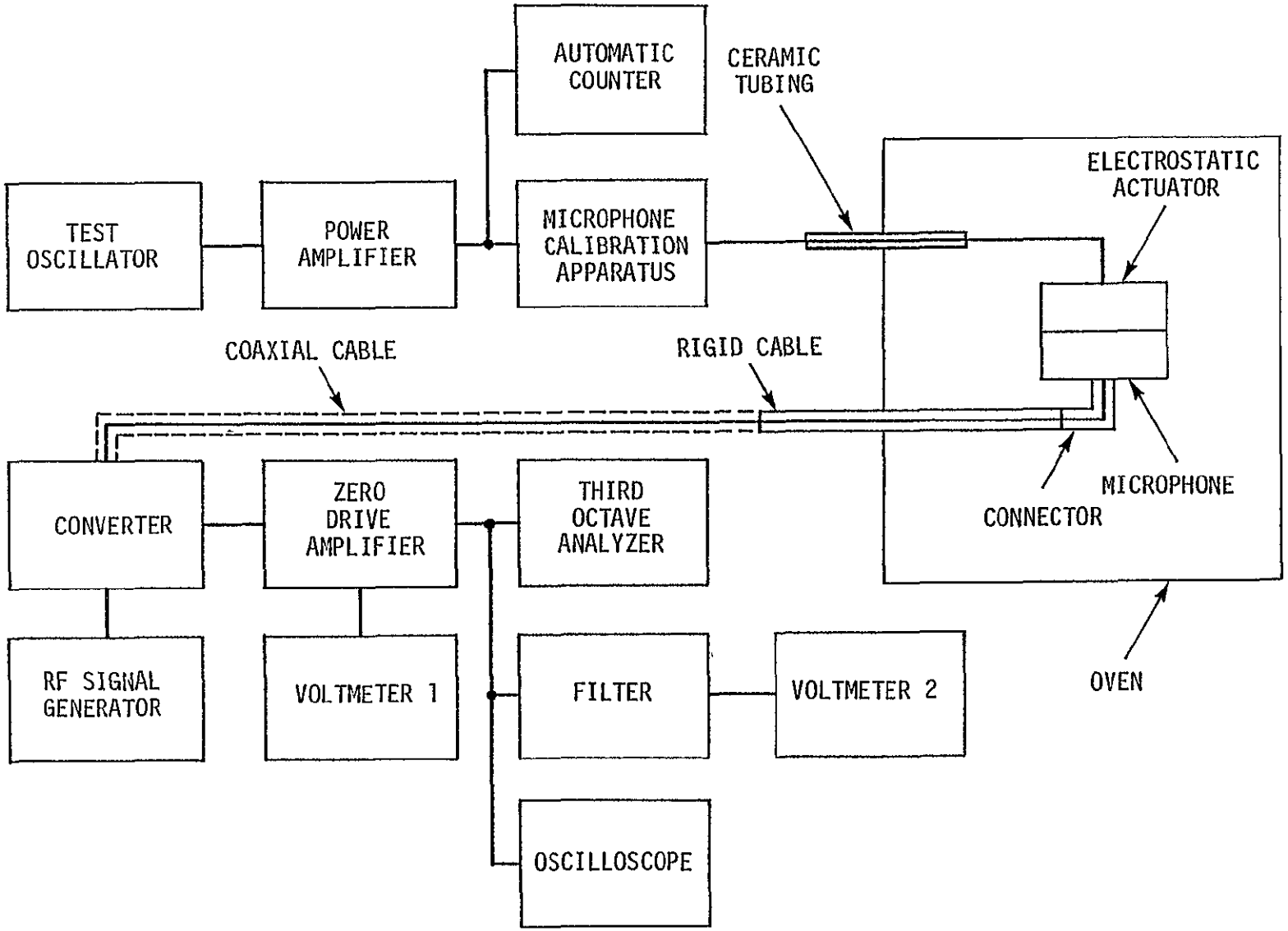

Figure 23. Experimental arrangement for measuring frequency response. Microphone calibration apparatus = B&K 4142, third octave analyzer = B&K 3347, filter = Kronhite 3202, voltmeter 1 = HP3403C; voltmeter 2 = HP427A; coaxial cable = RG 11A/U (5.59 m), remaining components are the same as those in figure 17

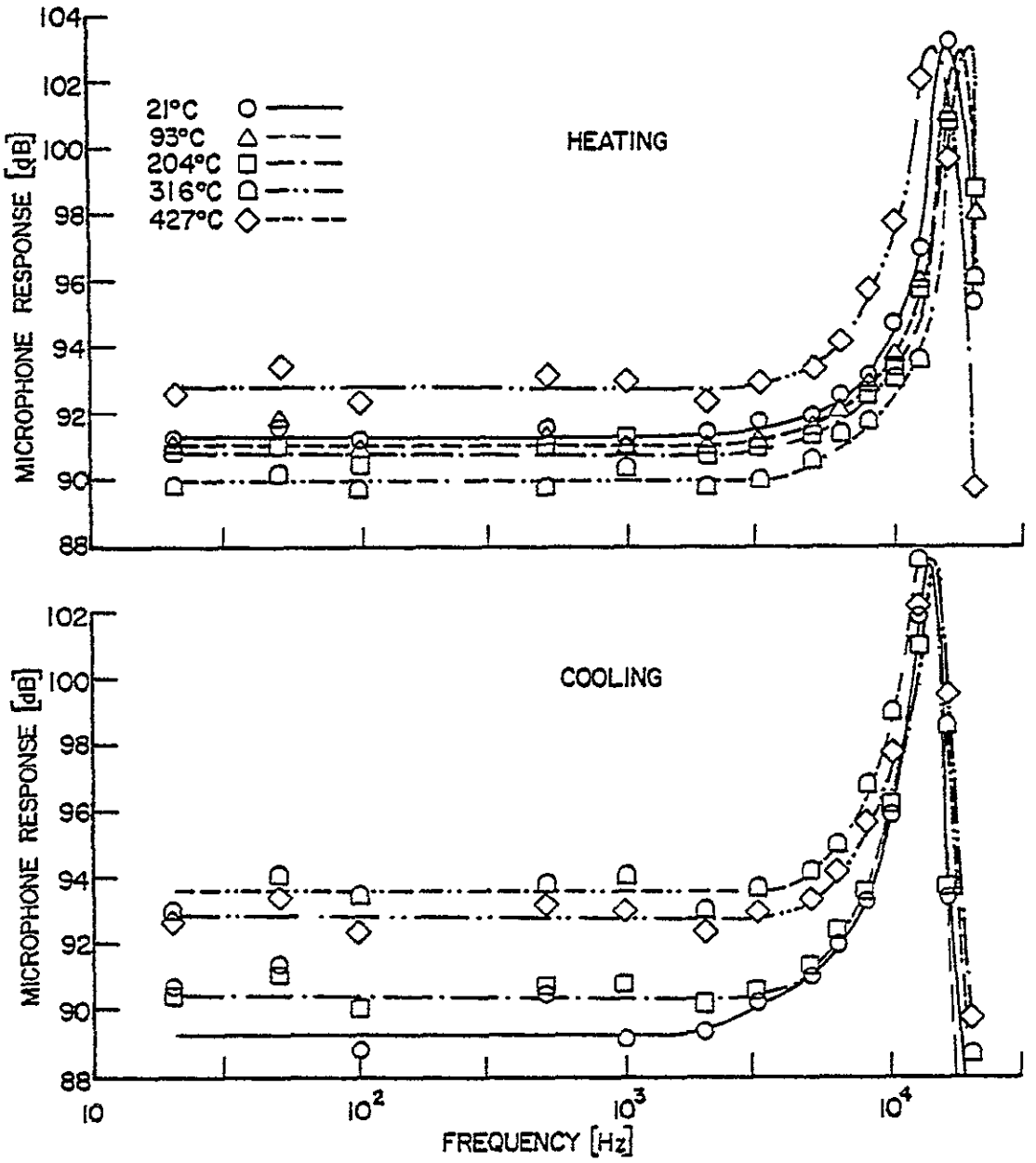

Figure 24 Frequency response of microphone 1 during heating and cooling Because of membrane replacement the membrane tension (4282.4 N/m) and gap (4.208×10^{-5} m) differ from those listed in table 7

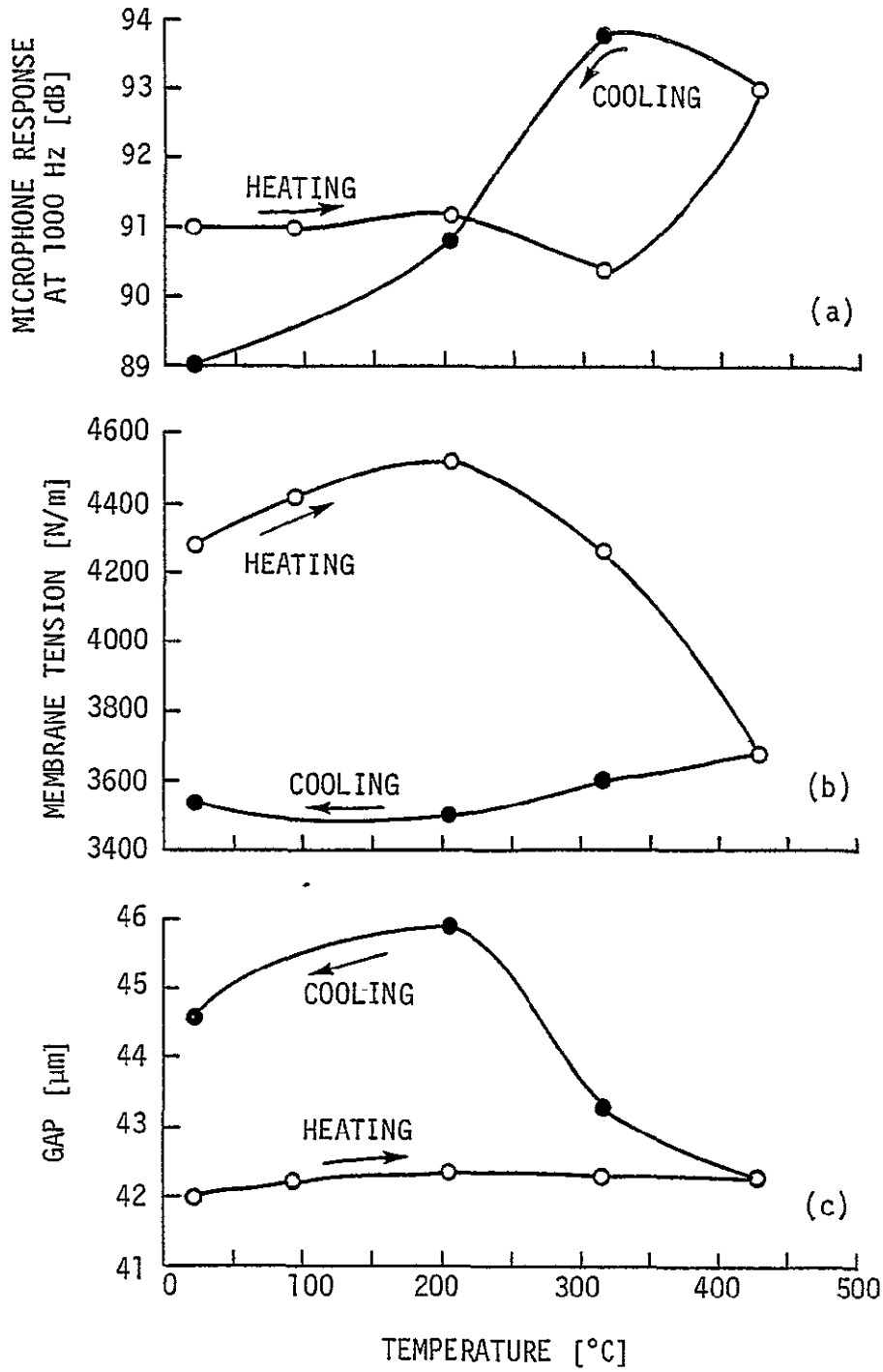

Figure 25. Temperature dependence of (a) microphone response at 1000 Hz, (b) membrane tension, and (c) gap of microphone 1

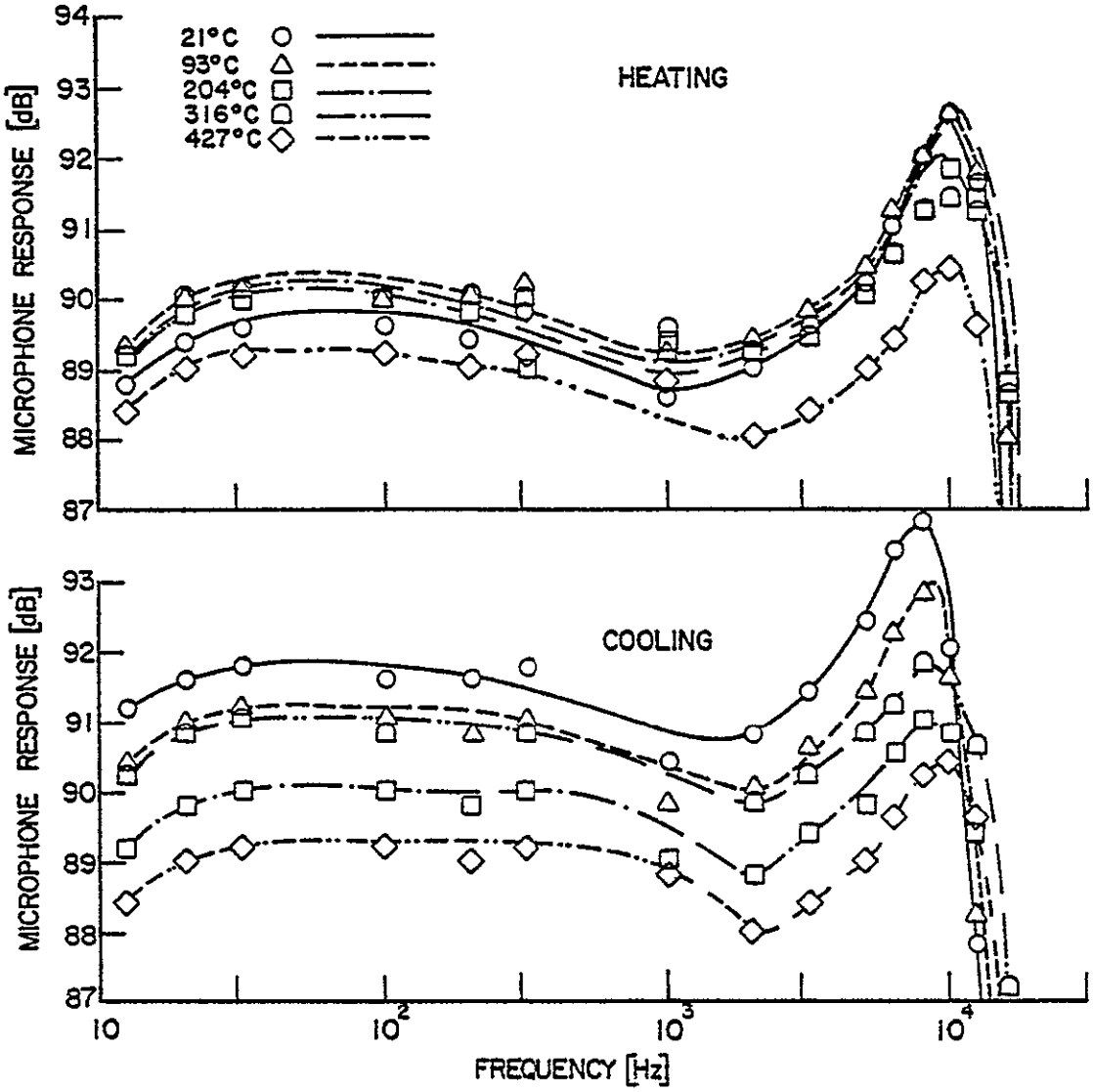

Figure 26. Frequency response of microphone 1 with reduced tension and gap during heating and cooling. Tension = 2733.1 N/m Gap = 2 903 × 10^{-5} m

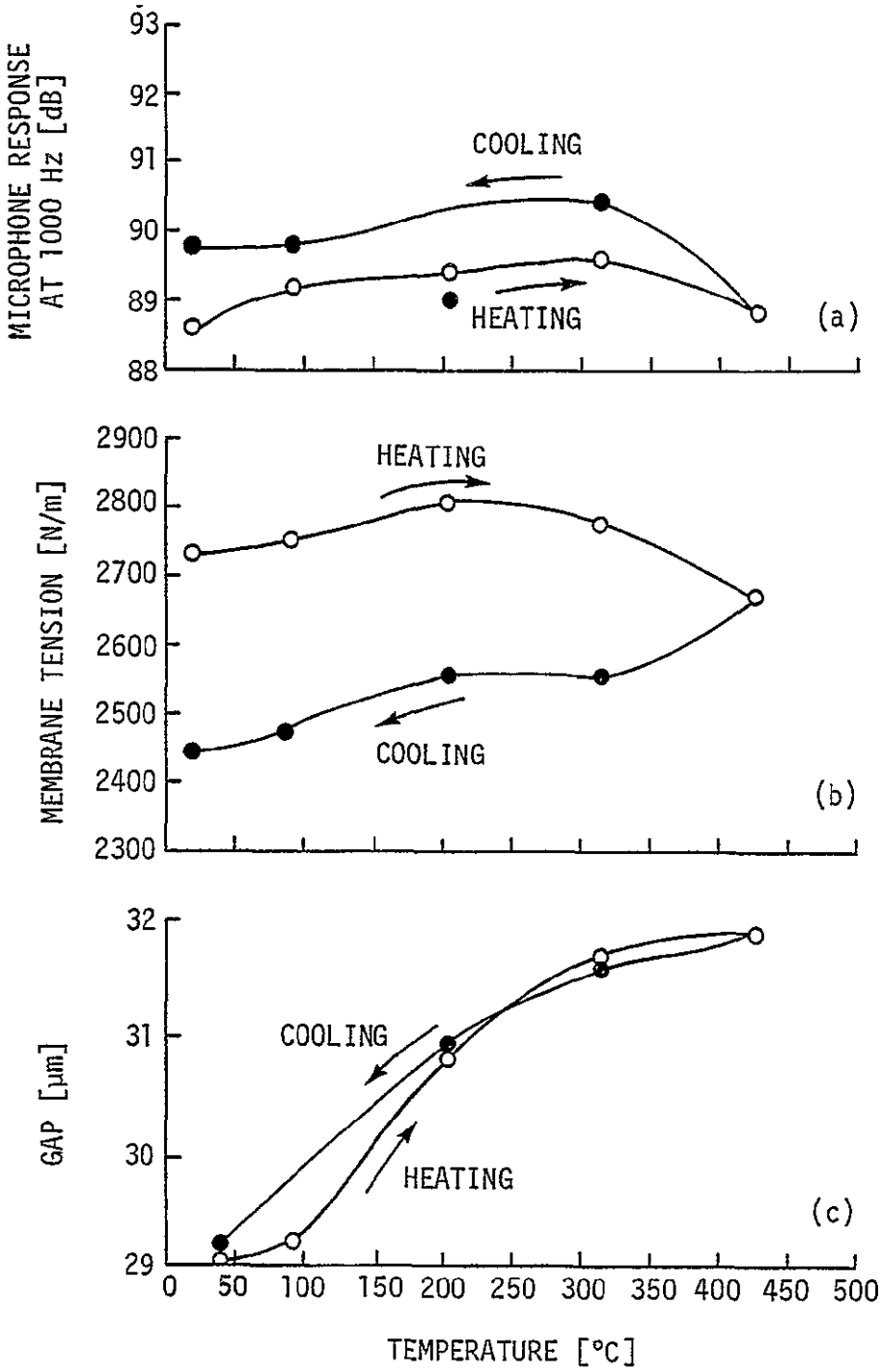

Figure 27 Temperature dependence of (a) microphone response at 1000 Hz, (b) membrane tension, and (c) gap of microphone 1 with reduced tension and gap.

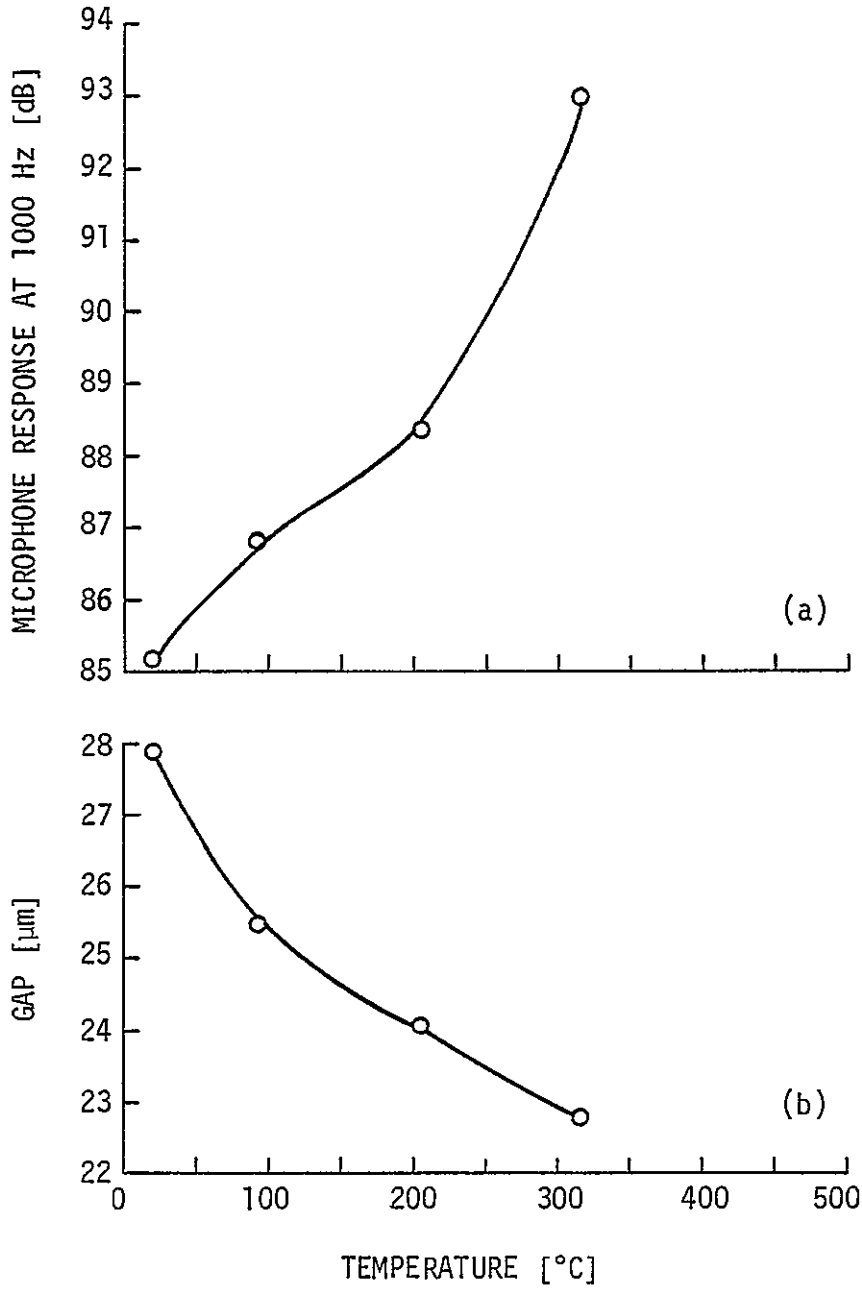

Figure 28. Temperature dependence of (a) microphone response at 1000 Hz and (b) gap of microphone 1 with type 347 stainless steel backplate.

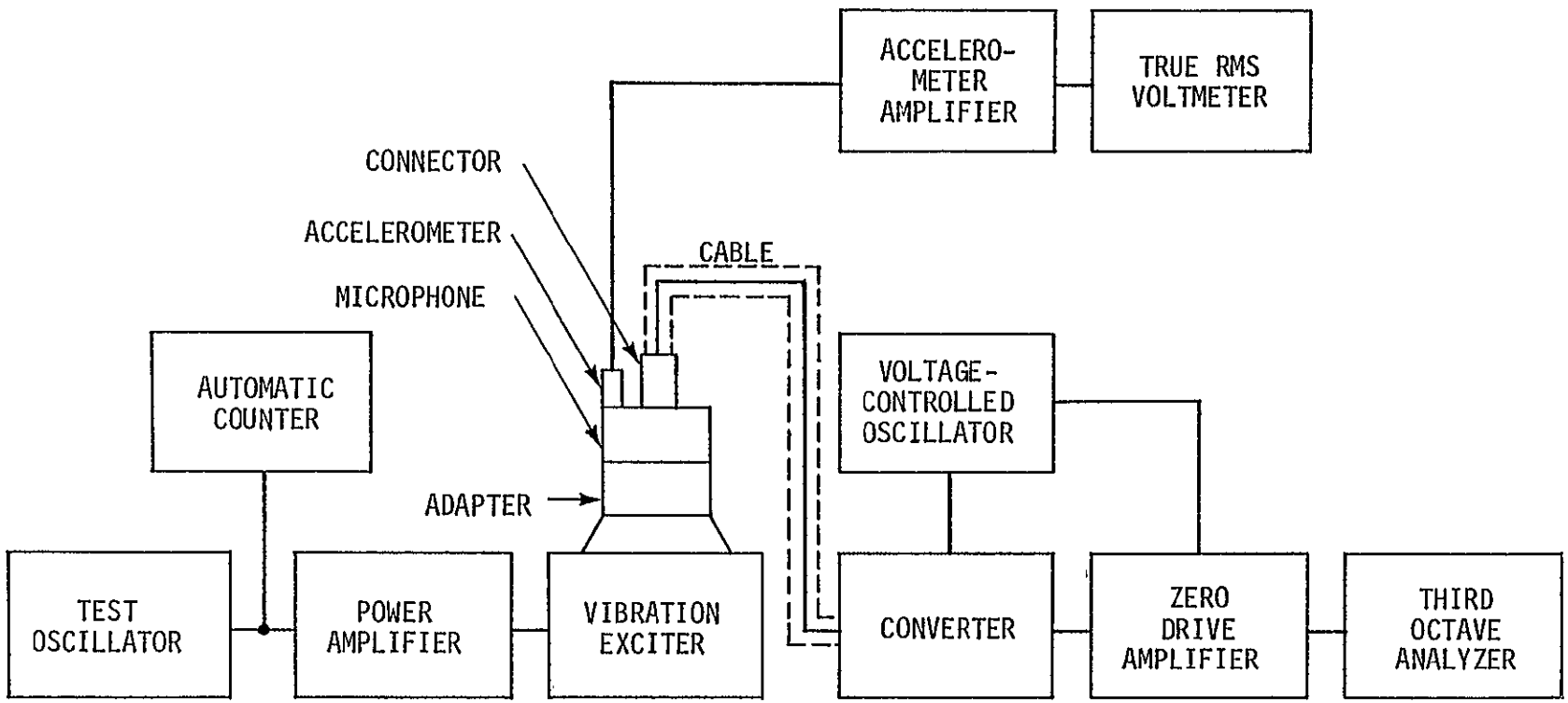

Figure 29 Experimental arrangement for measuring vibration sensitivity. Vibration exciter = B&K 4809, third octave analyzer = B&K 3347; accelerometer = BB&N 501-159, cable = RG 11 A/U (5.72 m); voltage-controlled oscillator = Hope VCO-100A, remaining components are the same as those in figure 17.

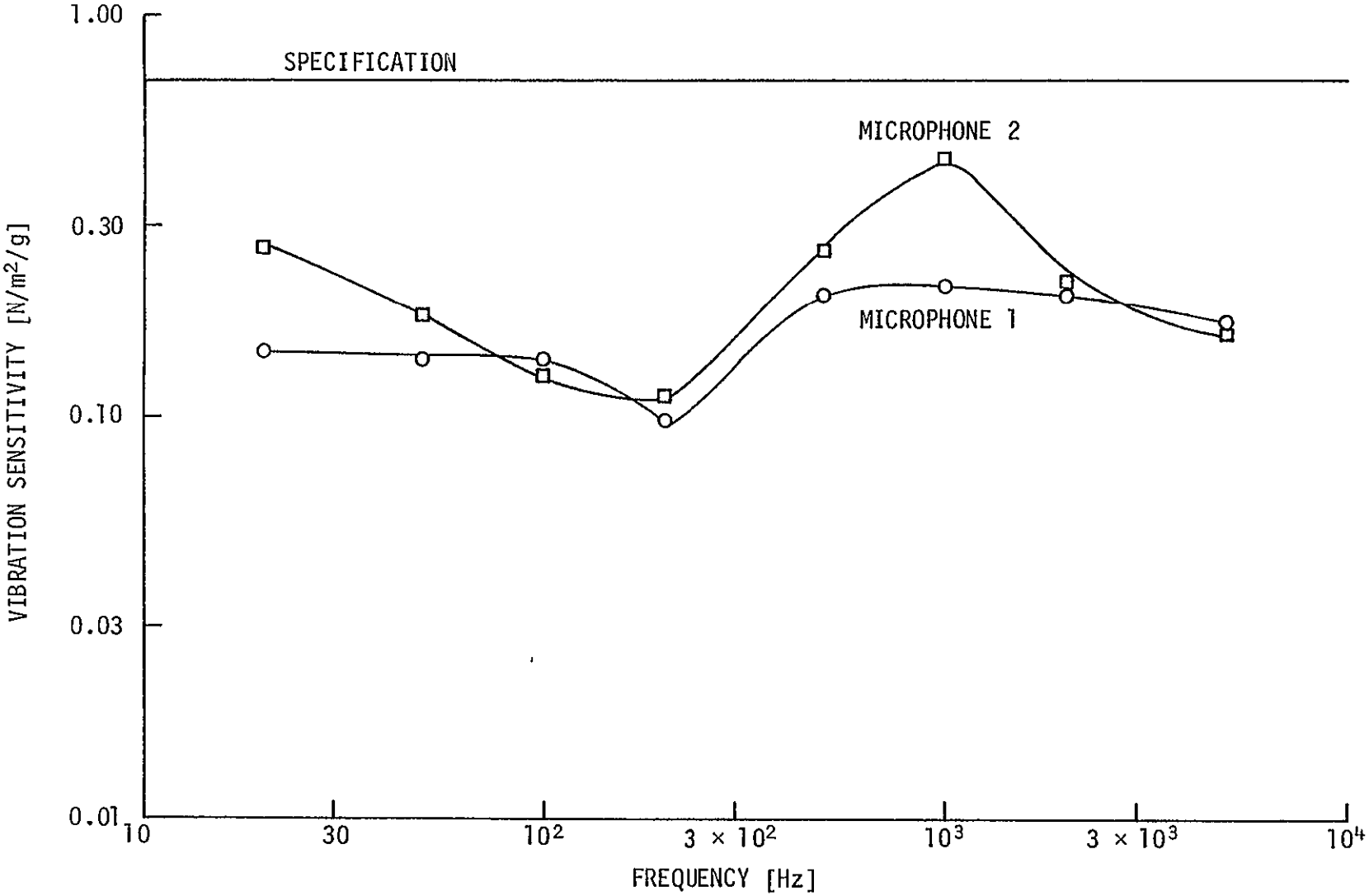

Figure 30 Vibration sensitivity spectrum of ○ microphone 1 and □ microphone 2. The horizontal line indicates the maximum vibration sensitivity permitted by the specification (0.6895 $N/m^2/g$).

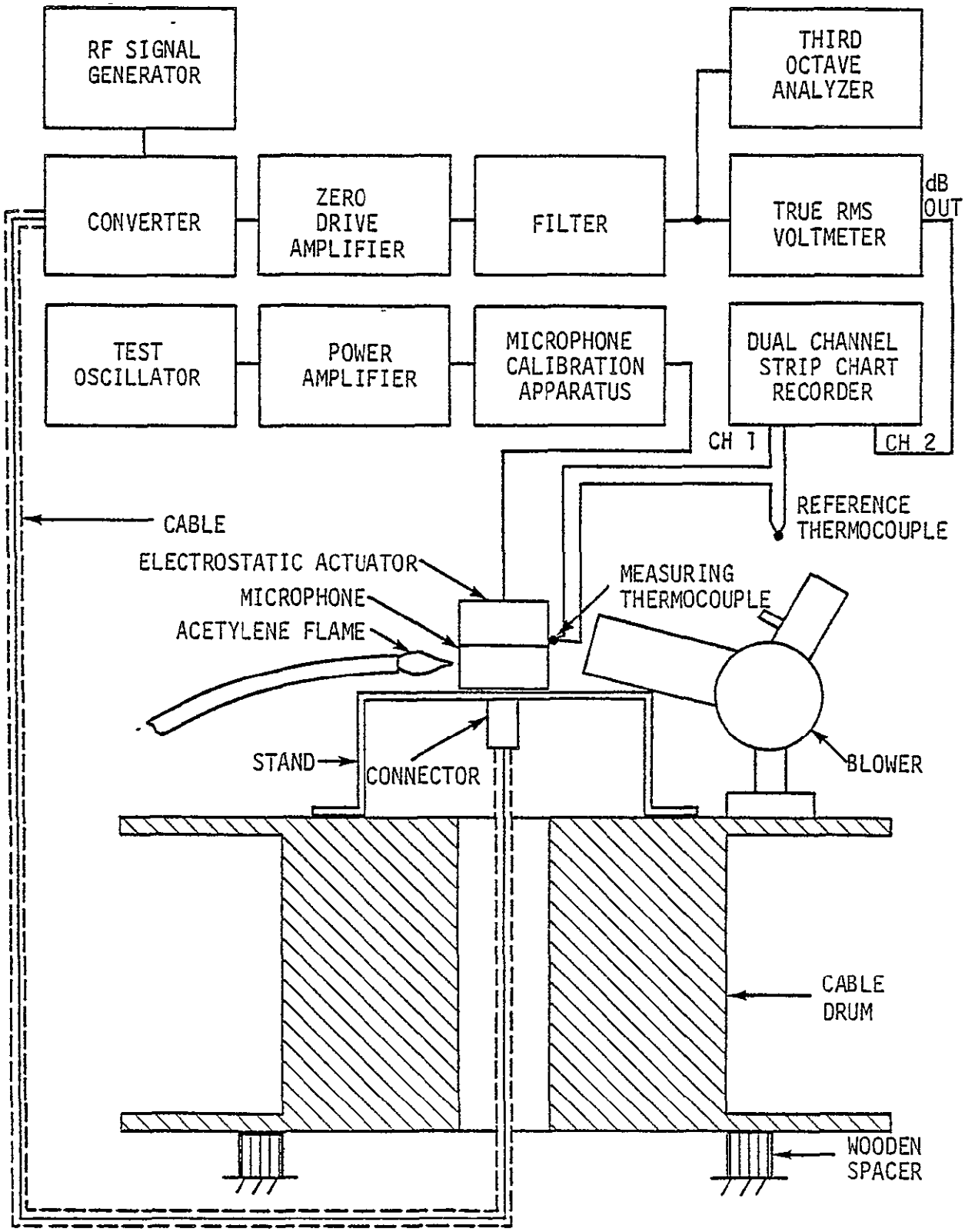

Figure 31 Experimental arrangement for thermal shock test. Filter = EDMAC 8010A, dual channel strip chart recorder = Leeds and Northrup Speedomax, cable = RG 11A/U (7.62 m), remaining components are the same as those in figure 23

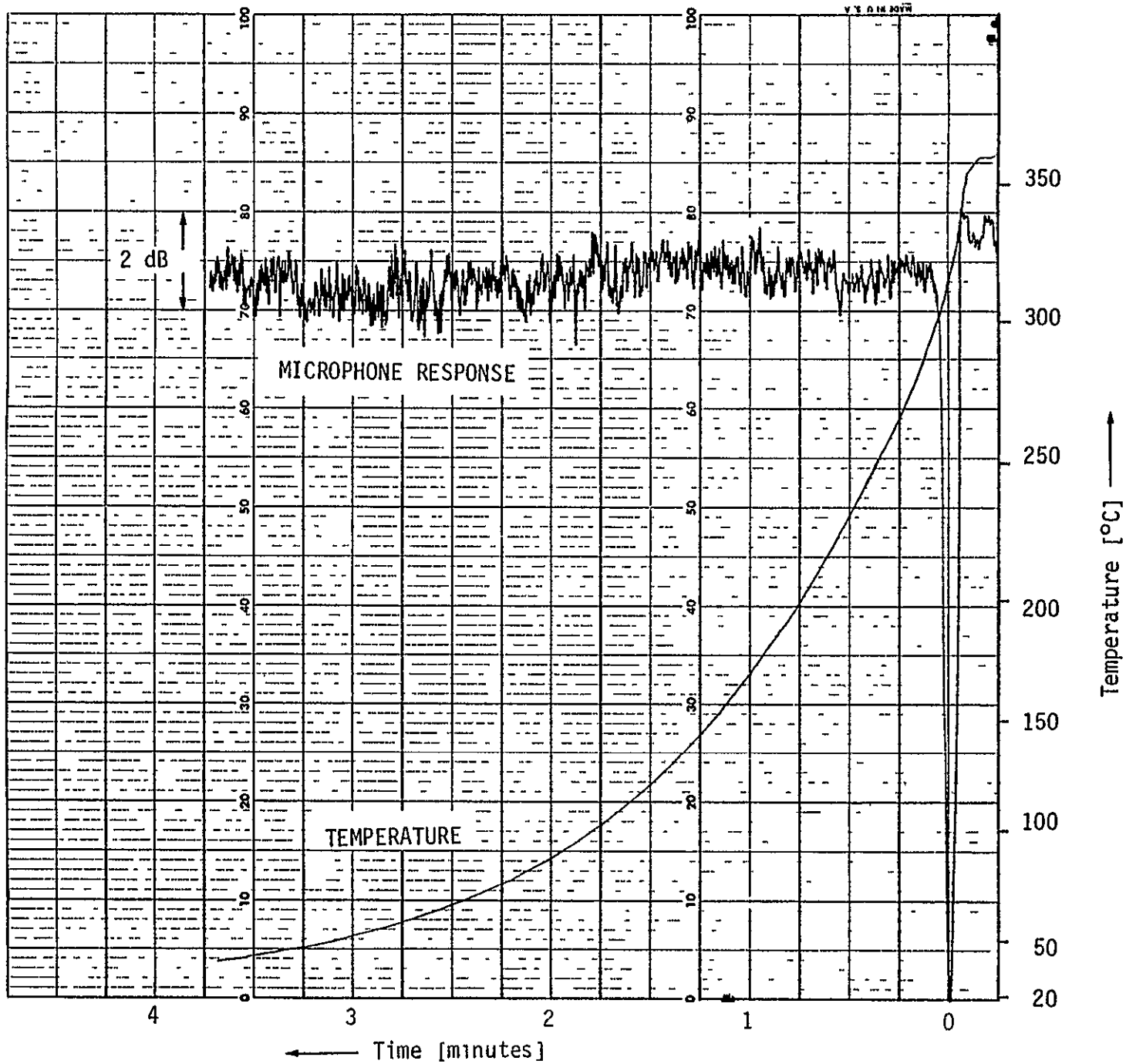

Figure 32. Time history of microphone response to a steady electrostatic actuator signal during thermal shock test. Blower was turned on at time t = 0